Structural investigation of membrane proteins by electron microscopy

Moscicka, Katarzyna Beata

Structural investigation of membrane proteins by Electron Microscopy

Katarzyna Beata Mościcka

Printed by GrafiMedia Rijksuniversiteit Groningen, The Netherlands

The work described in this thesis was carried out in the Elektron Microscopy group of the Groningen Biomolecular Science and Biotechnology Institute (GBB) of the University of Groningen (The Netherlands), and was financially supported and subsidized by the Nederlands Proteomic Center (NPC)

ISBN: 978-90-367-3743-2 printed version
ISBN: 978-90-367-3744-9 electronic version

RIJKSUNIVERSITEIT GRONINGEN

Structural investigation of membrane proteins by Electron Microscopy

Proefschrift

ter verkrijging van het doctoraat in de
Wiskunde en Natuurwetenschappen
aan de Rijksuniversiteit Groningen
op gezag van de
Rector Magnificus, dr. F. Zwarts,
in het openbaar te verdedigen op
vrijdag 17 april 2009
om 13.15 uur

door

Katarzyna Beata Mościcka
geboren op 13 december 1978
te Lublin, Polen

Promotor: Prof. dr. E. J. Boekema

Beoordelingscommissie: Prof. dr. B.W. Dijkstra
Prof. dr. A.J.M. Driessen
Prof. dr. I. J. van der Klei

ISBN: 978-90-367-3743-2
ISBN: 978-90-367-3744-9

„If we knew what it was we were doing, it would not be called research, would it?”

Albert Einstein

Contents

Chapter 1

Part 1. Introduction to proteins: physiology, structure and mechanism.

1. Proteins and protein structures

The word “protein” is derived from the Greek word prôtos, meaning “primary” or “first rank of importance.” Proteins form the very basis of life. They regulate a variety of activities in all known organisms on all levels, from replication of the genetic code to transporting oxygen, and are generally responsible for regulating the cellular machinery and consequently, the phenotype of an organism. Proteins accomplish their task by an incredible fine-tuning of interactions between various substrates such as DNA and RNA, metabolites and other proteins. Knowing the structure of the protein, we can probe for its function and potentially apply the new knowledge to various genome projects, such as mapping the functions of proteins in metabolic pathways for whole genomes and deducing evolutionary relationships.

Protein structural organization

Proteins have several different levels of organization. They become highly organized and efficient biological machines through many types of ionic and molecular interactions within the protein itself. The first level of protein structure is its primary structure. The primary structure of a protein is the linear sequence of its constituent amino acids. The next level of organization is the secondary structure of the protein.

Secondary structure is a regular structure brought about via hydrogen bonding mainly within the peptide backbone. The most common secondary structure elements in proteins are the alpha helix and the beta sheet. In membrane proteins, long membrane-spanning alpha

helices and beta sheets are the essential components in making the next level of folding, the tertiary structure. Covalent interactions between cysteine groups, noncovalent electrostatic interactions between polar groups, and Van der Waals interactions between non-polar R groups are very common in tertiary structures. A major driving force in determining the tertiary structure of globular proteins is the hydrophobic effect. The polypeptide chain generally folds such that the side chains of the non-polar amino acids are "buried" within the structure and the side chains of the polar residues are exposed on the outer surface.

Quaternary Structure is the combination of two or more chains or subunits, to form a complete unit. The interactions between the chains are not different from those in tertiary structure, but are distinguished only by being interchain rather than intrachain. Many membrane proteins are multisubunit complexes, and all proteins discussed in this theses are examples. In some cases protein subunits can form flexible, multimeric rings of over 10 copies, and these are the perfect examples where EM can make a major contribution in solving structures, as will be presented in this thesis.

1.2 Membrane proteins

Membrane proteins play many crucial roles in the cell and take center stage in processes ranging from basic small-molecule transport to sophisticated signaling pathways. They are also prime contemporary or future drug targets, and it has been estimated that more than half of all drugs currently on the market are directed against membrane proteins (Klabunde et al. 2002). It is still frustratingly hard to obtain high-resolution three-dimensional (3D) structures of membrane proteins, and they represent less than 1% of the structures in the Protein Data Bank (Berman et al. 2000). Even if the number of experimentally known membrane protein structures is on the rise (White 2004; Oberai et al. 2006), methods to predict their topology (i.e., the transmembrane segments and their in-out orientation across the membrane) and fold type from the amino acid sequence will be needed for many years to come.

As mentioned before, α-helices and β-barrels are important in integral membrane proteins and many of them have two basic architectures: an α-helix bundle or a β-barrel sheet. Helix-bundle proteins are found in all cellular membranes, except possibly the bacterial outer membrane, and represent an estimated 20% to 25% of all open reading frames (ORFs) in fully

sequenced genomes (Keseler et al. 2005). The number of β-barrel membrane proteins is more uncertain because they are more difficult to identify by sequence gazing; for bacteria, a rough estimate, based on the fact that all known β-barrel proteins are in the outer membrane and hence are made with an N-terminal signal peptide, suggests that they account for no more than a few percent of all ORFs. The EcoCyc database currently lists 58 outer membrane and 511 inner membrane proteins out of a total of 4332 proteins; the number of inner membrane proteins in *Escherichia coli* has been estimated to be close to 1000 (Krogh et al. 2001). Because all current membrane protein topology and structure prediction schemes first seek to identify the transmembrane segments, they are obviously quite different, and their variations depend on the class of protein for which they are designed. In general long hydrophobic transmembrane helices are easier to recognize in an amino acid sequence than the much shorter and less hydrophobic transmembrane β-strands, and partly for this reason, much more bioinformatics work has been devoted to the helix bundle proteins—another instance of the well-known dictum "always go for the easy problems."

1.3 Structure

Membrane protein structure determination is proceeding and exciting, driven by the hope that structures can connect decades of biochemical and biophysical observations to protein function and mechanism. As science as a whole unravels increasingly complex and finely tuned functionality, can structure determination continue to keep pace, or will new methodologies and perspectives be required? Evolution has exploited three categories of molecular-level organization in order to achieve efficient and diverse membrane protein functions: structure, molecular dynamics, and environmental constraints. As suggested schematically in Figure 2, they are inextricably linked, each influencing the other, collectively dictating membrane protein function. By recasting the structure-function relationship in this way, we suggest that a comprehensive view of membrane protein function may be more readily achieved (Sachs et al. 2006).

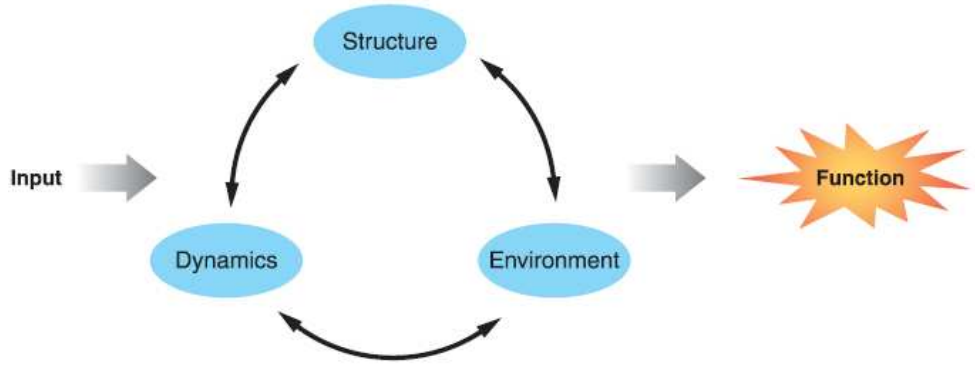

Figure 1. *Schematic representation showing three categories of molecular-level organization needed to achieve efficient and diverse membrane protein functions.*

Any model for predicting function should start with a structure. Static structures can elegantly illuminate the structure-function relationship. Nowadays, articles presenting atomic structures include astonishing details including protein oligomerization and complexation, lipidation, glycosylation, and the presence of structural water and lipid molecules, suggesting that future models may need to account for a high level of complexity and structural variability. Oligomerization is increasingly seen as a common motif in membrane proteins (Engelman et al. 2005). As the authors point out, distinguishing between dimers and higher order oligomers is far from trivial. Although this difficulty may be primarily due to experimental limitations such as dissociation by detergent, it may also reflect true biological variability. In most studied cases, oligomerization serves a functional role, and this function most likely drove its evolution.

1.4 Protein-protein interactions

The final step on the structure prediction ladder is the prediction of quaternary structure, i.e., protein-protein interactions. This is especially pertinent for membrane proteins because membrane-integral protein domains in most cases seem to be encoded by separate polypeptides rather than as multidomain polypeptides as often found in globular proteins (Liu et al. 2004). Large-scale experimental protein-protein interaction studies tend to ignoremembrane proteins, although some data are now starting to appear in the literature (Gavin et al. 2002; Stenberg et al. 2005; Lasserre et al. 2006).

The current state of predicting interactions between membrane proteins may be summarized in a few words: much remains to be done. For example, a recent attempt to predict interacting proteins in the *Saccharomyces cerevisiae* membrane proteome by integrating data, such as amino acid sequence, annotated function, subcellular localization, mRNA and protein abundance, transcriptional co-regulation, and gene knock-out phenotype, resulted in a predictor that could only identify 40% of 304 experimentally well-documented gold standard interactions while minimizing the number of false-positive predictions (Xia et al. 2006).

Part 2. Structure investigation of matrix and membranes proteins from different organism by Electron Microscopy

2 The peroxisome

2.1 The peroxisome: structure, function, and peroxisomal biogenesis

The peroxisome is a single-membrane organelle ubiquitous in nearly all eukaryotic cells. It is the most recently discovered subcellular organelle (De Duve and Baudhuin 1966). Peroxisomes, together with glyoxysomes of plants and glycosomes of trypanosomes, belong to the microbody family, which has gained a great functional diversity, from yeast to humans. Unlike chloroplasts and mitochondria, these organelles do not contain endogenous DNA, and hence all their proteins are nuclear encoded, synthesized in the cytosol, and post-translationally imported into the peroxisome (Lazarow and Fujiki 1985). Peroxisomes are very dynamic and display large plasticity in response to changes in environmental conditions. Under normal growth condition, the mature peroxisome presents a globular shape with a diameter of 0.1-1 μm (Fig. 2; van den Bosch et al. 1992).

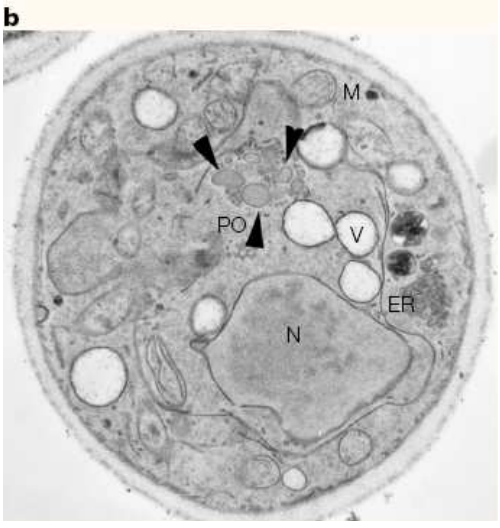

Figure 2*. An electron micrograph of a Saccharomyces cerevisiae cell during restoration of peroxisome biogenesis shows a cluster of peroxisomes (PO) and their distribution relative to the lipid droplets (V), endoplasmic reticulum (ER),mitochondria (M) and nucleus (N).*

The peroxisomal protein content is variable among species, and therefore, the metabolic functions can be adjusted according to cellular needs. Peroxisomes in fungi and plants play a central role in the β-oxidation of fatty acids and the detoxification of the hydrogen peroxide thereby produced (Poirier et al. 2006). The importance of the peroxisome is underscored by the existence of numerous human genetic disorders. Peroxisomal disorders are defined as a group of human inherited diseases in which either the peroxisome biogenesis or one or more peroxisomal functions are impaired.

The discovery that peroxisome proliferation can be induced in bakers' yeast *S. cerevisiae* by oleic acid was the start of a periode of extensive research on the biogenesis of the organelle in yeast (Veenhuis et al. 1987). When cells were grown on oleic acid as the sole carbon source, peroxisomes become essential for growth because they represent the exclusive site of fatty acid degradation in yeast. This important discovery allowed the screening of *pex* mutants affected in the biogenesis of peroxisomes (Erdmann et al. 1989; Erdmann et al. 1991) with *PEX* being the acronym for the corresponding gene, the gene products were named peroxins (Distel et al. 1996). Peroxins are involved in ways in the peroxisomal development: 1) formation of the peroxisomal membrane, 2) peroxisome proliferation and 3) compartmentalization of peroxisomal matrix proteins.

Important studies also involved the emerge of peroxisomal membrane, which has been a point of discussion for a long time. First data suggested that peroxisomes generate by budding from the endoplasmic reticulum (ER) (Novikoff and Shin 1964), which were based on ultrastructural studies using electron microscopy. Later, Lazarow and Fujiki (1985) demonstrated that peroxisomal matrix proteins are synthesized on free ribosomes in the cytosol and these proteins are imported posttranslationally in pre-existing peroxisomes. Based on these results, a ''growth and division model'' was proposed (ER-independent model), which predicted that peroxisomes multiply autonomously like mitochondria or chloroplasts. More recent studies, based mainly on real-time fluorescence microscopy combined with biochemical data, provided evidence for the ER being the source of origin of peroxisomal membranes, at least during de novo formation (Van der Zand et al. 2006; Hoepfner et al. 2005). This process requires the membrane protein Pex3p, which is localized at first in the ER. It concentrates in foci that bud off in a Pex19p-dependent manner which mature to functional peroxisomes. Based on data from plant and mammalian cells, peroxisomes are believed to constitute a semi-autonomous part of the secretory pathway (Hoepfner et al.

2005). However, in yeast new peroxisomes are believed to arise primarily by duplication of the pre-existing peroxisomes (Mottley and Hettema, 2007; Nagotu et al. 2007). In conclusion, we can say that peroxisomes contain an elaborate fission and proliferation machinery. Pex11p was among the first components of this device which were discovered, and together with Pex25p and Pex27p play a role in controlling size and number of *S. cerevisiae* peroxisomes. The scission of peroxisomal membranes has recently been connected to the function of the dynamin-related proteins (DLPs) Vps1p and Dnm1p, as well as the Dnm1p-anchoring protein Fis1p, all of which are also involved in fission processes of mitochondria (Van der Zand et al. 2006). The peroxisomes are still clustered after the fission event. These clusters are thought to be dissociated by the membrane proteins Pex28p and Pex29p of *S. cerevisiae.* Pex30p, Pex31p and Pex32p in *S. cerevisiae* further regulate the size of peroxisomes. These peroxins act downstream of Pex28p and Pex29p, but not much is known about their molecular function.

Last but not at least Inp1p regulates the movement of peroxisomes during cell division and thus peroxisomal inheritance in yeast. It is supposed to link peroxisomes to a cortical anchor to retain them in the mother cell and bud. Inp2p is a peroxisomal receptor for Myo2p which moves peroxisomes along polarized actin filaments into the bud of the dividing cell (Fagarasanu et al. 2006).

2.2 Peroxisomal protein targeting and sorting

Cargo recognition and peroxisomal targeting

The peroxisomal matrix enzymes are translated by polyribosomes and translocated into the peroxisomal matrix by specific targeting signals. Most of the peroxisomal matrix proteins are equipped with a C-terminal targeting motif, which has been classified as the targeting signal 1 (PTS1). The PTS1 motif consists of just three amino acids—SKL—or a conservative variant (Subramani et al. 2000; Gould and Collins 2002). Only some peroxisomal enzymes use a different targeting signal, the amino-terminally located PTS2. Import of PTS1 and PTS2 proteins requires around 20 *PEX* genes and their products; the peroxins (Table 1).

Table 1. Features of known peroxins	
Protein	Characteristics
Peroxins involved in the biogenesis of the peroxisomal membrane and in matrix protein import	
Pex1p	A large (100-150 kDa) AAA ATPase in yeast and humans. Interacts with Pex6p and other peroxins. Defects in Pex1p are by far the most common cause of PBDs (peroxisome biogenesis disorders).
Pex2p	An ~40-kDa integral PMP (peroxisomal membrane protein) with a carboxy-terminal, cytosolically exposed zinc RING domain. Has been identified in yeasts and humans, interacts with Pex10p and is defective in casual genes for CG (complementation group) 10 of the PBDs.
Pex3p	A ~40-kDa protein which traffics through the ER; membrane receptor for PMP in yeast and humans that binds Pex19p and is defective in CG12 of the PBDs.
Pex4p	A small (20–24 kDa) peroxisome-associated ubiquitin-conjugating enzyme that interacts with Pex22p. Has been identified in several yeast species, but so far there is no report of Pex4p in any metazoan.
Pex5p	An ~70-kDa, predominantly cytosolic/partly peroxisomal protein that is found from yeasts to humans. Contains a PTS1-binding domain in its carboxy-terminal, tetratricopeptide-repeat-containing half, interacts with several peroxins (Pex8p, Pex10p, Pex12p, Pex13p and Pex14p) and is defective in CG2 of the PBDs.
Pex6p	An ~100-kDa AAA ATPase found in all eukaryotes. Interacts with Pex1p and is defective in CG4 of the PBDs.
Pex7p	An ~40-kDa, WD40-repeat-containing protein that binds the PTS2. Defective in CG11 of the PBDs. Pex7p is conserved from yeast to humans but is absent in the nematode *Caenorhabditis elegans*.
Pex8p	A variably sized (60–80 kDa). Pex8p is the sole peroxin that resides in the peroxisome matrix; it interacts with Pex5p. It is found in yeast and other fungi, but has not been identified in higher eukaryotes.
Pex10p	An ~35-kDa integral PMP; RING finger protein; E3 ligase for Ubc4p dependent ubiquitination of Pex5p. Has been identified in yeasts, plants, fungi and humans, interacts with Pex2p, Pex5p and Pex12p, and is defective in CG7 of the PBDs.
Pex12p	An ~40-kDa integral PMP, RING finger protein. It has been identified in yeasts and humans, interacts with Pex5p and Pex10p, and is defective in CG3 of the PBDs.
Pex13p	An ~44-kDa integral PMP with a carboxy-terminal, cytosol exposed SH3 domain. Has been identified in yeasts and humans, interacts with Pex5p and Pex14p, and is defective in CG13 of the PBDs.
Pex14p	An ~40-kDa PMP, receptor docking complex component. Present in yeasts and humans; binds to Pex5p, Pex13p and Pex17p.
Pex15p	A 44-kDa integral PMP.
Pex16p	In humans, Pex16p is a 36-kDa PMP that traffics through the ER; membrane receptor for PMP recruitment in mammalian cells.
Pex17p	An ~25-kDa integral PMP that interacts with Pex14p. Pex17p is the third component of the proposed receptor docking complex. It has been identified in yeast and other fungi, but so far has not been detected in higher eukaryotes, including humans.
Pex18p	A 31-kDa soluble protein involved only in PTS2-protein import. It is highly similar to Pex21p, and might act as a Pex7p chaperone. Identified only in *S. cerevisiae*.
Pex19p	A 33-kDa farnesylated protein of yeasts and humans. Predominantly cytosolic/partly peroxisomal, binds all known integral PMPs and recognizes many PMP-targeting signals. Is defective in CG14 of the PBDs.
Pex20p	A 46-kDa soluble protein involved only in PTS2-protein import. Co-receptor required for Pex7p binding cargo; *S. cerevisiae* has functional homologs Pex21p/Pex18p instead.

Pex21p	A 31-kDa soluble protein involved only in PTS2-protein import, is highly similar to PEX18, and might act as a Pex7p chaperone. Identified only in *S. cerevisiae*. .
Pex22p	A 20-kDa integral PMP of yeasts that interacts with Pex4p.
Pex26p	Integral peroxisomal membrane proteins that bind Pex6p. Indentified in various filamentous fungi and mammals.
Peroxins involved in peroxisome proliferation	
Pex11p	An ~25-kDa integral PMP required for normal peroxisome abundance. Many species contain several *PEX* genes. Pex11 protein(s) are present in all eukaryotes.
Pex23p	A 46-kDa integral PMP. Identified only in in all fungi. *S. cerevisiae* Pex23p, Pex31p and Pex32p are exclusively required for peroxisome proliferation. Human cells do not appear to have Pex23p orthologs.
Pex24p	PMP known in *Y. lipolytica*. Pex24p peroxin is conserved in all yeast species. Remarkably, the genomes of filamentous fungi (and the fission yeast *S. pombe*) encode only a single protein with similarity to Pex24p.
Pex25p	Peripheral PMP; interacts with paralog Pex27p, recruits Rho1p to peroxisomes.
Pex27p	Interacts with paralog Pex25p.
Pex29p	PMP, Pex29p is conserved in all yeast species. Remarkably, the genomes of filamentous fungi (and the fission yeast *S. pombe*) encode only a single protein with similarity to Pex29p.
Pex31p	PMP; contains dysferlin domain. Human cells do not appear to have Pex31p orthologs.
Pex32p	Only present in yeast (including *S. pombe*) but not in filamentous fungi. PMP; contains dysferlin domain Human cells do not appear to have Pex32p orthologs.
Other proteins involve in peroxisome biogenesis	
DRPs	Dynamin-related proteins include Vps1p and Dnm1p in yeast and Dlp1p in mammalian cells
Fis1p/Mdv1p/Caf4p	DRP recruitment to peroxisomes
Rho1p	Guanosine triphosphatase involved in actin assembly on peroxisomes; interacts with Pex25p and Pex30p.
Myo2p	Motor that propels peroxisomes along actin cables
Inp1	PMP involved in retention of peroxisomes in mother and daughter cells by attaching peroxisomes to the cell cortex
Inp2	PMP involved in peroxisome movement through interaction with Myo2

PTS1 proteins are recognized by Pex5p, whereas PTS2 proteins are recognized by Pex7p. In mammals, the long isoform of Pex5p (Pex5L) is also required for PTS2-protein import, as it binds to Pex7p and is required for Pex7p transit to peroxisomes. These observations indicate that Pex5p is the direct or indirect import receptor for all newly synthesized and folded peroxisomal matrix enzymes (nsPMEs) in these species. The matrix proteins with PTSs are recognized in the cytosol. Pex5p is a predominantly cytosolic, partly peroxisomal protein that cycles between the cytosol and peroxisomes, which indicates that peroxisomal-protein import involves a complex interplay of cytosolic and peroxisomal events. PTS2, the second peroxisomal targeting signal is located near the amino-terminus and consists of the consensus sequence RLXXXXX(H/Q)L (Lazarow 2006). In yeasts, only a small number of matrix proteins contain a PTS2. Many more PTS2 proteins contains plants

(Reumann et al. 2004). Like Pex5p, Pex7p shuttles between the cytosol and peroxisome during cargo translocation. Pex5p is known to be an globular protein, probably oligomer. Fluorescent measurement revealed that the pH affects the oligomeric state of Pex5p. Upon shifting the pH from 6.0 to pH 7.2 the Pex5p from monomers forms larger oligomeric forms (Boteva et al. 2003).

Receptor –cargo docking to the peroxisomal membrane

After the protein-receptor interaction, the protein complex will interact with docking partners at the peroxisomal membrane (Purdue et al. 2001). At least 12 of the known membrane associated peroxins are directly involved in the import process for peroxisomal matrix proteins. In *S. cerevisiae* the docking complex is comprised of Pex13p and Pex14p, and also Pex17p. Pex17p is a peroxisomal membrane protein (PMP) which associates with Pex14p in a tight core complex. It has been reported that Pex17p possibly interacts through coiled-coil motifs found in several families of proteins (Elgersma et al. 1996). The fact that Pex17p interacts with Pex14p (Huhse et al. 1998; Snyder et al. 1999), led to the conclusion that these three peroxins might form a receptor-docking complex. Pex13p is an integral PMP whose amino- and carboxyl-termini both extend into the cytosol. In *S. cerevisiae* the amino-terminal domain binds the PTS2 receptor Pex7p. The carboxy-terminal region contains a Src-homology-3 (SH3) domain which directly binds the PTS1 receptor Pex5p as well as Pex14p (Pires et al. 2003). Pex14p is a peroxisomal membrane protein involved in the docking of Pex5p. In addition, Pex5p loaded with cargo exhibits a higher binding affinity to Pex14p than to Pex13p (Urquhart et al. 2000). Pex14p is therefore believed to be the docking-site for Pex5p.

Translation, receptor recycling and cargo release

Until now, there was much discussion in the field of peroxisomes about the function of the receptor-cargo complex. It can either enter the peroxisome lumen, as proposed in the "extended shuttle hypothesis" (Fig. 3), or remaining embedded in the peroxisome membrane. In the latter case the cargo can be released into the peroxisome matrix with the receptor remaining protease protected, according to the "simple shuttle hypothesis" (Kunau 2001; Smith and Schnell 2001).

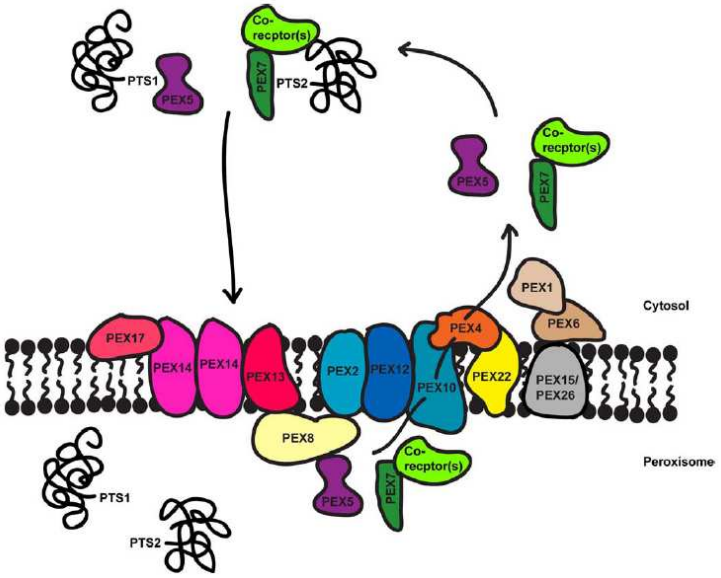

Figure 3*. Overview of peroxisomal matrix protein import. Matrix proteins have either a PTS1 or PTS2 targeting signal that binds to acytosolic receptor, Pex5p and Pex7p respectively (with or without co-receptors) which targets the protein to the docking complex (Pex13p, Pex14p and also Pex17p in yeast). The receptors translocate with their cargo into the peroxisome lumen, release their cargo and are recycled back into the cytosol. The RING-finger complex (Pex2p, Pex1p0 and Pex12p) associates with the docking complex via Pex8p (in yeast) and is required for receptor recycling. Pex10p is linked to the E2 ubiquitin conjugating enzyme, Pex4p, which is anchored to the membrane by Pex22p. Pex5p release from the membrane requires Pex4p-dependent monoubiquitination, which is ATPdependent. The RING-finger peroxins are the putative E3 ligases for this process. The AAA-proteins Pex1p and Pex6p are also involved in receptor release and are attached to the peroxisomal membrane via Pex15p in yeast and Pex26p in mammals. Little is known about the recycling of Pex7p, although two of its co-receptors, Pex18p and Pex20p, have been shown to be ubiquitinated (Brown and Baker 2008).*

However, a fraction of Pex5p is found in the lumen of peroxisomes which gave rise to the “extended shuttle hypothesis” of peroxisomal protein import (Van der Klei and Veenhuis 1996). This model suggests that the PTS receptors do not release the cargo proteins after the docking step but instead enter the peroxisomal matrix together with the cargo proteins. The receptors release their cargo in the peroxisomal lumen and are subsequently recycled to the cytosol. The same hypothesis was found in the mammals (Gouveia et al. 2003; Dammai and

Subramani 2001). Also, in *S. cerevisiae* Pex5p was found to interact with Pex8p, the only known peroxin bound to the trans side of the membrane. This indicates that Pex5p can traverse the membrane or at least be inserted into it to such an extent that it is exposed to the *trans* side.

Receptor-release to the cytosol

In addition to the docking complex, multiple Pex proteins participating in the import cycle have been identified. In addition to a role in the docking complex, multiple Pex proteins participating in the import cycle have been identified. The receptor recycling complex involves: (1) the RING finger proteins Pex2p, Pex10p, and Pex12p transiently anchored to the docking complex by Pex8p (in the yeast - Agne et al. 2003), (2) the ubiquitin-conjugating enzyme Pex4p anchored by Pex22p, and (3) a complex of AAA ATPases: Pex1p and Pex6p, anchored to the membrane by Pex15p (in *S. cerevisiae* or Pex26p in mammals). Ubiquitination of the import receptor (Pex5p) is emerging as an important aspect of import. The ubiquitination of Pex5p or Pex18p has been considered a signal for their export back to the cytosol (Platta et al. 2004; Kiel et al. 2005; Kragt et al. 2005). Monoubiquitination of Pex5p by Pex4p is required for release of Pex5p from peroxisomal membranes (Platta et al. 2007), whereas polyubiquitation of Pex5p by Ubc4p (Kiel et al. 2005 ; Kragt et al. 2005) and the E3 ligase activity of Pex10p is required for a mechanism to target receptors for degradation when receptor recycling is impaired. However, the detailed machinery for this process has not been elucidated yet. Remarkably, proteins locked in a folded conformation by chemical crosslinking or stabilizing drugs can also be imported into peroxisomes. Moreover, proteins lacking a PTS can be imported into peroxisomes in association with a protein containining a PTS. These facts suggest that proteins may be imported into peroxisomes in a folded or multimeric state, which is different from the mitochondrial and chloroplast protein import process.

Structure determination of peroxisome matrix and membrane complexes is still ongoing research. Several results describing Pex5p and the docking-complex containing Pex14p, Pex17p and Pex13p have been published (Boteva et al. 2003; Agne et al. 2003). Despite the accumulating biochemical knowledge structural studies on Pex protein complexes are lacking almost completely, although some individual proteins, such as Pex5p, have been

studied by X-ray diffraction (Gatto et al. 2000). This lack of knowledge stimulated the study of protein complexes by EM and single particle analysis, as we will report in this Thesis. Chapter 2 of this Thesis presents structural data of a complex between Pex5p and Pex20p, involved in peroxisomal matrix protein import from *Hansenula polymorpha* using single particle image analysis. Chapter 3 describes the different biochemical isolation methods together with BN-PAGE (Blue Native Page electrophoresis) and mass spectrometry to obtain one of the most important peroxisomal import machinery multimeric complex: the docking complex containing Pex14p, Pex17p, and a minor fraction of Pex13p.

3. Secondary transporters

3.1 Introduction

All together, archaeal, eukaryotic and bacterial organelles have a large number of integral membrane proteins and protein complexes involved in transport across the membrane (Konings et al. 1996). Most of the transport proteins have recently been classified in different families based on their sequence similarities. This led to the identification of 250 transporter families, of which secondary transporters represent the largest functional category, comprising 85 families (Boush and Saier 2004).

Secondary transporters drive the transport across the membrane by using free energy stored in ion and/or solute gradients. In general, they are classified in three groups based on the mode of energy coupling: 1- uniporters catalyse the translocation of a single solute across the membrane, 2- symporters couple transport of two or more solutes in the same direction, and 3- antiporters couple the movement of solutes in opposite directions. Many of the secondary transporters exchange a substrate at one side of the membrane for another substrate at the other side of the membrane. This exchange mode differs from the antiport mode in that the translocation of the two substrates in the two directions is not obligatorily coupled. Often, exchange is a partial reaction catalyzed by symporters.

3.2 Structure

Secondary transporters are found in the membranes of all biological cells. They come in a great sequence diversity and to date the Transporter Classification system (TC) developed

by Saier and co-workers lists some 85 families in the Porters (uniporters, symporters and antiporters) category (Saier 2000). The 85 families of secondary transporters do not represent as many different global structures. It has been shown by hydropathy profile analysis that many of the families belong to the same structural class (Lolkema et al. 1998) which probably means that they are evolutionary related. The hydropathy profiles report a specific folding pattern of proteins in membranes and are therefore capable of detecting distant evolutionary relationships between protein families.

The folding of secondary transporters is as a bundle of hydrophobic α-helices that are more or less oriented perpendicular to the membrane plane axis. At the two sides of the membrane the transmembrane segments are connected by hydrophilic loops of variable lengths. So far we know only four high-resolution structures of secondary transporters. These structures have provided a first glimpse on the structural and mechanistic diversity that may be expected to be present in the many different families of secondary transporters. One of them is the glutamate transporter homologue Glt_{Ph} from the archaeon *Pyrococcus horikoshii* (Yernool et al. 2004). It has been crystallized and the three-dimensional structure was solved at a resolution of about 2.7 Å (Boudker et al. 2007). The glutamate transporter family is one of the families that forms a separate structural class, also called dicarboxylate/cation symporters. GltT is a secondary transporter which translocates two cations, a proton and a sodium ion, and, therefore, is driven by the proton and sodium ion motive forces (Von Heyne et al. 1991). The DAACS family forms a structural class by itself (ST[4], named Secondary Transporters [4]).

The other two secondary transporters, CitS of *Klebsiella pneumoniae* and GltS of *Escherichia coli*, are both found in the structural class ST[3]. CitS belongs to the 2-hydroxycarboxylate transporter (2HCT) family and it is found in bacteria. CitS of *Klebsiella pneumoniae* is well-studied member of the family which is termed Na^+-citrate symporter.
GltS instead, from *Escherichia coli* is a secondary transporter that transports glutamate in symport with Na^+ ions and belongs to the Glutamate: Na^+ (ESS) symporter family (Heyne et al. 1991). 2HCT and ESS family members show highly similar hydropathy profiles which is the base of their classification in one and the same class. Studies of CitS proteins of *Klebsiella pneumoniae* give insight into the structure of class ST[3]. The structural model of the transporters shows a core of two homologous domains consisting of five trans membrane

segments (TMS) each that are connected by a large cytoplasmic loop region. The hydrophaty profile of the protein suggested the presence of 12 putative transmembrane domains (TMSs) that traverse the membrane in a zigzag fashion. However, a direct alignment of the hydropathy profile of the GltS protein family and the profile of the 2-hydroxycarboxylate transporter (2HCT) family revealed a high similarity suggesting a similar folding in the membrane. The CitS protein of *Klebsiella pneumoniae* of the 2HCT family consists of 11 transmembrane segments and comparison of both family profiles suggested that GltS would consists of 10 transmembrane segments with both termini exposed to the periplasm. Accessibility of cysteine residues introduced at the N- and C- termini of GltS and the three C-terminal loops of GltS were in agreement with the model based on the hydropathy profile alignment with 10 transmembrane segments (Sobczak end Lolkema 2003).

3.3 Quaternary structure

The structure determination of these proteins is still limited. Some evidence indicates that CitS of *K. pneumoniae* in the 2HCT family and GltS of *E. coli* in the ESS family exist as multimers, probably as a homodimers. The enzymes, solubilized in the detergent Triton X-100, were shown to run as a dimer on blue native PAGE (Kästner et al. 2003; Veenhoff et al. 2002). Moreover, an observation made during the purification of biotin acceptor domain (BAD)-tagged CitS, already strongly suggested the dimeric structure of the protein (Pos et al. 1998).

Electron microscopy (EM) is a proven method to study the structure of (membrane) proteins. EM data indicate that the two transporters from the ESS and 2HCT families, share a similar subunit structure – quaternary structure. There is evidence for differences in size and shape of CitS and GltS (~ 100 kDa) and in size and shape of CitS transporters to which the Biotin Acceptor Domain *(*BAD) of the oxaloacetate decarboxylase of *Klebsiella pneumoniae* with a mass of 10 kDa was attached.
Chapter 4 of this thesis presents a structural study of the quaternary structure of the secondary transporters GltT, CitS and GltS in which two-dimensional projections maps of several GltT, CitS and GltS particles were analyzed.

4. Secretin of Type IV Pilus system in pathogenic *Neisseria*

4.1 Introduction

Neisseria gonorrhoeae and *Neisseria meningitidis* are two pathogenic members of the genus *Neisseria* that cause infections which are associated with significant mortality of their exclusive human hosts. These pathogenic bacteria interact with blood, plasma and exudate fluid. They also adhere to and invade epithelial and endothelial cells (McGee et al. 1983; Van Putten et al. 1998). Several bacterial components are involved in the modulation of pathogen–host cell interactions, including type IV pili, Opa proteins and porins. The expression of pili, emanating from the bacterial surface, appears to be of paramount importance to the pathogenic process. Neisserial pili are ordered arrays of polymerized protein subunits termed pilin.

Neisseria gonorrhoeae pilus variation results from homologous recombination between a single complete pilin gene or expression locus and multiple partial pilin gene copies or silent alleles (Haas and Meyer 1986; Swanson et al. 1986; Koomey and Falkow 1987) and an analogous mechanism is thought to operate in *Neisseria meningitidis* pilus variation (Aho et al. 1987; Perry et al. 1988; Blake et al. 1989). Neisserial pilins show a high degree of homology with pilins of other pathogenic Gram-negative bacteria, including *Pseudomonas aeruginosa* (Strom and Lory 1986), *Vibrio cholerae* (Faast et al. 1989), enterotoxigenic *Escherichia coli* (Giron et al. 1994) and enteropathogenic as well as opportunistic pathogens within the genera *Eikenella* (Tønjum et al. 1993) and *Moraxella* (Frøholm and Sletten 1977). Collectively, this family of surface appendages has been termed type-IV pili (Ottow 1975). As in both *Neisseria* species, these related pilus colonization factors appear to be essential for infectivity and disease.

4.2 Type IV pili

Type IV pili are very important in the early stages of infection of human hosts. Type IV pili form filaments of a regularly ordered protein with a length of 1,000-4,000 nm and a diameter of 5 to 6 nm, which protrude from the cell surface of many bacteria of medical, environmental and industrial importance. They are also responsible for attachment to specific

epithelial tissue receptors during tissue colonization and mediate a variety of functions, including adhesion, twitching motility, and competence for DNA uptake (Heckels 1989; Virji et al. 1992). The type IV pilus is a helical polymer of pilin protein subunits and is capable of rapid polymerization or depolymerization, generating large motor forces in the process.

Currently, there is a lot of research ongoing concerning the biochemistry, genetics and functions of type IV pili. Collins and co-workers (2005) showed specific interaction between the outer membrane secretin PilQ and the type IV pilus fiber by using transmission electron microscopy. The authors showed that purified type IV pili, to which the purified PilQ oligomer had been added, caused PilQ to be located at one end of the pilus fiber. Determination of the three-dimensional structure of the PilQ-type IV pilus complex at 26 Å resolution showed that the cavity within the protein complex was filled. Craig and co-workers (2006) revealed a detailed *Neisseria gonorrrhoea* Type IV pili structure by quantitative fitting of a 2.3 Å full-length pilin crystal structure into a 12.5 Å resolution 3D reconstruction map solved by cryo-electron microscopy.

Besides that, very little is known about *Neisserial* pilus biogenesis, and the genes encoding the component proteins are scattered throughout the *N. meningitidis* and *N. gonorrhoeae* genomes (Tønjum and Koomey 1997). The only pilus biogenesis proteins that are associated with the outer membrane and that have been characterized to date are PilC, PilP, and PilQ. They are called secretins of Type IV pili.

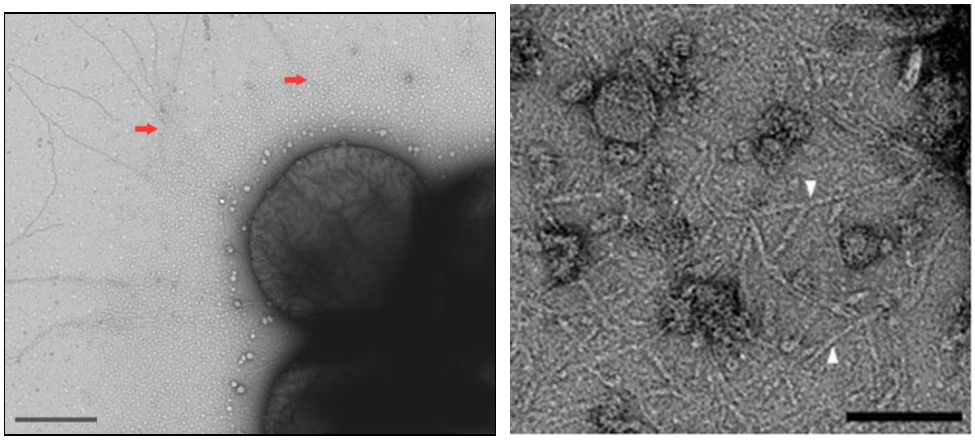

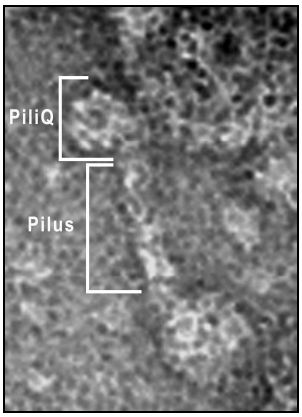

C

Figure 4*. Electron micrographs of negatively stained WT type IV pili cells and the PilQ-type IV pilus complex interaction.*

(A) A typical Neisseria bacterium with a diameter of about 2 μm with attached pili. The long pili are pointed by black arrows. Scale bar equals 0,5 μm.

(B) Tfp fibers visualized by TEM in uranyl acetate. Several fibers can be seen (pointed by white arrows). Scale bar represents 100 nm.

(C)PilQ-type IV pilus complexes with a distinctive hammer-like side-on view.

4.3 PiliQ secretin from *Neisseria species*

Identification and individual characterization of pilus biogenesis together with their coordinated functions and interactions in pilus assembly are still poorly understood. One of the integral elements in these processes is the PilQ multimer. PilQ of pathogenic *Neisseria strains* is an abundant outer membrane protein which forms a large multimer composed of 10 to 12 subunits (Drake et al. 1997; Drake and Koomey 1995). The PilQ complex is involved in the surface expression of Tfp, and meningococcal mutants missing or expressing defective PilQ are devoid of pili and pilus-associated phenotypes. A total of 200 to 300 conserved C-terminal residues in the transmembrane region of the PilQ monomer exhibit high sequence

homology to other secretins and are essential for oligomerization into a functional complex (Guilvout et al. 1999; Nouwen et al. 2000).

Collins and co-workers in 2001 showed that PilQ in *Neisseria meningitidis* forms a large 960-kDa homododecameric complex, which was analyzed by transmission electron microscopy by using negatively stained specimens. The projection map generated from 296 particles had an estimated resolution of 2.6 nm. They indicate that oligomeric PilQ adopts a donut-like structure with an external ring that is 16.5 nm in diameter surrounding a central cavity that is 6.5 nm in diameter. Self-rotation and power spectrum analysis demonstrated the presence of 12-fold rotational symmetry, showing that PilQ is organized as a ring of 12 identical subunits. This symmetry determination is questionable, because the data hardly permit to see consistent features at the subunit level. A few years later, the same authors presented a 3D structure of the PilQ complex visualized by cryo-negative EM staining. The structure shows a large central cavity, which was closed at the poles by 'plug' and 'cap' features, and four 'arm' features at the sides. The results suggested that the PilQ complex is the channel through which the moving pilus fibre (polymerized PilE) is extruded and retracted from the bacterial surface (Collins et al. 2004 and 2005). The dodecameric complex of the PilQ subunits forms an extremely stable structures that is resistant to heat and SDS treatment.

So far, the structure of the outer membrane PiliQ secretin complex of *Neisseria meningitidis* is well studied. Despite that, the structure of the PiliQ secretins of Type IV pili systems from related species, such as *Neisseria gonorrrhoea***,** remains unsolved. Therefore, in the last chapter of this Thesis, chapter 5, we have analyzed the PiliQ complex from *Neisseria gonorrrhoea* by using EM and single particle image analysis. Structural differences of the PiliQ secretin system of type IV pili from two pathogenic *Neisseria* strains are also compared and analysed by EM.

5. Application of Electron Microscopy to the Structural Analysis of Proteins

Electron microscopy (EM) is nowadays a wide-spread technique to study protein structure. Over the last two decades the technique of single particle EM has been successfully applied to many types of water-soluble and membrane-bound proteins. This Thesis describes

EM studies performed on matrix, membrane- and membrane-associated complexes from yeasts and bacteria.

5.1 Protein structure determination

Understanding of the processes underlying the passage from a DNA sequence to a protein structure and from a structure to its function and dynamics it is still a demanding process. Among the disciplines in the structural biology field that can contribute to answering these fundamental questions are X-ray crystallography, nuclear magnetic resonance (NMR), electron microscopy (EM) and molecular dynamics (MD). These are the most powerful approaches for macromolecular structure determination. Up till now, X-ray crystallography is one of the most successful tools to solve the structure from small to very large molecules. NMR is the other well-established method for determining atomic structures of relatively small proteins and allows the dynamics of a protein to be measured. Despite progress in understanding crystallization and robotic automation of systematic crystallization approaches, many biological proteins do not arrange themselves in perfectly ordered 3D crystals necessary to perform X-ray diffraction and also many other proteins are simply too large to be approached by NMR spectroscopy.

Electron microscopy has become a progressively more important technique for structural determination of small and large macromolecules. Over the last 3 decades, EM has also evolved into a powerful technique able to deliver three-dimensional (3D) structures of the studied complexes at the higher resolution necessary to visualize structural details of molecules (on the scale of nanometers) rather than of the gross architecture of cells (on the scale of micrometers) (Stahlberg and Walz 2008).

EM structure analysis can be performed on samples from ordered assemblies such as 2D crystals to asymmetric randomly oriented individual particles. The latter objects are rather easy to examine by EM, especially for soluble proteins. Electron crystallography of two-dimensional crystals yields the highest resolution data, since crystals present the largest numbers of proteins in well defined positions and orientations. Until very recently, electron crystallography has been the only EM technique that has reached sufficient resolution to produce atomic models of proteins. The 2D crystals used in electron crystallography are the

reason for the high resolution that can be achieved by this technique, because the crystallization accomplishes the alignment of the molecules, which therefore does not need to be done computationally. Thus, the better the order of the 2D crystals, the higher the resolution that can be achieved. Moreover it has the potential to provide structural information at near-atomic level. Because electron crystallography uses 2D crystals, it has proven particularly useful in structural studies of membrane proteins (Hite et al. 2007), although it was also used to determine the structure of the tubulin dimer (Nogales et al. 1998), light-harvesting complex II (Kühlbrandt et al. 1994), aquaporin (Murata et al. 2000; Ren et al. 2001) and bacteriorhopsin (Henderson et al. 1990). Notably, a recent density map obtained with doublelayered 2D crystals of aquaporin-0 at a resolution of 1.9 Å revealed water molecules in the channel of the protein as well as nine lipid molecules surrounding each monomer (Gonen et al. 2005). Besides electron crystallography, electron tomography is another novel technique to determine the 3D structure of unique objects, which can bring completely new insights into the proteins. Currently, the resolution of 3D reconstructions of biological, beam-sensitive samples rarely exceeds 50 Å because electron tomography still has some limitations. However, it has made stunning progress. In a landmark paper, electron tomography of a vitrified *Dictyostelium* cell revealed the organization of subcellular structures in the filipodium, including the rough endoplasmatic reticulum and the actin cytoskeleton (Medalia et al. 2002). The tomogram also revealed individual proteasomes, demonstrating that even the structure of macromolecular complexes can be determined in their native environment. Other recent successes of electron tomography include the visualization of the architectures of enveloped viruses (Grünewald et al. 2003), nuclear pore complex (Beck et al. 2007), bacterial cytoskeleton (Kürner et al. 2005), flagellar motor (Murphy et al. 2006), axonemes (Nicastro et al. 2006), magnetosomes (Komeili et al. 2006), and clathrin-coated vesicles (Cheng et al. 2007).

Although lagging behind in resolution with respect to electron crystallography, this technique can reveal structural features and conformational changes that underlie the function of the protein.

EM specimen preparation

EM specimen preparation techniques aim to prevent fundamental problems in the radiation sensitivity of the biological material. Biological specimens consist of up to 80%

water, requiring the samples to be prepared in a way that protects them from structural damage upon dehydration in the vacuum of the electron microscope. Important issue factor is that biological specimens also consist mainly of light atoms, and the density of proteins is very close to that of vitrified ice, making them low-contrast objects.

For individual particles two main specimen preparation methods have been developed to achieve high contast. Initially, biological specimens were prepared for EM by negative staining. Negative staining was introduced by Brenner and Horne at the end of the fifties (Brenner and Horne 1959). One of the methods of providing high contrast of the image in the electron microscope is to dry and embed the specimen in a layer of electron-dense heavy metal salts. The biological material surrounded by a heavy-metal ("negative stain") layer, is considerably increasing the scattering contrast lacking in the absence of stain. This method is not only very fast and straightforward, but also highly reproducible.

Amongst the most effective heavy metal salts that have been found to be suitable for this method are uranyl acetate, sodium- and potassium phosphotungstate and ammonium molybdate. Uranyl oxalate can replace unbuffered uranyl acetate, which has a very low pH, if proteins turn out to be unstable at low pH, as proposed by the former group leader E.F.J. Van Bruggen (Mellema et al. 1967).

One of the important aspects, in addition to negative staining is a glow-discharge device. It is often employed to make the surface of the support film more hydrophilic. It facilitates the absorption of the protein to the film and gives a better stain distribution. Using this method, the signal-to-noise ratio is much improved. Negative staining is effective at revealing the outer surface and therefore the quaternary structure of a protein molecule. However, there are a few dissadvantages of this method. While negative staining is fast and easy to use, there are possible distortions of the molecules resulting from the staining/drying procedure, causing the low attainable resolution of around 20 Å. Because of the limited penetrating ability of the stain, and the fact that the image is formed mainly by the stain-protein boundary, the structural information is restricted to topographical features of the molecule surface.

However, distortions of the molecules can be reduced by cryo-negative staining methods (Adrian et al. 1998; Ohi et al. 2004). This is the second and advanced fast preparation technique for a thin layer of hydrated specimen at liquid nitrogen temperature. Preparation methods to obtain ice-embedded protein specimens were developed in the eighties by Dubochet and colleagues (Adrian et al. 1984).Vitrification of the unstained specimen in its native buffer solution is the method of choice. In the preparation of cryosamples, the specimen is rapidly frozen (by plunging the EM grid into liquid ethane) and becomes thus embedded in a layer of vitreous (amorphous) ice (Dubochet et al. 1988). Then the grid is transferred to the electron microscope in special nitrogen-cooled holders. Although this technique preserves the specimen virtually artifact-free in a near-native environment, images of vitrified specimens are very noisy and have a contrast that is an order of magnitude lower than that of stained specimens.

To prevent proteins and supermolecular assemblies from denaturation and dehydration one can use air-drying in the presence of sustaining media such as glucose (Unwin and Henderson 1975) or trehalose (Hebert et al. 1997). Embedding in sugar in this way generates a non-volatile water-like environment for protein molecules, thus sustaining the specimen and taking advantage of the decrease of radiation damage at low temperature. Unfortunately the contrast using this method is even lower than in ice, since sugar almost matches the density of the protein.

One of the other methods invented by Dubochet and colleagues in 1998, combine the two techniques of vitreous-ice embedding and negative staining. The specimen preparation is very similar to the thin-film vitrification technique used for preparing cryo-EM specimens, except for the addition of a heavy metal salt at a concentration of several percent. The advantages of this method are two-fold. Firstly, the high contrast of cryo-negatively stained sample can be imaged close to focus and thus better preserves the high-resolution information. Secondly, the signal-to-noise ratio is higher, so improving the visualisation of the sample with a high amount of detail.

5.2 Electron Microscopy

The first electron microscope prototype was built in 1931 by the German engineers Ernst Ruska and Max Knoll in Berlin. Although this initial instrument was capable of

magnifying objects by only four hundred times and had a modest resolution of about 200 Å it demonstrated the principles and potency of an entirely different type of microscope. The Siemens company already produced commercial TEM microscopes in 1939, but actually the first practical electron microscope was built at the University of Toronto in 1938, by Eli Franklin Burton and students Cecil Hall, James Hillier, and Albert Prebus. A steadfast search for improvements has perfected the electron microscope of the last 70 years towards a powerful research tool to investigate matter at a resolution beyond 1.0 Å. Currently researchers use various types of microscopes to examine biological materials (such as microorganisms and cells), a variety of large molecules, medical biopsy samples, metals and crystalline structures and the characteristics of various surfaces. The electron microscope is also used extensively for inspection, quality assurance and failure analysis applications in industry, including, in particular, semiconductor device fabrication.

Image formation

In a conventional transmission electron microscope, a thin specimen is irradiated with a coherent electron beam of uniform current density. A schematic representation of the image formation in the electron microscope is depicted in Figure 5. Electrons are emitted from the electron gun and the electron beam is deflected through a two or three stage condenser lens system, which ensures that the incident electron beam falling on the specimen is parallel (for simplicity this is not depicted on the picture) with a tunable size. The incident electron beam passes through the specimen by which the electrons are scattered or non-scattered by the atoms of the specimen. Scattered electrons further interact with the magnetic field of the objective lens. The objective lens provides the formation of either an image or diffraction pattern of the specimen. The electron intensity distribution behind the specimen is magnified with a three or four stage lens system and viewed on a fluorescent screen or recorded by cameras. If the electrons are considered to interact with the specimen atoms as elementary particles the contrast in an electron micrograph arises from elastic and inelastic scattering. When the beam of electrons is deflected by the positively charged nucleus without loss of energy, the deviation angle is mostly large and scattered electrons can be removed by the objective aperture. This part of the contrast is called scattering contrast. For thick specimens or for heavy-metal stained specimens it is the major contribution in the final contrast. When the electrons undergo inelastic scattering with loss of energy, the interaction with the lenses is different due to chromatic aberration effects. The result is a blurring of the image and the

consequence of the energy loss is an increase in background noise and radiation damage as a side-effect. The contribution of inelastically scattered electrons can, however, be removed from the final image by filtering, as will be discussed in the next section. Filtering is useful for unstained specimens, but for negatively stained membrane proteins, as studied in this thesis the remaval is not crucial for obtaining higher quality data.

When the electron beam is considered as waves, the contrast arises from interference between non-scattered waves without a phase shift and scattered waves with additional phase shift. This is called phase contrast and it can be optimized by a right amount of defocusing of the objective lens and properties of the objective lens such as its spherical aberration constant. Thin specimens or unstained biological specimens are typically weakly scattering and such specimens are considered as phase objects. In practice, the final image always results from a combination of phase contrast and scattering contrast at a ratio depending on the type of specimen.

The final image can be recorded by direct exposure of a photographic emulsion or an image plate or digitally by a CCD camera. The acceleration voltage of up to date routine instruments is 120 to 200 kV. Medium-voltage instruments work at 200-500 kV to provide a better transmission and resolution, and in high voltage electron microscopy (HVEM) the acceleration voltage is in the range 500 kV to 3 MV. The acceleration voltage determines the velocity, wavelength and hence the resolution (ability to distinguish the neighbouring microstructural features) of the microscope.

Electron microscopes can also be used to generate and view diffraction patterns of samples. These are usually from samples that contain a repeated motif, such as 2D crystals (sheets one layer thick) of proteins. In the back focal plane of the objective lens, a difraction image is formed. Depending then on the positioning of the intermediate lens, the difraction pattern or the image will be magnified and displayed on the view screen.

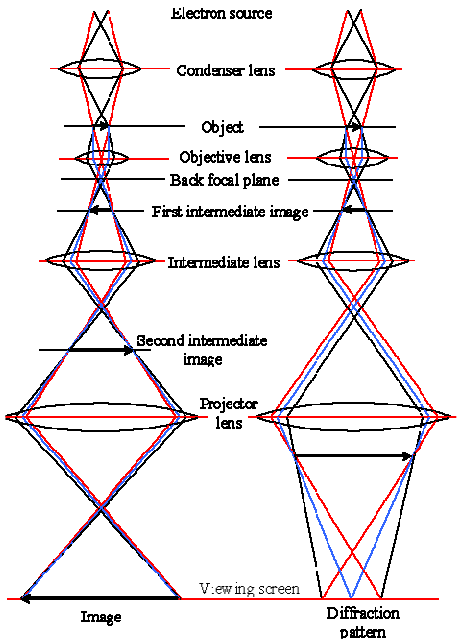

***Figure 5**. Schematic diagram showing the principle of image formation in an EM. An arrow shows the part of the image which is magnified by the sets of the objective and projection lenses and reprojected on the image plane.*

5.3 Image analysis as a method to increase resolution and signal-to-noise ratio

Generally speaking, an electron microscopy image of biological material suffers from a very low signal-to-noise ratio (SNR). The introduction of digital image processing made it possible to determine the 2D and 3D structures of biological molecules from very noisy EM images. The idea of increasing the SNR in electron images started by Aaron Klug, a Nobel prize laureate in 1982, and his colleagues from Cambridge in the sixties. Application to unstained specimens was first discussed by Glaeser in 1971 (Glaeser 1971) and applied by Nigel Unwin and Richard Henderson to bacteriorhodopsin crystals in two classical papers, the most cited piece of work in protein EM (Unwin and Henderson 1975; Henderson and Unwin 1975).

The first attempts to average single particle projections came just at the time of the crystallographic approach in the seventies (Frank 1975), although most of the basic tools were developed in the eighties, such as the use of statistical analysis to separate particle projections

from different angles (van Heel and Frank 1981) and schemes to obtain 3D reconstructions (Frank et al. 1988). In the single particle averaging approach computer programs are used to average images of equivalent molecules to increase the SNR, but improvement of the SNR depends not only on the number of images that are averaged but also on the correct alignment of the images such that the averaging actually improves the signal. In principle, the attained resolution (the minimum size of the structural detail that can be resolved) depends on the number of images averaged, their homogeneity (they should represent the same protein in the same orientation), and the accuracy of alignment; however, in practice the problem is difficult and remains the subject of vigorous research.

In addition, the computer is used to combine projection images of the molecule in different orientations to calculate a 3D reconstruction, thus overcoming the problem that electron microscopes can only record 2D images. Underlying 3D reconstruction are two implicit notions, namely, that electron microscope images are true projections of the imaged molecule and that all images represent identical molecules.

5.4 Novel developments in electron microscopy

Much of the current and future progress in molecular EM relies on developments in instrumentation, from specimen preparation to data acquisition. There is a lot of recent progress, for instance, the FEI Vitrobot has made it possible for the non-experienced user to obtain, within a short time, usable cryo-EM grids for single-particle EM and electron tomography. In general, automation of procedures of data acquisition and particle picking has tremendously shortened processing time. Most of the progress has been achieved in the instumentation of transmission electron microscopes driven by the materials sciences. The introduction of highly coherent and bright field emission gun (FEG) electron sources made it possible to record highly defocused images with only a limited loss in resolution. Because recording pictures at higher defocus values boosts the image contrast tremendously, FEG instruments have been crucial for obtaining higher resolution structures of biological specimens with their weak-phase-object characteristics. Stable EM electronics and specimen stages allowed for longer exposure times, which is beneficial for the coherence of the illumination and may result in lower beamdamage per dose (Chen et al. 2008).

Charge-coupled-device (CCD) cameras revolutionized imaging because they allow images to be captured in digital format, avoiding the time-consuming processes of developing and scanning photographic film. Initial CCD cameras had small imaging areas (typically 1K x 1K chips); recently the first camera with an 8K x 8K chip was introduced. Improvement in better data collection strategies are still under development. Together with higher acceleration voltages, energy filters made it possible to image thicker specimens and thus became essential for electron tomography. Operated in the so-called zero-loss mode, the energy filter removes inelastically scattered electrons, which are responsible for much of the noise in electron micrographs, thus improving the SNR of images, and also of electron diffraction patterns (Yonekura et al. 2002). Unstained biological samples are weak phase objects and thus create little image contrast.

The current way to enhance contrast is to take images at high defocus. Similar to the effect of a Zernike phase plate for light microscopy (Zernike 1935; Zernike 1955), the phase-shifted electrons then produce strong phase contrast when they interfere with the non-phase-shifted electrons in the image-recording medium. Such phase plates are currently under development, but the various designs still need to overcome significant technical challenges to become of practical use (Schroeder et al 2008). Another part of progress was done on aberration-corrected electron lenses. It has allowed material scientists to record much higher resolution images. Instruments free of spherical aberration have a clean transfer of features to a very high resolution, but the concomitant loss of contrast for the low-resolution frequencies makes this innovation less useful for biological samples with their low inherent contrast (Evans et al. 2008). The combination of an aberration-corrected imaging system with a phase-shifting device could, however, deliver an instrument with strong contrast and high-resolution transfer characteristics. However, even when combined with a phase-shifting device, the low tolerance of focus variations for an aberration-corrected lens system may prevent its use for imaging large, tilted biological samples. This problem could potentially be addressed by using “spot scan” imaging with dynamic focus adjustment, in which a series of small image frames is made with a focussed electron beam, the actual “spot”. At least for untilted biological samples, an electron optical imaging system that combines lenses corrected for spherical and also chromatic aberration (Haider et al. 2007) with a phase-shifting device, may deliver images of biological specimens of unprecedented quality, potentially revolutionizing molecular EM as we know it today.

Outline of this Thesis

The work described in this thesis is mainly performed within the research group Electron Microscopy. The research in this group is concentrating on the structural investigation and characterisation of protein complexes by using sigle particle electron microscopy. This thesis is focused on investigation of matrix and membrane proteins from different organisms belonging to yeasts or bacteria. Transmission electron microscopy in combination with single particle analysis and proteomics techniques have been the main tools in this study.

Chapter 2 of this thesis deals with a structural characterisation of Pex5p and Pex20p, peroxins involved in peroxisomal matrix protein import in the yeast *Hansenula polymorpha*. EM analysis showed that Pex5p is a tetramer. Upon addition of multimeric Pex20p, the conformation of tetrameric Pex5p changed from a closed conformation with a diameter of 115 Å into an open conformation of 134 Å. The results also indicated that the Pex5p-Pex20p complex was capable to bind native, folded catalase, a peroxisomal PTS1 protein. This suggests that the Pex5p-Pex20p complex may be functional as receptor complex.

Chapter 3 discusses Pex proteins involved in matrix transport over the peroxisomal membrane. We have performed a survey of the major peroxisomal membrane protein complex Pex14p, Pex13p and Pex17p by using Blue-Native polycrylamide gel electrophores (BN-PAGE) in combination with biochemical characterization and mass spectrometry. It appeared that purification of the peroxisomal membranes is crucial, but difficult to achieve by classical methods such as differential and sucrose density centrifugation since cells have a large excess of mitochondrial mebranes. The mitochondrial protein complexes obscure the peroxisomal ones in 1D and 2D PAGE analysis and a structural characterisation of the major peroxisomal membrane protein complexes is difficult to achieve.

In **chapter 4** the results of an analysis of the secondary transporters GltT, CitS and GltS using single particle electron microscopy is presented. Since the CitS and GltS particles are expected to be at the lower size limit of what is feasible for the technique, GltT protein with known structure was included as a reference particle. Evidence has been presented that the GltT protein assembles into a trimeric structure. EM analysis indicated that the other two

transporters from the ESS and 2HCT families, share a similar subunit structure. Both CitS and GltS (~ 100 kDa) showed to be dimers. Unfortunatelly, because of the small dimensions of proteins (~100 kDa) together with the low signal-to-noise ratio of EM images, and the unstructured detergent shell around membrane proteins, we were unable to reveal much detail in these proteins. Additional data were obtained by applying single particle averaging on proteins of mutants. We could show differences in size and shape of CitS transporters to which the Biotin Acceptor Domain *(*BAD) of the oxaloacetate decarboxylase of *Klebsiella pneumoniae* with a mass of 10 kDa was attached.

Chapter 5 focuses on a structural characterization of the Type IV secretion system from prokaryotes. For this investigation, intact membrane structures from *Neisseria species* were studied by electron microscopy. We have concentrated on PilQ, which is a member of the secretin family of outer membrane proteins and is specifically involved in secretion of type IV pili in *Neisseria meningitides* and *Neisseria gonorrhoeae.* We have investigated the quaternary structure of PilQ from *N. gonorrhoeae* analyzed by transmission electron microscopy. Oligomeric PilQ adopts a structure with two rings: an undefined inner and anh outer that is composed of 14 protein densities in *Neisseria gonorrhoeae.* At the periphery, seven external spikes bind to the second ring. In *Neisseria meningitides* the second ring is absent in many of the particles, but when it is present it is composed on 19 copies of an protein. The structure data have been extended by analysing the structures from specific knock-outs of Pili proteins in *Neisseria gonorrhoeae*. In one of them, a change in the second ring plus absence of the spikes was found.

REFERENCES

Adrian M., Dubochet J., Lepault J. and McDowall A.W. (1984) Cryo-electron microscopy of viruses. Nature 308, 32-36.

Adrian, M., Dubochet, J., Fuller, S.D. and Harris, J.R. (1998) Cryonegative staining, Micron 29, 145–160.

Agne, B., Meindl, N.M., Niederhoff, K., Einwachter, H., Rehling, P., Sickmann, A., Meyer, H.E., Girzalsky, W.and Kunau, W.H. (2003) Pex8p: an intraperoxisomal organizer of the peroxisomal import machinery. Mol. Cell. 11, 635-646.

Boudker, O., Ryan, R.M., Yernool, D., Shimamoto, K. and Gouaux, E. (2007) Coupling substrate and ion binding to extracellular gate of a sodium-dependent aspartate transporter. Nature 445, 387-393.

Beck, M., Lucič, V., Förster, F., Baumeister, W. and Medalia, O. (2007) Snapshots of nuclear pore complexes in action captured by cryo-electron tomography. Nature 449, 611–615.

Berman, H.M., Westbrook, J., Feng, Z., Gilliland, G., Bhat, T.N., Weissig, H., Shindyalov, I.N. and Bourne P.E. (2000) The Protein Data Bank. Nucleic Acids Res. 28, 235–242.

Blake, M.S., MacDonald, C.M. and Klugman, K.P. (1989) Colony morphology of piliated *Neisseria meningitidis*. J. Exp. Med. 170, 1727–1736.

Borden, K.L. and Freemont, P.S. (1996) The RING finger domain: a recent example of a sequence-structure family. Curr Opin Struct Biol 6, 395-401.

Bouwmeester, T., Bork, P., Seraphin, B., Kuster, B., Neubauer, G. and Superti-Furga, G. (2002) Functional organization of the yeast proteome by systematic analysis of protein complexes. Nature 415, 141–147.

Brenner, A. and Horne, R.W. (1959) A negative staining method for high resolution electron microscopy of viruses. Biochim.Biophys.Acta 34, 60-71.

Brown, L. A. and Baker, A. (2008) Shuttles and cycles: transport of proteins into the peroxisome matrix (Review). Mol. Memb. Biol. 25, 363-375.

Busch, W. and Saier, M.H.Jr. (2004) The IUBMB-endorsed transporter classification system. Mol. Biotechnol. 27, 253-262.

Chen, J. Z., Sachse, C., Xu, C., Mielke, T., Spahn, C. M. and Grigorieff, N. (2008) A dose-rate effect in single-particle electron microscopy, J. Struct. Biol. 161, 92–100.

Cheng, Y., Boll, W., Kirchhausen, T., Harrison, S. C. and Walz, T. (2007) Cryo-electron tomography of clathrin-coated vesicles: structural implications for coat assembly, J. Mol. Biol. 365, 892–899.

Collins, R.F., Frye, S.A., Kitmitto, A., Ford, R.C., Tønjum, T. and Derrick, J.P. (2004) Structure of the *Neisseria meningitidis* Outer Membrane PilQ Secretin Complex at 12 Å Resolution. J. Biol. Chem. 279, 39750-39756.

Collins, R.F., Frye, S.A., Balasingham S., Ford, R.C., Tønjum, T. and Derrick, J.P. (2005) Interaction with Type IV Pili Induces Structural Changes in the Bacterial Outer Membrane Secretin PilQ. J. Biol. Chem. 280, 18923-18930.

Craig, L., Volkmann, N., Arvai, A.S., Pique, M.E., Yeager, M., Egelman, E.H. and Tainer, J. (2006) Type IV Pilus Structure by Cryo-Electron Microscopy and Crystallography: Implications for Pilus Assembly and Functions. Molecular Cell 23, 651-662.

Dammai, V. and Subramani, S. (2001) The human peroxisomal targeting signal receptor, Pex5p, is translocated into the peroxisomal matrix and recycled to the cytosol. Cell 105, 187-196.

De Duve, C. and Baudhuin, P. (1966) Peroxisomes (microbodies and related particles). Physiol. Rev. 46, 323-357.

Drake, S.L. and Koomey, M. (1995) The product of the PilQ gene is essential for the biogenesis of type IV pilus in *N. gonorrhoeae*. Mol. Microbiol. 18, 975–986.

Drake, S., Sandstedt, S.A. and Koomey, M. (1997) PilP, a pilus biogenesis lipoprotein in *Neisseria gonorrhoeae*, affects expression of PilQ as a high molecular mass multimer. Mol. Microbiol. 23, 657–668.

Dubochet, J., Adrian, M., Chang, J.J., Homo, J.C., Lepault, J., Mc-Dowall, A.W. and Schultz, P. (1988) Cryo-electron microscopy of vitrified specimens, Q. Rev. Biophys. 21, 129–228.

Engelman, D.M. (2005) Membranes are more mosaic than fluid. Nature 438, 578–580.

Evans, J.E., Hetherington, C.J., Kirkland, A.I., Chang, L.Y., Stahlberg, H. and Browning, N.D. (2008) Low-dose aberration corrected cryo-electron microscopy of organic specimens. Ultramicroscopy 108, 1636-1644.

Erdmann, R., Veenhuis, M., Mertens, D. and Kunau, W.-H. (1989) Isolation of peroxisome-deficient mutants of *Saccharomyces cerevisiae*. Proc. Natl. Acad. Sci. USA 86, 5419–5423.

Erdmann, R., Wiebel, F.F., Flessau, A., Rytka, J., Beyer, A., Fröhlich, K.U. and Kunau, W.-H. (1991) PAS1, a yeast gene required for peroxisome biogenesis, encodes a member of a novel family of putative ATPases. Cell 64, 499–510.

Faast, R., Ogierman, M.A., Stroeher, U.H. and Manning, P.A. (1989) Nucleotide sequence of the structural gene, *tcpA*, for a major pilin characterization of the gene cluster specifying expression of subunit of *Vibrio cholerae*. Gene 85, 227–231.

Fagarasanu, M., Fagarasanu, A. and Rachubinski, R.A. (2006) Sharing the wealth: peroxisome inheritance in budding yeast. Biochim. Biophys. Acta 1763, 1669–1677.

Frank, J. (1975) Averaging of low exposure electron micrographs of non-periodic objects. Ultramicroscopy 1, 159-162.

Frank, J., Verschoor, A., Wagenkenecht, T., Radermacher, M., Carazo, J.M. (1988) A new non-crystallographic image-processing technique reveals the architecture of ribosomes. Trends Biochem. Sci. 13, 123-127.

Frøholm, L.O. and Sletten, K. (1977) Purification and N-terminal sequence of a fimbrial protein from *Moraxella nonliquefaciens.* FEBS Lett. 73, 29–32.

Gatto, G.J., Geisbrecht, B.V., Gould, S.J., Berg, J.M. (2000) Peroxisomal targeting signal-1 recognition by the TPR domains of human PEX5. Nature Str. Biol. 7, 1091-1095.

Gavin, A.C., Bosche, M., Krause, R., Grandi, P., Marzioch, M., Cruciat, C.M., Remor, M., Hofert, C., Schelder, M., Brajenovic, M., Ruffner, H., Merino, A., Klein, K., Hudak, M., Dickson, D., Rudi, T., Gnau, V., Bauch, A., Bastuck, S., Huhse, B., Leutwein, C., Heurtier, M.A., Copley, R.R., Edelmann, A., Querfurth, E., Rybin, V., Drewes, G., Raida, M., Stenberg, F., Chovanec, P., Maslen, S.L., Robinson, C.V., Ilag, L.L., von Heijne, G. and Daley, D.O. (2005) Protein complexes of the Escherichia coli cell envelope J. Biol. Chem. 280, 34409–34419.

Glaeser,R.M. (1971) Limitations to significant information in biological electron microscopy as a result of radiation damage. J Ultrastruct.Res. 36, 466-482.

Gonen, T., Cheng, Y., Sliz, P., Hiroaki, Y., Fujiyoshi, Y., Harrison, S. C., and Walz, T. (2005) Lipid-protein interactions in doublelayered two-dimensional AQP0 crystals, Nature 438, 633–638.

Gould, S.J. and Collins, C.S. (2002) Opinion: peroxisomal-protein import: is it really that complex? Nat Rev Mol Cell Biol 3, 382-389.

Grünewald, K., Desai, P., Winkler, D.C., Heymann, J.B., Belnap, D.M., Baumeister, W. and Steven, A.C. (2003) Three-dimensional structure of herpes simplex virus from cryo-electron tomography, Science 302, 1396–1398.

Guilvout, I., Hardie, K.R., Sauvonnet, N. and Pugsley, A.P. (1999) Genetic dissection of the outer membrane secretin PulD: are there distinct domains for multimerization and secretion specificity? J. Bacteriol. 181, 7212–7220.

Gouveia, A.M., Guimaraes, C.P., Oliveira, M.E., Reguenga, C., Sa-Miranda, C., Azevedo, J.E. (2003) Peroxisomal Disorders and Regulation of Genes 544, 219-220.

Haas, R. and Meyer, T.F. (1986) The repertoire of silent pilus genes in *Neisseria gonorrhoeae*: evidence for gene conversion. Cell 44, 107–115.

Haider, M., Müller, H., Uhlemann, S., Zach, J., Loebau, U. and Hoeschen, R. (2007) Prerequisites for a C(c)/C(s)-corrected ultrahighresolution TEM, Ultramicroscopy 108, 167–178.

Heckels, J.E. (1989) Structure and function of pili of pathogenic *Neisseria* species. Clin. Microbiol. Rev. 2, 66–73.

Hebert, H., Schmidt-Krey, I., Morgenstern, R., Murata, K., Hirai, T., Mitsuoka, K. and Fuijyoshi, Y. (1997) the 3.0 A projection structure of microsomal gluthatione transferase as determined by electron crystallography of p 21212 two-dimensional crystals. J. Mol.Biol. 271, 751-758.

Heiland, I. and Erdmann, R. (2005) Biogenesis of peroxisomes. Topogenesis of the peroxisomal membrane and matrix proteins. FEBS Journal 272, 2362-2372.

Henderson, R. and Unwin, P.N.T. (1975) 3-dimensional model of purple membrane obtained by electron microscopy. Nature 257, 28-32.

Henderson, R., Baldwin, J.M., Ceska, T.A., Zemlin, F., Beckmann, E., and Downing, K.H. (1990) Model for the structure of bacteriorhodopsin based on high-resolution electron cryo-microscopy. J Mol.Biol. 213, 899-929.

Heyne, R.I., De Vrij, W., Crielaard, W. and Konings, W.N. (1991) Sodium ion-dependent amino acid transport in membrane vesicles of *Bacillus stearothermophilus*. J. Bacteriol. 173, 791-800.

Hite, R.K., Raunser, S. and Walz, T. (2007) Revival of electron crystallography, Curr. Opin. Struct. Biol. 17, 389–395.

Hoepfner, D., Schildknegt, D., Braakman, I., Philippsen, P. and Tabak, H.F. (2005) Contribution of the endoplasmic reticulum to peroxisome formation. Cell 122, 89–95.

Holroyd, C. and Erdmann, R. (2001) Protein translocation machineries of peroxisomes. FEBS Lett. 501, 6–10.

Kästner, C.N., Prummer, M., Sick, B., Renn, A., Wild, U.P. and Dimroth, P. (2003) The citrate carrier CitS probed by single-molecule fluorescence spectroscopy. Biophys. J. 84, 1651-1659.

Keseler, I.M., Collado-Vides, J., Gama-Castro, S., Ingraham, J., Paley, S., et al. 2005. *Nucleic Acids Res.* 33:D334–37

Kiel, J.A., Emmrich, K., Meyer, H.E. and Kunau, W.H. (2005) Ubiquitination of the peroxisomal targeting signal type 1 receptor, Pex5p, suggests the presence of a quality control mechanism during peroxisomal matrix protein import. J Biol Chem 280, 1921-1930.

Klabunde, T. and Hessler, G. (2002) Drug Design Strategies for Targeting G-Protein-Coupled Receptors. ChemBioChem 3, 928–944.

Komeili, A., Li, Z., Newman, D.K. and Jensen, G.J. (2006) Magnetosomes are cell membrane invaginations organized by the actinlike protein MamK, Science 311, 242–245.

Koomey, J.M. and Falkow, S. (1987) Cloning of the *recA* gene of *Neisseria gonorrhoeae* and construction of gonococcal RecA− mutants. J. Bacteriol. 169, 790–795.

Konings, W.N., Kaback, H.R. and Lolkema, J.S. (1996) Transport processes in eukaryotic and prokaryotic organisms. Elsevier Science B.V., Amsterdam, The Netherlands.

Kragt, A., Brouwer, T.V., van den Berg, M. and Distel, B. et al. (2005) The Saccharomyces cerevisiae peroxisomal import receptor Pex5p is monoubiquitinated in wild type cells. J Biol Chem 280, 7867-7874.

Krogh, A., Larsson, B., von Heijne, G. and Sonnhammer, E.L. (2001) Predicting transmembrane protein topology with a hidden Markov model: Application to complete genomes. J. Mol. Biol. 305, 567–580.

Kunau WH. (2001) Peroxisomes: the extended shuttle to the peroxisome matrix. Curr. Biol. 11, 659-662.

Kühlbrandt, W., Wang, D.N. and Fujiyoshi, Y. (1994) Atomic model of plant light-harvesting complex by electron crystallography, Nature 367, 614–621.

Kürner, J., Frangakis, A.S. and Baumeister, W. (2005) Cryoelectron tomography reveals the cytoskeletal structure of *Spiroplasma melliferum*, Science 307, 436–438.

Lasserre, J.P., Beyne, E., Pyndiah, S., Lapaillerie, D., Claverol, S. and Bonneu, M. (2006) A complexomic study of Escherichia coli using two-dimensional blue native/SDS polyacrylamide gel electrophoresis. Electrophoresis 27, 3306–3321.

Lazarow, P.B. and Fujiki,Y. (1985) Biogenesis of peroxisomes. Annu. Rev. Cell Biol. 1, 489-530.

Lazarow PB. 2006. The import receptor Pex7p and the PTS2 targeting sequence. Bioch. Bioph. Acta-Molec. Cell Res. 1763, 1599-1604.

Liu, Y., Gerstein M. and Engelman, D.M. (2004) Transmembrane protein domains rarely use covalent domain recombination as an evolutionary mechanism. Proc. Natl. Acad. Sci. USA 101, 3495–3497.

Lolkema, J.S. and Slotboom, D.J. (1998) Hydropathy profile alignment. A tool to search for structural homologues of membrane proteins. FEMS Microbiol. Rev. 22, 305–322.

McGee, Z.A., Stephens, D.S., Hoffman, L.H., Schlech, W.F. 3rd and Horn, R.G. (1983) Mechanisms of mucosal invasion by pathogenic Neisseria. Rev. Infect. Dis. 5, 708–714.

Medalia, O., Weber, I., Frangakis, A. S., Nicastro, D., Gerisch, G. and Baumeister, W. (2002) Macromolecular architecture in eukaryotic cells visualized by cryoelectron tomography, Science 298, 1209–1213.

Mellema, J.E., van Bruggen, E.F.J. and Gruber, M. (1967) Uranyl oxalate as a negative stain for electron microscopy of proteins. Biochim. Biophys. Acta 140, 180-182.

Murata, K., Mitsuoaka, K., Hirai, T., Walz, T., Aare, P., Heymann, J.B., Engel, A. and Fujiyoshi, Y. (2000) Structural determinants of water permeation through aquaporin-1. Nature 407, 599-605.

Murphy, G.E., Leadbetter, J.R. and Jensen, G.J. (2006) In situ structure of the complete Treponema primitia flagellar motor, Nature 442, 1062–1064.

Nicastro, D., Schwartz, C., Pierson, J., Gaudette, R., Porter, M.E. and McIntosh, J.R. (2006) The molecular architecture of axonemes revealed by cryoelectron tomography, Science 313, 944–948.

Nogales, E., Wolf, S.G., and Downing, K.H. (1998) Structure of the β- tubulin dimer by electron crystallography, Nature 391, 199–203.

Nouwen, N., Stahleberg, H., Pugsley, A.P. and Engel, A. (2000) Domain structure of secretin PulD revealed by limited proteolysis and electron microscopy. EMBO J. 19, 2229–2236.

Novikoff, A.B. and Shin, W.Y. (1964) The endoplasmatic reticulum in the golgi zone and ist relations to microbodies, golgiapparatus and autophagic vacuoles in rat liver cells. J. Mikros. Oxford 3, 187–206.

Oberai, A., Ihm, Y., Kim, S. and Bowie, J.U. (2006) A limited universe of membrane protein families and folds. Protein Sci. 15, 1723–1734.

Ohi, M., Li, Y., Cheng, Y. and Walz, T. (2004) Negative staining and image classificationOpowerful tools in modern electron microscopy, Biol. Proced. Online 6, 23–34.

Ottow, J.C.G. (1975) Ecology, physiology, and genetics of fimbriae and pili. Annu. Rev. Microbiol. 29, 79–108.

Perry, A.C., Nicolson, I.J. and Saunders, J.R. (1988) *Neisseria meningitidis* C114 contains silent, truncated pilin genes that are homologous to *Neisseria gonorrhoeae pil* sequences. J. Bacteriol. 170, 1691–1697.

Platta, H.W., Girzalsky, W. and Erdmann, R. (2004) Ubiquitination of the peroxisomal import receptor Pex5p. Biochem J 384, 37-45.

Platta, H.W., El Magraoui, F., Schlee, D., Grunau, S., Girzalsky, W. And Erdmann, R. (2007) Ubiquitination of the peroxisomal import receptor Pex5p is required for its recycling. J. Cell Biol. 177, 197-204.

Pires, J.R., Hong, X.J., Brockmann, C., Volkmer-Engert, R., Schneider-Mergener, J., Oschkinat, H. and Erdmann, R. (2003) The ScPex13p SH3 domain exposes two distinct binding sites for Pex5p and Pex14p. J. Mol. Biol. 326, 1427-1435.

Poirier, Y., Antonenkov, V.D., Glumoff, T. and Hiltunen, J.K. (2006) Peroxisomal beta-oxidation--a metabolic pathway with multiple functions. Biochim Biophys Acta 12, 1413-1426.

Pos, K.M., Dimroth, P. and Bott, M. (1998) The Escherichia coli citrate carrier CitT: a member of a novel eubacterial transporter family related to the 2-oxoglutarate/malate translocator from spinach chloroplasts. J. Bacteriol. 180, 4160-4165.

Purdue, P.E. and Lazarow, P.B. (2001) Peroxisome biogenesis. Annu Rev Cell Dev Biol 17, 701-52.

Rachubinski, R.A. and Subramani, S. (1995) How proteins penetrate peroxisomes. Cell 83, 525-528.

Ren, J.S., Reddy, V.S., Cheng, A., Melnyk, P. and Mitra, A.K. (2001) Visualization of a water-selective pore by electron crysallography in vitrous ice. Proc. Natl. Acad. Sci. U.S.A 98, 1398-1403.

Reumann, S., Ma, C.L., Lemie, S. and Babujee, L. (2004). AraPerox. A database of putative Arabidopsis proteins from plant peroxisomes. Plant Physiol 136, 2587-2608.

Sacksteder, K.A. and Gould, S.J. (2000) Genetics of peroxisome biogenesis. Annu Rev Genet. 34, 623-652.

Saier, M.H.Jr. (2000) A functional-phylogenetic classification system for transmembrane solute transporters. Microbiol. Mol. Rev. 64, 354-411.

Schroeder, R.R., Barton, B., Schultheiss, K., Gramm, B. and Gerthsen, D. (2008) In-focus contrast: present state and future developments. In: M. Luysberg, K. Tillmann, T. Weinrich (eds.) EMC2008, Vol. 1, pp 69-70. Springer, Berlin, Heidelberg.

Smith, M.D., Schnell, D.J. (2001) Peroxisomal protein import: the paradigm shifts. Cell 105, 293-296.

Sobczak, I. and Lolkema, J.S. (2003) Accessibility of Cysteine Residues in a Cytoplasmic Loop of CitS of *Klebsiella pneumoniae* is Controlled by the Catalytic State of the Transporter. Biochemistry 42, 9789-9796.

Strom, M.S. and Lory, S. (1986) Cloning and expression of the pilin gene of *Pseudomonas aeruginosa* PAK in *Escherichia coli*. J. Bacteriol. 165, 367–372.

Swanson, J., Bergstrom, S., Robbins, K., Barrera, O., Corwin, D. and Koomey, J.M. (1986) Gene conversion involving the pilin structural gene correlates with pilus+ to pilus− changes in *Neisseria gonorrhoeae*. Cell 47, 267–276.

Stahlberg, H. and Walz, T. (2008) Molecular Electron Microscopy: State of the Art and Current Challenges. Molecular and Cellular Biology 16, 268-281.

Subramani, S., Koller, A. and Snyder,W.B. (2000) Import of peroxisomal matrix and membrane proteins. Annu Rev Biochem 69, 399-418.

Tabak, H.F., Hoepfner, D., Zand, A., Geuze, H.J, Braakman, I. and Huynen, M.A. (2006) Formation of peroxisomes: present and past. Biochim Biophys Acta, 2006. 1763, 1647-1654.

Tønjum, T., Weir, S., Bøvre, K., Progulske-Fox, A. and Marrs, C.F.(1993) Sequence divergence in two tandemly located pilin genes of factor export. Science 265, 612–614.

Tønjum, T., and Koomey, M. (1997) The pilus colonisation factor of pathogenic *Neisseria* species: organelle biogenesis and structure/function relationships. Gene 192, 155–163.

Unwin, P.N.T. and Henderson, R. (1975) Molecular structure determination by electron microscopy of unstained crystalline specimens. J. Mol.Biol. 94, 425-440.

Urquhart, A.J., Kennedy, D., Gould, S.J. and Crane, D.I. (2000) Interaction of Pex5p, the type 1 peroxisome targeting signal receptor, with the peroxisomal membrane proteins Pex14p and Pex13p. J. Biol. Chem. 275, 4127-4136.

Van Heel, M. and Frank, J. (1981) Use of multivariate statistics in analysing the images of biological macromolecules. Ultramicrocopy 6, 187-194.

Van den Bosch, H., Schutgen, R.B.H., Wanders, R.J.A. and Tager, J.M. (1992) Biochemistry of peroxisomes. Annu Rev Biochem 61, 157-97.

Van der Zand, A., Braakman, I., Geuze, H.J. and Tabak, H.F. (2006) The return of the peroxisome. J. Cell Sci. 119, 989–994.

Van Putten, J.P., Duensing, T.D. and Carlson, J. (1998) Gonococcal invasion of epithelial cells driven by P.IA, a bacterial ion channel with GTP binding properties. J. Exp. Med. 188, 941–952.

Veenhoff, L.M., Heuberger, E.H. M.L., Duurkens, H.H. and Poolman, B. (2002) Oligomeric state of membrane transport proteins analyzed with blue native electrophoresis and analytical ultracentrifugation. J. Mol. Biol. 317, 591-600.

Veenhuis, M., Mateblowski, M., Kunau, W.-H. and Harder, W. (1987) Proliferation of microbodies in Saccharomyces cerevisiae. Yeast 3, 77–84.

Virji, M., Alexandrescu, C., Ferguson, D.J., Saunders, J.R. and Moxon, E.R. (1992) Variations in the expression of pili—the effect on adherence of *Neisseria meningitidis* to human epithelial and endothelial cells. Mol. Microbiol. 6, 1271–1279.

Vizeacoumar, F.J., Torres-Guzman, J.C., Bouard, D., Aitchison, J.D. and Rachubinski, R.A. (2004) Pex30p, Pex31p and Pex32p form a family of peroxisomal integral membrane proteins regulating peroxisome size and number in Saccharomyces cerevisiae. Mol. Biol. Cell 15, 665–677.

White, S.H. (2004) The progress of membrane protein structure determination. Protein Sci. 3, 1948–1949.

Xia, Y., Lu, L.J. and Gerstein, M. (2006) Integrated prediction of the helical membrane protein interactome in yeast. J. Mol. Biol. 357, 339–349.

Yernool, D., Boudker, O., Jin, Y., Gouaux, E. (2004) Structure of a glutamate transporter homologue from Pyrococcus horikoshii. Nature 431, 811-818.

Yonekura, K., Maki-Yonekura, S. and Namba, K. (2002) Quantitative comparison of zero-loss and conventional electron diffraction from two-dimensional and thin three-dimensional protein crystals, Biophys. J. 82, 2784–2797.

Zernike, F. (1935) Das Phasenkontrastverfahren bei der mikroskopischen Beobachtung, Phys. Z. 36, 848–851.

Zernike, F. (1955) How I discovered phase contrast, Science 121, 345–349.

Chapter 2

The *Hansenula polymorpha* Peroxisomal Targeting Signal 1 receptor, Pex5p, functions as a tetramer

Katarzyna B. Mościcka, Sandra H. Klompmaker, Dongyuan Wang, Ida J. van der Klei & Egbert J. Boekema

ABSTRACT

We have studied *Hansenula polymorpha* Pex5p and Pex20p, peroxins involved in peroxisomal matrix protein import. *In vitro* binding experiments suggested that *H. polymorpha* Pex5p and Pex20p physically interact. We used single particle electron microscopy (EM) to analyze the structure of purified Pex5p and its possible association with Pex20p. Upon addition of Pex20p, a multimeric Pex20p complex was observed to be associated to the periphery of the Pex5p tetramer. In this Pex5p-Pex20p complex, the conformation of tetrameric Pex5p had changed from a closed conformation with a diameter of 115 Å into an open conformation of 134 Å. EM also indicated that the Pex5p-Pex20p complex was capable to bind native, folded catalase, a peroxisomal PTS1 protein. This suggests that the Pex5p-Pex20p complex may be functional as receptor complex.

Keywords: Pex5p, peroxisome; membrane transport; electron microscopy; *Hansenula polymorpha*

Published in FEBS Letters (2007), 581:*1758-1762*

INTRODUCTION

Peroxisomal matrix proteins are synthesized on free polyribosomes and directed to the organelle by specific peroxisomal targeting signals (PTSs). The routing of most matrix proteins depends on one of the two conserved PTSs, designated PTS1 and PTS2, which are recognized by the receptor proteins Pex5p or Pex7p, respectively.

The *PEX5* gene encodes the PTS1 receptor, Pex5p, which interacts with the PTS1 signal via a series of tetratricopeptide repeats (TPRs) within its C terminus. A crystal structure has been determined of a 41 kDa fragment of human Pex5p that includes six TPR motifs in complex with a small peptide containing a PTS1 sequence (Gatto et al. 2000; Gatto et al. 2003) or the sterol carrier protein (Stanley et al. 2006). This structure reveals the molecular basis for PTS1 recognition which is mostly formed by two clusters of three TPRs almost completely surrounding the PTS1-peptide.

However, whether or not Pex5p functions as an oligomer, is still a matter of debate. Gel filtration chromatography and electron microscopy studies indicated that human Pex5p (HsPex5p) is a homotetramer (Schliebs et al.1999). Fluorescence spectroscopy studies on Pex5p of the yeast *Hansenula polymorpha* (HpPex5p) indicated that HpPex5p also forms oligomers (Boteva et al. 2003). Moreover, HpPex5p oligomers were shown to bind PTS1 containing synthetic peptides, suggesting that this is indeed the conformation of a functional PTS1 receptor (Wang et al. 2003). On the other hand, recent studies on human Pex5p (HsPex5p) using sucrose density centrifugation revealed that HsPex5p is monomeric (Costa-Rodrigues et al. 2005). The behavior of HsPex5p in gel filtration chromatography, which indicated a high molecular weight of the native protein, was suggested to result from a non-globular shape of the protein. Studies on the N-terminal domain of HsPex5p pointed to an unfolded pre-molten globule-like structure, which may contribute to a non-globular shape of full length HsPex5p (Carvalho et al. 2006).

Pex7p is the receptor for the PTS2 signal. In higher eukaryotes (plants, mammals), Pex7p associates with Pex5p during peroxisomal protein import. In lower eukaryotes (yeasts, fungi) Pex7p binds to Pex20p (or Pex18p and Pex21p in *S. cerevisiae*; for a review see (Kiel et al. 2006). For PTS2 protein import Pex20p's most likely fulfill a similar function as Pex5p

in higher eukaryotes. Indeed, the N-terminal half of Pex5p's and Pex20p's share a few conserved domains and show similar dynamics during import (Kiel et al. 2006; Leon et al. 2006a). Like Pex5p also Pex20p has been reported to form oligomers (Otzen et al. 2005).

Our understanding of the structure of the peroxins involved in peroxisomal protein translocation is still limited. For initial characterization of such complexes single particle electron microscopy (EM) is a well-established technique to obtain information at a resolution of 10–20 Å (Frank, J. 2002; Van Heel et al. 2000). It is attractive for samples of mixed complexes with a mass above about 200 kDa, because the statistical analysis and classification procedures used are effective in sorting of (slightly) different projection views originating from different conformations or subunit compositions. In this study, the projection structures of HpPex5p and HpPex5p-HpPex20p complexes were investigated by single particle electron microscopy. The analysis shows that HpPex5p is a tetramer and that HpPex20p is able to induce a major conformational change leading to a rather open space in the centre of the HpPex5p tetramer. In a successive set of experiments we show that HpPex5p-HpPex20p complexes are able to bind folded copies of tetrameric catalase at the periphery. Since catalase is one of the major peroxisomal proteins this indicates that such HpPex5p-HpPex20p-catalase complexes are functional as receptor complex.

MATERIAL AND METHODS

Organisms and growth.

The *Hansenula polymorpha* strains used in this study are wild type (WT), *pex5, pex7* and *pex20*. Yeast cells were grown in a carbon-limited chemostat culture at 37˚C using 0.25% glucose as carbon source and 0.2% choline as nitrogen source at a dilution rate of 0.1 h^{-1}. Cells were harvested from steady state cultures. The levels of Pex5p and Pex20p were analyzed by western blotting using total cell lysates.

Expression and purification

Escherichia coli M15 cells containing plasmids pREP4 and pQE60- Pex20p-His_8 (Otzen et al. 2005) or pQE60- Pex5p-His_6 (Wang et al. 2003) were grown as described before. Expression of the *PEX5* or *PEX20* genes was induced by the addition of 1 mM isopropyl-1-thio-β-D-

galactopyranoside as detailed before (Wang et al. 2003; Otzen et al.2005). Cells were harvested by centrifugation. All subsequent steps were carried out at 4˚C. Pex5p was purified as detailed (Wang et al. 2003). To isolate the Pex5p-Pex20p complex, Pex5p-His_6 and Pex20p-His_8 were isolated by affinity chromatography using Ni-NTA (Qiagen). Cell pellets were resuspended in 40 ml buffer A (50 mM phosphate buffer, pH 7.4, 300 mM NaCl, 1% Tween 20, 10% glycerol, 0.2 mM β-mercaptoethanol, 1mM phenylmethyl sulfonyl fluoride, 1 mM sodium azide, 5 mM sodium fluoride, and Complete^{TM} (Roche, Almere, The Netherlands). Cells were disrupted using a French Press. The lysates were centrifuged (20 min, 10000g), and supernatants incubated for 1 hour with Ni-NTA (Qiagen, 500 mg protein/ ml resin). Subsequently, the resin was extensively washed with buffer B (50 mM phosphate buffer, pH 7.4, 100 mM NaCl) containing increasing concentrations of imidazole (up to 40 mM). Bound proteins were eluted with buffer B containing 200 mM imidazole. Elution fractions were analyzed by SDS-PAGE followed by Coomassie brilliant blue staining and Western blotting using antibodies raised against Pex5p or Pex20p. Fractions highly enriched in Pex5p-His_6 or Pex20p-His_8, respectively were pooled. Equal portions of these fractions were mixed and incubated for one hour on ice. Then, the Pex5p-His_6 - Pex20p-His_8 mixture was subjected to gel filtration chromatography (Superose 12) using 50 mM potassium phosphate buffer, pH 7.4 as running buffer. The elution fractions were analyzed by SDS-PAGE followed by Coomassie brilliant blue staining and Western blotting using anti-Pex5p and anti-Pex20p antibodies. The first fractions that eluted from the column and contained both Pex5p-His_6 and Pex20p-His_8 were used for electron microscopy.

Gel filtration experiments to estimate the mass of Pex5p and Pex5p-Pex20p complexes were performed on a Superose 6 size exclusion column on an AKTA FPLC system, equipped with a UV detector with catalase, ferritin, thyroglobulin as marker proteins.

***In vitro binding studies*.**

Pex5p-His_6 and Pex20p-His_8 were produced in *E. coli* and purified using Ni-NTA agarose as detailed above. Fractions containing Pex20p or Pex5p were diluted 10 times using buffer A and incubated with Ni-NTA agarose for 1 hour at 4 ^{o}C. Methanol grown *H. polymorpha* wild type or *pex7* cells were disrupted using glass beads. Cell homogenates were centrifuged at 4 ^{o}C for 5 minutes at 20000×g to remove unbroken cells and cell debris. Supernatants were loaded onto the Ni-NTA agarose containing either Pex20p-His_8 or Pex5p-His_6 and incubated for one hour at

4 ^{o}C with continuous rotation. After extensive washing with buffer B containing increasing concentrations of imidazole (from 10 mM up to 40 mM), Pex20p-His_8 or Pex5p-His_6 together with the bound proteins were eluted with buffer B containing 250 mM imidazole. The elution fractions were analyzed by Western blotting.

Preparation Pex5p-Pex20p complexes with catalase

Crystalline catalase from bovine liver (from Sigma-Aldrich) at a stock concentration of 20 mg/ml was diluted with water to the final concentration of 33 μg/ml. 5 μl of Pex5p-Pex20p complexes from the best fractions were incubated with 1 μl catalase for 1h at room temperature and immediately prepared for EM.

Electron Microscopy and Single-Particle Analysis

Negatively stained Pex5p, Pex5p-Pex20p and Pex5p-Pex20p complexes mixed with catalase were prepared with 2% uranyl acetate on glow-discharged carbon-coated copper grids. Electron microscopy was performed on a Philips CM12 FEG electron microscope operated at 120 kV. Images were recorded with a Gatan 4K slow-scan CCD camera at 80000 x magnification with a pixel size (after binning the images) of 3.75 Å at the specimen level, with "GRACE" software for semi-automated specimen selection and data acquisition. About 6000 images were recorded and about 7520 single particle projections from Pex5p, 6071 projections from Pex5-20 complexes, 1300 from Pex5-20p-catalase and 5800 single catalase projections were selected, respectively. Single-particle analysis was performed with the Groningen Image Processing ("GRIP") software package on a PC cluster. Selected single-particle projections (128 x 128 pixel frame) were aligned by a multireference alignment and reference-free alignment procedures according to (Van Heel et al. 2000; Penczek et al. 1992). Next, particles were subjected to multivariate statistical analysis, followed by hierarchical ascendant classification (HAC) (Van Heel et al. 2000). The resolution of the class averages was measured by Fourier Ring Correlation according to (Van Heel 1987). After several cycles of multireference alignments, statistical analysis and classification the best projections from each set were averaged.

RESULTS AND DISCUSSION

We recently performed a detailed comparative study on *H. polymorpha pex* mutants, which were identically grown in chemostat cultures (Koek and Van der Klei, unpublished results). Unexpectedly, in samples of steady state cultures we observed that the levels of HpPex5p were reduced in cells lacking Pex20p (*H. polymorpha pex20* cells), whereas HpPex20p levels were lower in the absence of Pex5p (in *H. polymorpha pex5*), as shown in Fig. 1. This indicates that HpPex5p and HpPex20p may stabilize each other *in vivo*. To analyze whether this apparent stabilization is related to a physical interaction between both proteins, we performed *in vitro* interaction studies. Crude extracts of *H. polymorpha* wild type cells were loaded onto columns containing either immobilized His-tagged HpPex5p or HpPex20p, purified from *E. coli*. As shown in Fig. 2A (lane 2), Pex20p from the *H. polymorpha* extract co-eluted with Pex5p-His_6. The cytosolic enzyme pyruvate carboxylase (Pyc1p), used as a negative control, did not co-elute with Pex5p-His_6. Moreover, Pex20p was not detected in the eluate when an empty column was used (Fig. 2A, lane 1). In a reverse approach, using a column containing Pex20p-His_8, Pex5p from the *H. polymorpha* extract co-eluted with Pex20p-His_8 (Fig. 2B, Lane 2). Again, the Pyc1p control protein did not co-elute with Pex20p-His_8 and no Pex5p was present in the elution fraction when an empty column was used (Fig. 2B, lane 1). Co-elution of Pex5p with Pex20p and vice versa was also observed when crude extracts of *H. polymorpha* cells were used in which the PTS2 receptor Pex7p was absent (*H. polymorpha pex7* cells), indicating Pex7p is not required for association of Pex5p with Pex20p (Fig. 2A,B lane 3).

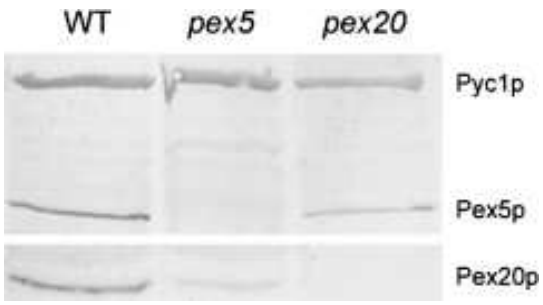

Figure 1. *Pex5p and Pex20p levels in cells of H. polymorpha WT and pex mutants. Shown are steady-state levels of Pex5p and Pex20p in WT and pex5 and pex20 mutants grown in chemostat cultures on glucose/choline. Pex5p and Pex20p levels were analyzed by Western blotting using specific antibodies against Pex5p and Pex20p, respectively. Pex5p and Pex20p are both evident in WT cells. In pex5 cells Pex5p is absent as expected. However, in addition the level of Pex20p is strongly reduced in pex5 cells. Similarly, Pex20p is absent in pex20 cells, but Pex5p levels are slightly reduced. Equal amounts of protein were loaded per lane. The cytosolic protein pyruvate carboxylase (Pyc1p) was included as a loading control*

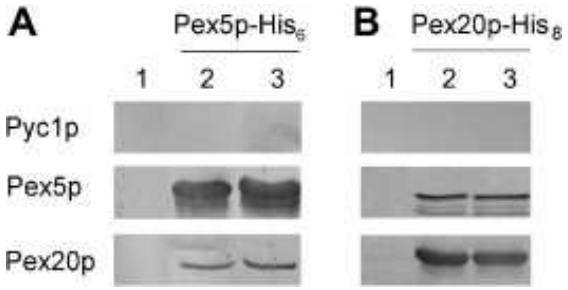

Figure 2. *H. polymorpha Pex5p and Pex20p physically interact in vitro. (**A,B**) Pex5p-His$_6$ (lanes 2 and 3 in (**A**))or Pex20p-His$_8$ (lanes 2 and 3 in (**B**)), produced in E. coli, were immobilized on Ni-NTA columns. Empty Ni-NTA columns (lane 1) were used as controls. Crude extracts of H. polymorpha WT (lanes 1 and 2) or pex7 cells (lane 3) were loaded onto the columns. After washing with buffer, the His-tagged proteins together with bound proteins were eluted using imidazole. Equal portions of the elution fractions were loaded onto an SDS–PAGE gel and subjected to Western blot analysis using antibodies against pyruvate carboxylase (Pyc1p), Pex5p or Pex20p as indicated.*

In order to study the structure of Pex5p and its association with Pex20p, both proteins were produced in *E. coli*, purified (see Fig. 3A,B) and analyzed by electron microscopy (EM).

EM of negatively stained purified Pex5p complexes indicated high numbers of tetrameric particles in one type of projection (not shown). In specimens of the Pex5p-Pex20p mixture small numbers of the same type of closed tetramer were observed (black arrowhead, Fig. 4), but the vast majority of the tetramers was slightly expanded. Many of these open tetramers had one and occasionally two or three globular masses attached (white arrowheads, Fig. 4). A total number of about 14,000 projections of the Pex5p, Pex5p-Pex20p and Pex20p particles were analyzed by single particle electron microscopy. Analysis shows that the purified Pex5p forms a closed tetramer with a diameter of 115 Å (Fig. 5A). This four-fold symmetrical top-view is almost the only type of projection and side-views were very rare. Apparently molecules can not attach to the carbon support film in any stable side-view position, which indicates that the tetramer should be rather flat (see also below for the shape of catalase). Thus it is very likely that each ¼ of the tetramer is compatible to a monomer of Pex5p, if compared to other multi-subunit complexes with known composition and exact mass. With an estimated height of 50-70 Å, a diameter of 115 Å and a mass of a tetramer of 4 x 67 kDa, the tetramers are for instance compatible with the $\alpha_3\beta_3$ F_1 ATP synthase subcomplex (6 x ~55 kDa; 110 Å diameter; height ~ 85 Å) [17]. Indeed, the behaviour of HpPex5p in gel filtration chromatography (not shown) also suggests that the protein is not monomeric, because it eluted in the same range as the marker proteins catalase and ferritin (440 kDa). However, it is in general impossible to draw firm conclusions from size exclusion chromotography about the exact number of copies of a multimeric protein such as Pex5p.

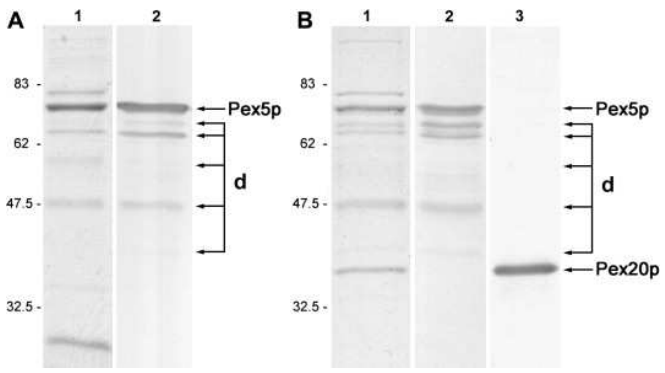

Figure 3. *Purification of Pex5p-His$_6$ and Pex5p-His$_6$/Pex20p-His$_8$ complexes. H. polymorpha Pex5p-His$_6$ and Pex20p-His$_8$ were produced in E. coli. (**A**) Lane 1 shows a Coomassie brilliant blue stained gel of the protein fraction containing HpPex5p. The major protein band at ≈67 kDa represents Pex5p, as is evident from the Western blot decorated with anti-Pex5p antibodies (lane 2). The higher protein band of approx. 80 kDa visible in lane 1 represents Escherichia coli hsp70 as was evident from mass spectrometry analysis (data not shown). The few minor bands of lower molecular weight most likely represent Pex5p degradation products as they are recognized by the anti-Pex5p antibodies (lane 2, indicated by d). (**B**) A gel of a Pex5p and Pex20p containing fraction obtained upon gel filtration of a mixture of Pex5p and Pex20p. Lane 1 shows a gel stained with Coomassie brilliant blue. Lane 2 shows the corresponding Western blot decorated with anti-Pex5p antibodies and lane 3 the corresponding blot stained with anti-Pex20p antibodies. The Pex5p degradation bands are indicated by d.*

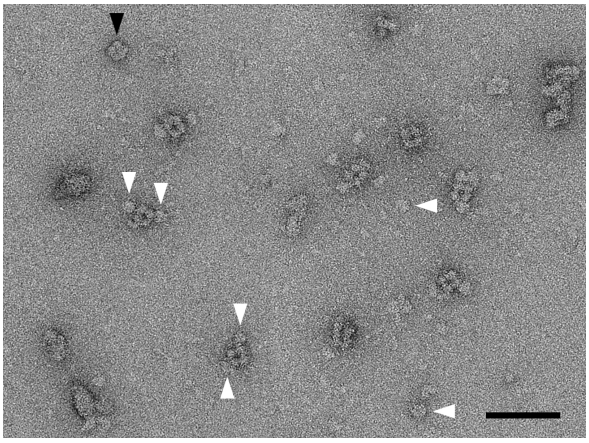

Figure 4. *Electron micrograph of negatively stained Pex5p–Pex20p complexes. The black arrowhead points to a Pex5p tetramer in the closed conformation; the white arrowheads indicate Pex20p in the open conformation, either attached to Pex5p or as single complexes. The bar indicates 50 nm.*

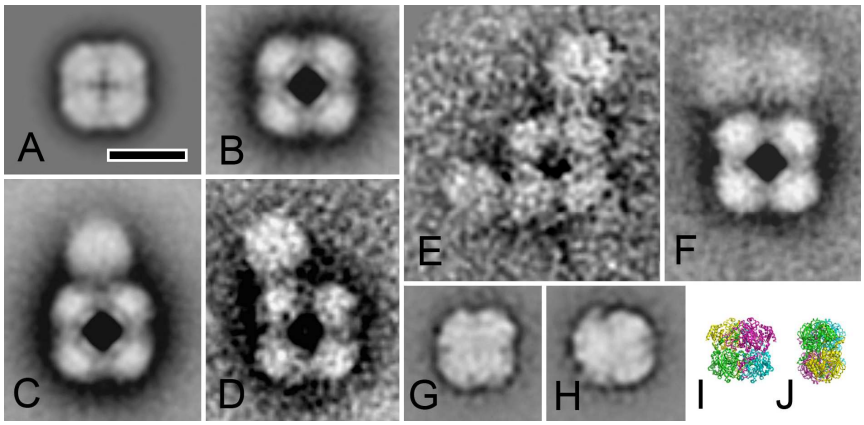

Figure 5. *Single particle image analysis of Pex5p, Pex5p–Pex20p and Pex5p–Pex20p-catalase complexes. (**A**) Average projection map of purified Pex5p in the closed conformation. (**B**) Average projection map of purified Pex5p in the open conformation. (C) Main view of the Pex5p–Pex20p complex. (**D**) Average map of a small class of Pex5–Pex20p complexes in which the upper Pex20p multimer is displaced. (**E**) Another class of Pex5p–Pex20p complexes in which a Pex20p multimer second multimer is binding to the left side of the Pex5p tetramer. (F) Main class of Pex5p–Pex20p-catalase complexes (**G,H**) main views of purified catalase tetramers. (**I**) High-resolution catalase X-ray model in a position similar to the EM projection of image G, in which it is slightly tilted out of its fourfold symmetrical view. (**J**) Side-view of the X-ray model (Sugadev et al.UNPUBLISHED) in which two monomers are almost in overlap with two others. Fourfold symmetry was imposed on images of (**A**) and (**B**) after completion of analysis. The bar equals 10 nm.*

The EM analyses also revealed that in the Pex5p-Pex20p sample about 75% of the Pex5p tetramers is complexed with a globular mass of about 80 Å in 1-3 copies (Fig. 5C-E). Additional EM experiments with purified Pex20p revealed similar-shaped 80 Å globular densities (not shown), indicating that these globular densities are composed of a Pex20p multimer. In the majority of the Pex5p tetramers the Pex20p multimer binds at the interface between two monomers (Fig. 5C), in small subsets it is displaced (Fig. 5D, E). Previous fluorescence correlation spectroscopy experiments have indicated that the 35 kDa Pex20p protein forms multimers with a mass of about 200 kDa, probably hexamers (Otzen et al. 2005). Unfortunately, the data did not resolve the inner features of Pex20p, probably due to multiple orientations. The resolution in the EM maps of Fig. 5(A, B) is about 20 Å, but in the one of Fig. 5D only about 30 Å. However, the binding of most of the Pex20p multimers to the

Pex5p tetramer is rather specific (Fig. 5C). Binding of Pex20p leads to an unexpected increase in the diameter of the tetramers from 115 Å to 134 Å and a pronounced change of the overall conformation. The increase was observed in 98% of the tetramers from the Pex5p-Pex20p batch, even if no Pex20p was bound (Fig. 5B), which was the case in 25% of the tetramers. Probably, such tetramers had lost the Pex20p multimer after the conformational change upon preparation for EM, because in 5% of Pex5p-Pex20p complexes the Pex20p multimer is almost detached (see upper multimer in Fig. 5E). About 15% of the Pex5p tetramers has a second or third Pex20p complex attached (Fig. 5E and not shown).

The Pex5p-Pex20p complexes eluted from the gelfiltration column before the marker protein thyroglobulin (669 kDa), confirming that both proteins are present in complexes that are larger than the Pex5p tetramers.

Subsequently, we aimed to study the binding of potential cargo to the Pex5p-Pex20p complexes. To this end, the PTS1 protein catalase was used. Single catalase tetramers could be averaged with reasonable detail after statistical analysis and classification (Fig. 5G, H). Figure 4(G) shows a class-sum which matches the high-resolution X-ray structure of catalase of Fig. 5I. Side-views of the catalase tetramer, such as presented in Fig. 5 (J), were not observed. Samples of Pex5p-Pex20p complexes incubated with catalase were inspected for larger complexes. Small numbers of Pex5p-Pex20p-catalase complexes could be observed. Classification indicates only binding of catalase at the periphery of the Pex5p tetramers, preferentially next to a Pex20p multimer. An averaged sum of the best 153 complexes shows, however, a fuzzy appearance of the Pex20p multimer (left) and the catalase tetramer (Fig. 5F). The assumed catalase density has the expected overall dimensions deduced from the purified catalase, but can not be assigned more positively. However, we do not consider the second density to be another Pex20p multimer, because we did not find any significant numbers of such particles with two Pex20p multimers at one side of the Pex5p tetramer before admission of catalase. The blurred circumference of the catalase in Fig. 5(F) strongly suggests that it is bound at slightly different positions within the Pex5p-Pex20p-catalase complexes. Hence no further conclusions on the precise binding of catalase (in top- or side view orientation) can be drawn.

Our data convincingly demonstrate that *H. polymorpha* Pex5p is arranged as a tetramer. Also, the conformational change of the Pex5p tetramer associated with Pex20p

binding is clearly resolved. The widening of the tetramer most likely occurs via a major rearrangement of protein domains. This rearrangement could lead to replacement of the hinge region, which has been assigned in the atomic structure (Gatto et al. 2000) and which could lead to a movement of TPRs1-3 in respect to TPRs 4-6. It would be tempting to fit the atomic X-ray structure into the EM map of Pex5p. However, the fact that the X-ray structure only contains a fragment of Pex5p and that the EM map has a much lower (20 Å) resolution makes it impossible to relate them at the current stage. This prevents speculating about domains of Pex5p which might be important for cargo transport at the atomic level. Further research will be necessary to clarify if the open centre has this specific function, or if it is a secondary effect of a conformational change in the centre of each Pex5p monomer. Nevertheless, the lower-resolution EM data clearly indicate that the peripheral binding of Pex20p and catalase to the Pex5p tetramer appears to be relevant. Since also folded proteins can be translocated over the peroxisomal membrane (Goodman et al. 2006b), we speculate that the Pex5p-Pex20p-catalase complex is a structural entity that can be transported over the membrane. This would suggest that - like in higher eukaryotes - import of PTS1 and PTS2 proteins also converges at the level of the receptor complexes in lower eukaryotes, as recently suggested (Kiel et al. 2006).

The *H. polymorpha* Pex5p-Pex20p complex is one of the few complexes involved in the transport of folded proteins which has been structurally characterized. Another system is the twin-arginine (Tat) translocation system of bacteria, but this system has no structural similarity to the Pex5p-Pex20p complex (Oates et al. 2003).

Acknowledgements: Wilma Bergsma, Wilko Keegstra and Gert Oostergetel for help with electron microscopy, Anne Koek for growing yeast cells in chemostat cultures, Wim Huibers for performing mass spectrometry and Marten Veenhuis for discussions and critical reading of the manuscript. EJB acknowledges financial support from the Netherlands Proteomics Centre (NPC). DW and IvdK are supported by a grant of the Earth and Life foundation (ALW), which is subsidized by the Netherlands Organization for Scientific Research (NWO).

REFERENCES

Abrahams, J.P., Leslie, A.G.W., Lutter, R. and Walker, J.E. (1994) Structure at 2.8-Angstrom resolution of F1-ATPase from bovine heart-mitochondria. Nature 370 (6491), 621-628.

Aho, E.L., Murphy, G.L. and Cannon, J.G. (1987) Distribution of specific DNA sequences among pathogenic and commensal *Neisseria* species. Infect. Immun. 55, 1009–1013.

Boteva, R., Koek, A., Visser, N.V., Visser, A.J., Krieger, E., Zlateva, T., Veenhuis, M. and Van der Klei, I.J. (2003) Fluorescence analysis of the *Hansenula polymorpha* peroxisomal targeting signal-1 receptor, Pex5p. Eur. J. Biochem. 270 (21), 4332-4338.

Carvalho, A.F., Costa-Rodrigues, J., Correia, I., Costa Pessoa, J., Faria, T.Q., Martins, C.L., Fransen, M., Sa-Miranda, C. and Azevedo, J.E. (2006) The N-terminal half of the peroxisomal cycling receptor Pex5p is a natively unfolded domain. J. Mol. Biol. 356 (4), 864-875.

Costa-Rodrigues, J,, Carvalho, A.F., Fransen, M., Hambruch, E., Schliebs, W., Sa-Miranda, C. and Azevedo, J.E. (2005) Pex5p, the peroxisomal cycling receptor, is a monomeric non-globular protein. J. Biol. Chem. 280 (26), 24404-24411

Frank, J. (2002). Single-particle imaging of macromolecules by cryoelectron microscopy. Annu. Rev. Biophys. Biomol. Struct. 31, 309–319.

Gatto, G.J., Geisbrecht, B.V., Gould, S.J., Berg, J.M. (2000) Peroxisomal targeting signal-1 recognition by the TPR domains of human PEX5. Nature Str. Biol. 7 (12), 1091-1095.

Gatto, G.J., Maynard, E.L., Guerrerio, A.L., Geisbrecht, B.V., Gould, S.J. and Berg, J.M. (2003) Correlating structure and affinity for PEX5:PTS1 complexes. Biochem. 42 (6), 1660-1666.

Kiel, J.A., Veenhuis, M. and van der Klei, I.J. (2006) PEX genes in fungal genomes: common, rare or redundant. Traffic 7 (10), 1291-1303.

Koek, A. (2006) Peroxisomes in *Hansenula polymorpha*. PhD Thesis University of Groningen, The Netherlands.

Leon, S., Zhang, L., McDonald, W.H., Yates, J., Cregg, J.M. and Subramani, S. (2006a) Dynamics of the peroxisomal import cycle of PpPex20p: ubiquitin-dependent localization and regulation. J. Cell Biol. 172 (1), 67-78.

Leon, S., Goodman, J.M. and Subramani, S. (2006b) Uniqueness of the mechanism of protein import into the peroxisome matrix: Transport of folded, co-factor-bound and oligomeric proteins by shuttling receptors. Biochim. Biophys. Acta 1762 (12), 1552-1564.

Oates, J., Mathers, J., Mangels, D., Kühlbrandt, W., Robinson, C. and Model, K. (2003) Consensus structural features of purified bacterial TatABC complexes. J. Mol. Biol. 330 (2), 277-286.

Otzen, M., Wang, D., Lunenborg, M.G.J. and van der Klei, I.J. (2005) *Hansenula polymorpha* Pex20p is an oligomer that binds the peroxisomal targeting signal 2 (PTS2). J. Cell. Sc. 118 (15), 3409-3418.

Penczek, P., Radermacher, M. and Frank, J. (1992) Three dimensional reconstruction of single particles embedded in ice. Ultramicr. 40 (1), 33-53.

Schliebs, W., Saidowsky, J., Agianian, B., Dodt, G., Herberg, F.W. and Kunau, W.H. (1999) Recombinant human peroxisomal targeting signal receptor PEX5. J. Biol. Chem. 274 (9), 5666–5673.

Stanley, W. A., Filipp, F.V., Kursula, P., Schuller, N., Erdmann, R., Schliebs, W., Sattler, M. and Wilmanns, M. (2006) Recognition of a functional peroxisome type 1 target by the dynamic import receptor pex5p. Mol. Cell. 24 (5), 653-663.

Sugadev, R., Balasundaresan, D., Ponnuswamy, M.N., Kumaran, D., Swaminathan, S. and Sekar, K. The crystal structure of bovine liver catalase. UNPUBLISHED, PDB entry: 1TGU.

Van Heel, M. (1987) Similarity measures between images. Ultramicr. 21 (1), 95-100.

Van Heel, M., Gowen, B., Matadeen, R., Orlova, E.V., Finn, R., Pape, T., Cohen, D., Stark, H., Schmidt, R., Schatz, M. and Patwardhan, A. (2000) Single-particle electron cryo-microscopy: towards atomic resolution. Quat. Rev. Biophys. 33 (4), 307–369.

Wang, D., Visser, N.V., Veenhuis, M. van der Klei, I.J. (2003). Physical interactions of the Peroxisomal Targeting Signal 1 receptor Pex5p, studied by fluorescence correlations spectroscopy. J. Biol. Chem. 278 (44), 43340–43345.

Chapter 3

A search for peroxisomal membrane protein complexes by BN-PAGE, Mass Spectrometry and Electron Microscopy

Katarzyna B. Moscicka , Hans-Peter Braun & Egbert J. Boekema

ABSTRACT

In the last decades many of the Pex proteins, involved in protein transport over the peroxisomal membrane, have been genetically and biochemically characterized in detail and models of their interactions have been proposed. However, the models are not based on direct structural studies, such as single particle electron microscopy, which means that there are still many unsolved problems related to these large complexes. We explored the use of Blue-Native Gel electrophoresis (BN-PAGE), which is one of the best methods to purify large, transient membrane complexes, and in combination with biochemical characterization, and mass spectrometry looked for ways to assign subunit compositions and interactions.

Here, we have performed a pilot study of the major peroxisomal membrane complexes in the yeast species *Saccharomyces cerevisiae* and *Hansenula polymorpha*. We have monitored the presence and purification of large, hypothetical Pex complexes by using western blotting with specific antibodies against Pex14p. However, upon 1D and 2D/SDS Blue Native gels electrophoresis from peroxisomal fractions only few protein bands could be attributed to peroxisomes. In fact, no large Pex protein complexes were found, which we also proved by mass spectrometry. This could be related to a very low amount of peroxisomal membrane proteins compared to mitochondrial proteins. Peroxisomes were obtained by differential and sucrose density centrifugation and mitochondria were the major contaminating organelles in purified peak fractions. It appears that further purification of the initial membranes is crucial. This requires more advanced techniques and better separation protocols to separate peroxisomes from mitochondria.

INTRODUCTION

Eukaryotic cells are characterized by the presence of organelles that are involved in various metabolic processes (e.g. mitochondria, Golgi apparatus etc.). Microbodies including peroxisomes also belong to this group. They are ubiquitous organelles involved in numerous catabolic and anabolic pathways in eukaryotic cells (Van den Bosch et al. 1992). Their biogenesis can be conceptionally divided into different functional aspects including organelle segregation during the course of cell division, membrane biogenesis and import of matrix proteins (Kunau 1998). The function of peroxisomes depends on the organism, tissue, developmental stage and environmental conditions, like in the case of yeast and fungi.

In general, there are only low numbers of enzymes associated with the microbody membrane. Sulter and co-workers (1993) showed by freeze fracture electron microscopy that the peroxisome membranes possess a very low content of large integral membrane proteins. Based on their function, these membranes must contain proteins involved in matrix protein import, membrane protein insertion, organellar maintenance and solute transport.

The major group of known peroxisome-bound proteins are peroxins. To date 32 different peroxins have been indentified (Vizeacoumar et al. 2004; Van der Zand et al. 2006). Several of these proteins have been predicted to appear in larger homomeric or heteromeric complexes (Sacksteder and Gould 2000; Subramani et al. 2000; Agne et al. 2003). Many of the known peroxins are essential for peroxisomal matrix protein import. Both Pex5p and Pex7p are the import receptors that specifically recognize PTS1 and PTS2, respectively. PTS receptors are predominantly soluble proteins that bind their cargo proteins in the cytosol and then target them to the peroxisomal membrane, from where the matrix proteins are imported into the organelle and then the free receptors are recycled back to the cytoplasm (Marzioch et al. 1994; Dodt and Gould 1996). The steps in which the import receptor is membrane associated can be subdivided into three distinct stages: (I) docking of the receptor to the recognition machinery at the membrane (consisting of at least Pex13p, Pex14p and Pex17p), (II) transfer and release of cargo proteins and (III) dissociation of the receptor from the organelle into the cytoplasm (by Pex4p and Pex22p).

It is well established that Pex13p, Pex14p, and Pex17p contribute to or mediate the docking of the receptors to the *cis*-side of the peroxisomal membrane (Subramani et al. 2000; Holroyd and Erdmann 2001). Pex13p and Pex14p recognize and physically bind both of the import receptors, Pex5p and Pex7p. Lutz (2004) showed by using BN-PAGE that Pex14p was present as a protein complex of approximately 450-550 kDa and 900 kDa in *H. polymorpha* and *S. cerevisiae*, respectively.

A second group of membrane proteins consist of Pex2p, Pex10p, and Pex12p. These three peroxins are integral membrane proteins of peroxisomes and contain a RING zinc finger at the C-terminal part. Impaired function of these three peroxins results in the failure of matrix protein import, implying that RING peroxins are involved in the process of protein transport across the membrane, possibly as members of import machinery constituents. Moreover, Pex2p, Pex10p, and Pex12p are mutually distinct in their primary structure except for a commonly shared RING finger (Okumoto et al. 2000). Thus, the RING finger is probably important for the function of these peroxins. The RING finger domains to the *cis* side of the peroxisomal membrane (Holroyd and Erdmann, 2001) exhibit pairwise interactions, and bind the PTS1 receptor Pex5p (Chang et al. 1999). Association of these two subcomplexes into a large complex was observed. Moreover, epistasis analysis predicts that during the peroxisomal import process the RING finger peroxins act downstream of Pex13p, Pex14p, and Pex17p (Collins et al., 2000). This hypothesis predicts that the three RING finger peroxins function together and are involved in the translocation step for receptors and cargo (Gould and Collins 2002). Five other membrane bound peroxins, Pex1p, Pex6p, Pex4p, Pex22p, and Pex10p are reported to act subsequently to the RING finger peroxins and thus are implicated in posttranslocation events (Collins et al. 2000).

Although biochemical studies of peroxisomal protein complexes suggest many interactions, there are still many open questions which need to be solved about the spatial organization of these subcomplexes, even on the low-resolution level. One of the ways to determine subunit interaction is to use single particle electron microscopy, which is a well-established technique to obtain structural information about large biomolecules at a resolutionof 20 Å, or better. Schliebs et al. 1999 showed the structure Pex5p from human and several years later Moscicka et al. 2007 determined the structure of the Pex5p-Pex20p complex.

In this study we aim to analyse and identify protein complexes at the peroxisomal membranes of the two yeast species *Saccharomyces cerevisiae* and WT *Hansenula polymorpha* using blue native gel electrophoresis (BN-PAGE), mass spectrometry and electron microscopy.

Although we were able to isolate the peroxisome and detect the presence of Pex14p by antibodies in isolated fractions, we did not detect any large Pex complex present after protein solubilization. One of the reasons why it is difficult to detect such complexes is the fact that peroxisomal membrane protein complexes are difficult to separate from the much more abundant mitochondrial membrane complexes. Because we think that it is worth to continue attempts to obtain pure fractions of the largest Pex complexes for structural analysis we present of our analysis in the context of such attempts.

MATERIALS AND METHODS

Strains, media and growth conditions of S.cerevisiae and H.polymorpha

The yeast strain used in this study was wild-type *UTL- 7A* (Erdmann et al. 1991), producing ProtA-TEV-Pex14p. Complete and minimal media used for yeast culturing have been described previously (Erdmann et al. 1989). YNO medium contained 0.1% oleic acid, 0.05% Tween 40, 0.1% yeast extract, and 0.67% yeast nitrogen base without amino acids, adjusted to pH 6.0.

Hansenula polymorpha NCYC495 cells were grown at 37 ^{o}C on mineral medium (van Dijken et al. 1976) supplemented with 0.5 % (w/v) glucose or 0.5 % (v/v) methanol as a carbon source, and 0.25 % (w/v) ammonium sulfate as nitrogen source. Leucine was added at a final concentration of 30 μg ml^{-1}.

Isolation of peroxisome protein complexes from S.cerevisiae by using IgG-Sepharose

Oleate induced yeast cells were lysed according to Agne et al. 2003, using glass beads and lysis buffer (20 mM HEPES, 100 mM KOAc, 5 mM MgOAc [pH 7.5]) containing protease inhibitors (1mM phenylmethyl sulfonyl fluoride (PMSF), 1 mM sodium azide, , 2 μg/ml aprotinin, 0.35 μg/ml bestatin, 1 μg/ml pepstatin, 2.5 μg/ml leupeptin, 0.16 mg/ml

benzamidin, 5 µg/ml antipain, 5 mM sodium fluoride (NaF), 6 µg/ml chymostatin). Cell debris was sedimented, and the supernatant was centrifuged at 100,000 × g at 4 °C for 1 h. A protein concentration of 2.7 mg/ml was obtained. Membrane proteins were solubilized with the detergent digitonin (2% w/v final concentration) at 4°C for 1 hr. Unsolubilized material was removed by centrifugation (30 min., 18.000 × g). For affinity chromatography, the detergent extract was incubated with IgG-Sepharose (Pharmacia) for 12-14 h at 4°C over night on a rotary shaker and the sedimented material was centrifuged for 5 min. at 4 ^{o}C (1500 x g). Bound material was collected, followed by 4x washing with 125 volumes of solubilization buffer containing 1/10 of the detergent concentration used for solubilization together with protease inhibitors. To elute bound protein complexes, 70 U TEV-protease (Invitrogen) and 21 µl solubilization buffer (containing 1/10 detergent concentration) were added to the Sepharose followed by incubation at 16 °C for 2 hr. TEV protease eluates were collected by centrifugation 1 min. (50 x g), and the elution was repeated twice. The native elution fractions were pooled and used directly or stored in small aliquots at −80 °C until use. The purity of subfractions was analyzed by SDS-PAGE followed by silver staining and subsequent Western blot analysis or by two-dimensional blue native PAGE.

Isolation of peroxisomes from wt H. polymorpha by differential centrifugation and sucrose density centrifugation

Methanol induced yeast cells were prepared for homogenization by using pre-incubation buffer (100 mM Tris-HCl [pH 8.0], 50 mM EDTA [pH 8.0] and 140 mM β-Mercaptoethanol), protoplast buffer (50 mM potasium phosphate [pH 7.2], 1.2 M sorbitol) and homogenization buffer (5 mM MES [pH 5.5], 0.1 mM EDTA, 1 mM KCl and 1 M sorbitol) respectively, containing protease inhibitors (1mM PMSF, 2 µg/ml aprotinin, 0.35 µg/ml bestatin, 1 µg/ml pepstatin, 2.5 µg/ml leupeptin, 5 µg/ml antipain). The resulting homogenate of protoplasts was used for differential centrifugation steps (as described by van der Klei 2000), and the organellar pellet was subjected to sucrose density centrifugation. The pellet was resuspended very carefully in a solution of 40% (w/w) sucrose in buffer B (containing 5 mM MES [pH 5.5], 0.1 mM EDTA, 1 mM KCl) and the amount of protein loaded per gradient was 5 mg. Gradients were centrifuged for 2.5 hours and were harvested in 21 fractions. The organellar peak fractions were identified by performing alcohol oxidase (Verduyn et al. 1984) and cytochrome c oxidase (Douma et al. 1985) assays. The peroxisomal peak fractions were

pooled together and the sucrose concentration was measured and lowered to 44%. The collected material was spinned down for 30 min., 18,000 rpm. After spinning down, the supernatant was removed and the pellet was resuspended in lysis buffer [pH 7.5] (20 mM Hepes, 100 mM KOAc, 5 mM MgOAc) containing protease inhibitors (Complete^{TM}, 1mM PMSF, 2 µg/ml aprotinin, 0.35 µg/ml bestatin, 1 µg/ml pepstatin, 2.5 µg/ml leupeptin). To separate peroxisomal membranes from the peroxisomal matrix proteins, the pellet was centrifuged at 100,000 × g at 4 °C for 1 h. The pellet fraction containing peroxisomal membranes were store in small aliquots at - 80^{o}C until use.

Gel electrophoresis procedures and immunobloting

Protein concentrations were determined using the Bio-Rad Protein Assay system (Biorad GmbH, Munich, Germany) with bovine serum albumine as a standard. Proteins were separated by standard SDS-PAGE or one-dimensional Blue Native PAGE according to standard procedures (Schägger and von Jagow 1987). For subunit analysis, gel stripes including the resolved protein complexes were transferred horizontally onto a second gel dimension, which was carried out in the presence of SDS (two-dimensional Blue native/SDS-PAGE). Proteins were visualized by Coomassie Blue-colloidal staining (Neuhoff et al. 1985 and 1990), silver stain or blotted onto nitrocellulose filters. Blots were incubated with Pex14p antibody from *H. polymorpha*. Selected protein complexes were cut out from Coomassie Blue-stained two-dimensional blue-native gels and subunits were identified by mass spectrometry.

Electron Microscopy

Negatively stained specimens were prepared with 2% uranyl acetate on glow-discharged carbon-coated copper grids. Electron microscopy was performed on a Philips CM10 FEG electron microscope operated at 100 kV. Images were recorded at 34000 x magnification with a pixel size (after binning the images) of 3.75 Å at the specimen level.

RESULTS

Purification and solubilization of Peroxin Complexes from S.cerevisiae

In order to investigate peroxisomal membrane protein complexes, we first performed an isolation procedure from total cellular membranes of *S.cerevisiae* without separating organelles. Peroxin-containing complexes were isolated by IgG affinity chromatography, utilizing TEV-ProtA-tagged peroxins. Previous work on protein complexes of the respiratory chain from mitochondrial membranes had demonstrated that the solubilization conditions have a significant impact on the composition and integrity of the isolated complexes (Schägger and Pfeiffer, 2000). We aimed here to test efficient solubilization conditions and as a criterion for solubilization, we employed a centrifugation step of 100,000 × g for 1 h. We chose to follow enrichment in Pex complexes by monitoring protein A fusion of Pex14p because that protein has been implicated in multiple interactions with other peroxins. ProtA-TEV-Pex14p was isolated via IgG-Sepharose chromatography from supernatants obtained after solubilization with 1% digitonin.

Data obtained by Agne and co-workers (2003) indicated that only solubilization of the membranes with digitonin gives sufficient amounts of apparently intact peroxisomal membrane protein complexes. Aliquots of TEV protease eluates, representing equal amounts of membranes, were separated by SDS-PAGE and stained with Coomassie or silver staining, and whole lanes were analyzed by mass spectrometry and subsequently compared with yeast database searches. Pex14p could be detected by Western blotting decorated by a specific antibody against Pex14p (Fig. 2A). However, mass spectrometry analysis on several gels from independent solubilization experiments did not indicate any (large) Pex complexes present in the eluates (Fig. 2B). However, an electron microscopy analysis indicated the presence of the dimeric ATP synthase from mitochondria (Fig. 1). This complex is easy recognizable because of its large size and specific shape (Dudkina 2006).

Analysis of fractions from S. cerevisiae from affinity purification by electron microscopy.

Negatively stained specimens of the solubilized peroxisomal fractions were found to contain a large contamination with dimeric ATP synthease molecules, which is a

mitochondrial supercomplex that can be recognized by its characteristic shape (Fig. 1). Further investigation by BN-PAGE gel electrophoresis and mass spectrometry proved that the fractions contained a lot of contamination with mitochondria proteins and no peroxisomal proteins were found.

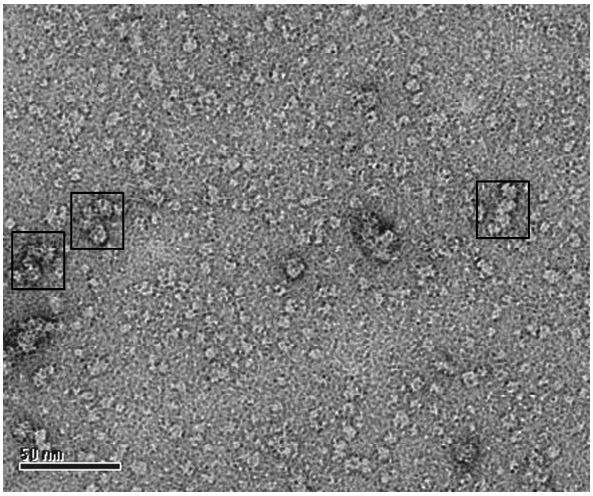

Figure 1. *Electron micrograph of a negatively stained membrane fraction after solubilization with 1% digitonin. The black boxes indicate ATP synthase dimers. Scale bar is 50 nm.*

In a next set of experiments, affinity purification from a total cellular fraction was abandoned. Instead, organelles were first separated only by differential centrifugation, according to the methods section (purification and solubilization of Peroxin Complexes from *S.cerevisiae*). From the peroxisomal fraction, membrane solubilization was performed with 5 % digitonin or with 10% n-dodecyl β-D-maltoside (DDM). The composition of generated fractions with 5% digitonin was tested by 1D blue native PAGE (Fig. 3). Several high molecular weight bands (MW) could be detected. The question now was to establish which of the protein bands observed after BN-PAGE are peroxisomal in nature. The reason for this is related to the fact that only a small portion of the total membrane proteins (approx. 5%, according to Janssen en Janssen 2001) represents peroxisomal proteins. This is in contrast to mitochondria, which contribute about 80% of the total membrane fraction. To check for the presence of specific mitochondrial complexes, solubilized membranes from mitochondrial peak fractions from *S. cerevisiae* were used as control (Fig. 3, lane 1). Comparison of the gel patterns indicates that some bands in the peroxisomal fraction run at a position where there is no strong profile of a mitochondrial protein, especially at the position of boxes 1, 5, 8 and 9 (Fig. 3, lane 2). Therefore 12 bands of interest were cut out and submitted to mass spectrometry (highlighted by boxes in Figure 3, lane 2). After detailed examinations, once again no Pex complexes were found in analysed bands. This suggest that an increase in

detergent concentration (from 1% to 5 % digitonin) or the change to a stronger detergent (10% n-dodecyl β-D-maltoside, data not shown) could not induce the isolation of any large peroxisomal complex.

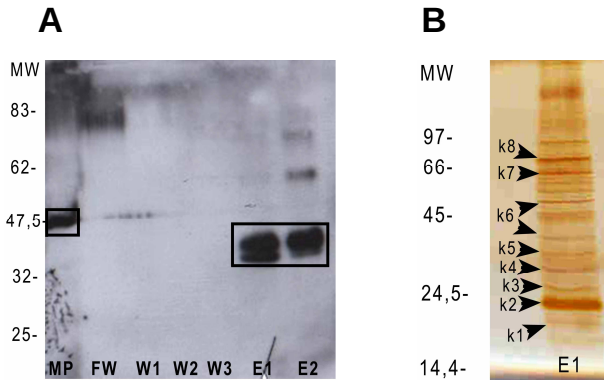

Figure 2. *Pex14p-containing complexes from peroxisomal membranes analyzed by immunoblotting and mass spectrometry. Protein complexes were solubilized with 1% digitonin from isolated membranes of S. cerevisiae cells producing Pex14p-TEV-ProtA and purified via IgG-Sepharose affinity chromatography. (A) Western blot decorated using α-Pex14p antibody. The data show that a Pex14p signal was detected in peroxisomal membrane pellet (MP), E1 (elution) and E2. The presence of the Pex14p is indicated by the black boxes. In FW (flow thro) and W1-3 (washing) no signal is detected (as predicted). (**B**) A silver stained gel where the bands from elute fraction (lane E1 gel A) were cut and analyzed by mass spectrometry (pointed by arrows). Bands analyzed by mass spectrometry:* ***K1 –*** *ubiquinol-cytochrome-c reductase or H+ transporting two-sector ATPase (maybe Pex11p);* ***K2 –*** *TEV protease band;* ***K3 –*** *VDAC1, outer mitochondrial membrane protein porin 1;* ***K4 –*** *heat shock protein HSP60 precursor, mitochondrial;* ***K5 –*** *YSCE1B NIB;* ***K6 –*** *ubiquinol-cytochrome-c reductase;* ***K7 –*** *heat shock protein HSP60 precursor, mitochondrial;* ***K8 –*** *heat shock protein SSA1 or SSA2. In analyzed bands no Pex14p or other Pex proteins were detected.*

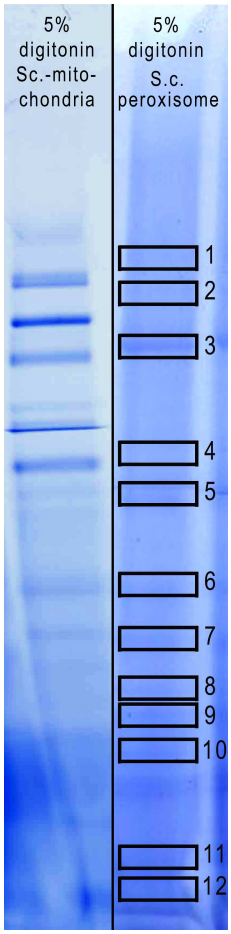

Figure 3. *Separation of peroxisomal protein complexes by BN-PAGE using a 4.5 - 16% gradient gel. The bands represent protein complexes found after solubilization of peroxisomal membranes from S. cerevisiae with 5% digitonin, in the supernatant after centrifugation to remove non-solubilized material. All visible bands were cut out and analysed by mass spectrometry. Boxes with numbers (1-12) mark bands analysed and assigned by mass spectrometry:* ***1****-cytochrome* c_1*;* ***2****- subunit 2 of ubiquinol cytochrome;* ***3****-ATP 1, beta subunit of ATPase;* ***4****- HSP60;* ***5****-Subunit of mitochondrial NAD(H)* specific isocitrate dehydrogenase*;* ***6****-CDC19, Pyruvate kinase;* ***7****-KGD1, component of the mitochondria alpha subunit;* ***8****- Alcohol dehydrogenase isoenzyme;* ***9****-CIT1, citrate synthase;* ***10****-Acetyl CoA hydrolase;* ***11****-Phosphoenolpyruvate carboxykinase;* ***12****-RPS1, Ribosomal protein 10*

Purification and solubilization of Peroxin Complexes from H. polymorpha

Since the investigations with *S. cerevisiae* gave only negative results, experiments were continued with starting material from *H. polymorpha*. In addition to the differential centrifugation step, an additional sucrose density gradient centrifugation was applied to improve the purification process. Organelles present in the homogenate of protoplasts prepared from methanol-grown *H. polymorpha* cells were separated by differential and sucrose density centrifugation (van der Klei 2000). Peroxisomal peak fractions were pooled and subjected to an osmotic shock, followed by centrifugation at 100,000 g in order to separate matrix components from the membranes. Several detergents were tested to solubilize peroxisomal membrane proteins. Aliquots of the washed membrane pellet were solubilized in

buffer containing digitonin or DDM (n-dodecyl β-D-maltoside) at different concentrations and were later centrifuged. A 1D Blue-native PAGE was carried out to monitor the protein complex composition from the peroxisomal yeast fractions of the sucrose gradient (data not shown), followed by 2D/SDS PAGE gel electrophoresis. The resulting bands were cut and analyzed by mass spectrometry. Peroxisomal fractions solubilized with 5% digitonin were submitted to 2D/SDS PAGE and visible spots (red circles) were analyzed by mass spectrometry (Figure 4B and C). Figure 4A presents a control experiment in which membranes isolated from mitochondrial peak fractions of *S. cerevisiae* were solubilized by 5% digitonin.

After detailed examinations by mass spectrometry, once again no large Pex complexes of interest, such as a docking complex composed of Pex14p, Pex17p, pex13p, were found in analysed spots. Nevertheless, the presence of several others peroxisomal proteins was detected (legend to figure 4). In parallel, we performed immunoblotting experiments with Pex14p (Fig. 2D) where we could detect its presence in the membrane fractions, but the observed molecular mass of 20 kDa suggests that the complex had already degraded during sample preparation. We have also used Pex10p antibody but the signal was not detected (data not shown). Our data clearly indicates that the membrane fractions were once again contaminated with mitochondrial proteins.

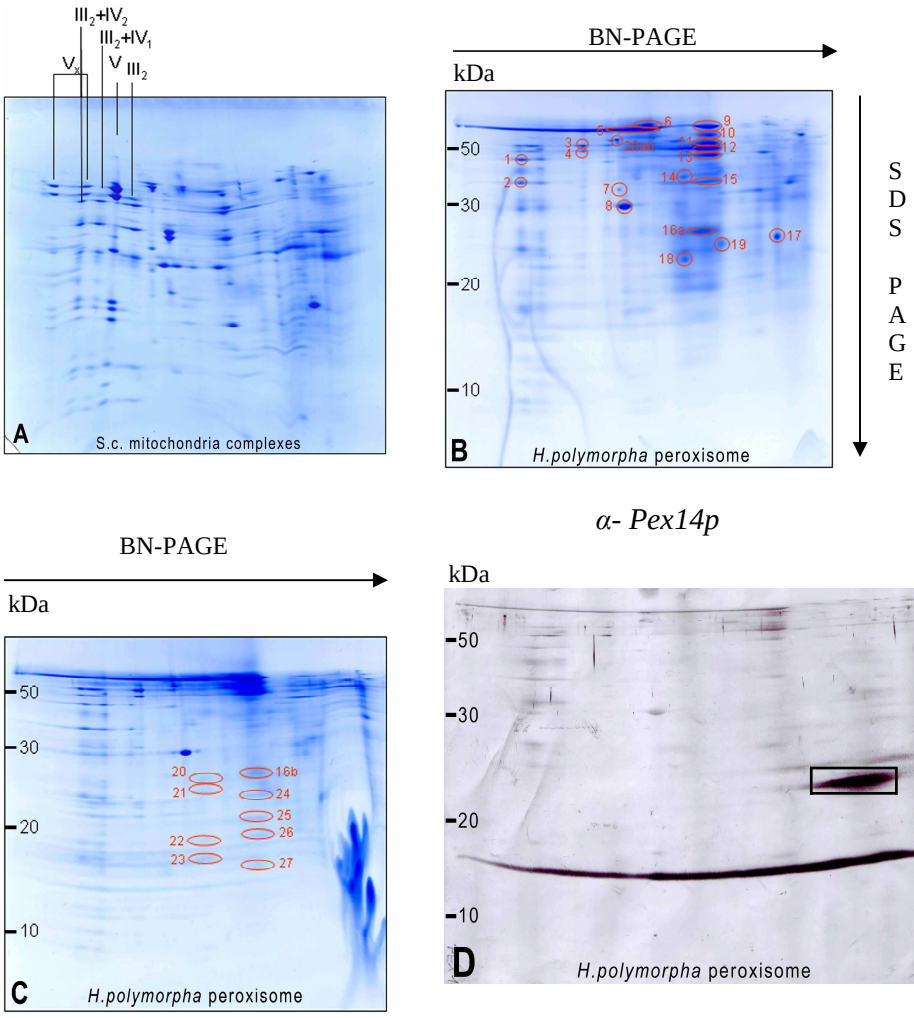

Figure 4*. Purification of the peroxisomal complexes by sucrose gradient ultracentrifugation. Peroxisomal membrane proteins from yeast were solubilized by digitonin (5 g detergent per g protein) and resolved by ultracentrifugation as described under "Material and Methods". All fractions were analyzed by one-dimensional Blue native-PAGE (data not shown) to monitor their protein complex content. (**A**) Mitochondrial membrane protein complexes from S. cerevisiae solubilized by 5% digitonin. (**B,C**) Peroxisomal protein complexes were identified by parallel two-dimensional Blue native-SDS-PAGE and identified by mass spectrometry. Fractions 1 to 28ab contain respectively: **1-** similarity to ubiquinol--cytochrome-c reductase 44K core protein; **2-** ubiquinol-cytochrome-c reductase 40K chain II precursor; **3-** F1F0-ATPase complex, F1 alpha subunit ; strong similarity to alpha subunit of H+transporting two- sector ATPase MGI2 - Kluyveromyces lactis; **4-** mitochondrial F1F0-ATPase subunit beta ; strong similarity to F(1)F(0)-ATPase complex beta subunit ATP; **5-** strong similarity to*

transketolase – S. cerevisiae; ***6-*** *strong similarity to transketolase – S. cerevisiae;* ***7-*** *transport protein USO1 – S. cerevisiae;* ***8-*** *Porin/voltage-dependent anion-selective channel protein ; strong similarity to mitochondrial outer membrane porin POR1/YNL055C – S. cerevisiae;* ***9-*** *strong similarity to transketolase – S. cerevisiae;* ***10-*** *strong similarity to TFIIIB 90 kDa subunit – S. cerevisiae;* ***11-*** *identity to thymocyte nuclear protein 1 ; strong similarity to hypothetical protein - Mus musculus;* ***12-*** *strong similarity to iso-1-cytochrome c – S. cerevisiae;* ***13-*** *similarity to protein required for mitochondrial iron-sulfur cluster biosynthesis; strong similarity to hypothetical protein – S. cerevisiae;* ***14-*** *Myosin-1 (Type II myosin); similarity to myosin-1 isoform (type II myosin) heavy chain S. cerevisiae;* ***15-*** *strong similarity to SMC chromosomal ATPase family member – S. cerevisiae;* ***16a-*** *similarity to integrin analogue gene USO1- S. cerevisiae;* ***16b-*** *similarity to SYnthetic lethal with cdcForty – S. cerevisiae; Pre-mRNA-splicing factor syf2;* ***17-*** *similarity to integrin analogue gene USO1- S. cerevisiae;* ***18-*** *Myosin-1 (Type II myosin); similarity to myosin-1 isoform (type II myosin) heavy chain S. cerevisiae;* ***19-*** *strong similarity to component of exocyst complex – S. cerevisiae;* ***20-*** *strong similarity to a protein essential for assembly of a functional mitochondrial ATPase complex – S. cerevisiae;* ***21-*** *no homology; weak similarity to AMP deaminase – S. cerevisiae;* ***22-*** *Putative peroxiredoxin-A (Thioredoxin reductase) (Peroxisomal membrane protein A) (PMP20); strong similarity to peroxisomal membrane protein 20 CbPMP20 - Candida boidinii;* ***23-*** *histone H3 ; strong similarity to histone H3 - Hypocrea jecorina;* ***24-*** *Emp24p; strong similarity to component of the COPII-coated vesicles, 24 kDa EMP24/YGL200C – S. cerevisiae;* ***25-*** *Putative peroxiredoxin-A (Thioredoxin reductase) (Peroxisomal membrane protein A) (PMP20); strong similarity to peroxisomal membrane protein 20 CbPMP20 - Candida boidinii;* ***26-*** *strong similarity to nucleoside diphosphate kinase – S. cerevisiae;* ***27-*** *Putative peroxiredoxin-A (Thioredoxin reductase) (Peroxisomal membrane protein A) (PMP20); strong similarity to peroxisomal membrane protein 20 CbPMP20 - Candida boidinii;* ***28-*** *Myosin-1 (Type II myosin); similarity to myosin-1 isoform (type II myosin) heavy chain – S. cerevisiae.* ***(D)*** *Immunological localization of Pex14p detected by antibody against that protein.*

DISCUSSION

In this report, we aimed to purifiy and characterize membrane-bound subcomplexes of the peroxisomal import machinery. These are the docking complex containing Pex14p, Pex17p, and Pex13p, and the RING finger complex comprising Pex2p, Pex10p, and Pex12p. We have tried to isolate the Pex14p complex from two different yeast species: *S. cerevisiae* and *H. polymorpha*. First we used the Pex14p-TEV-ProtA producing *S. cerevisiae* strain to isolate peroxin-containing complexes from peroxisomal membranes by IgG affinity chromatography. We chose the proteinA fusions of Pex14p as affinity target, because Pex14p has been implicated in multiple interactions with other peroxins. Secondly, with the same purpose of isolating peroxisomal membrane proteins, we used WT cells from *H. polymorpha.* In both methods, we have used BN-PAGE elecrophoresis together with mass spectrometry and electron microscopy for the analysis and presence of membrane proteins in protein complexes. Our analysis shows the presence of Pex14p by Western Blots (Fig. 2A). Upon comparison the *S. cerevisiae* protein patterns in Coomasie stained BN-PAGE gels (Fig. 3) prepared from membranes of purified mitochondrial fractions (lane 1, Fig. 3) and total peroxisomal membrane (lane 2, Fig. 3) we detected a number of 'peroxisomal' protein bands which were different from mitochondrial bands. However, detailed analysis by mass spectrometry showed no presence of any Pex protein in the gel. The same results were obtained in a second experiment were we used WT cells from *H. polymorpha*. In 2D/SDS PAGE gels (Fig. 4B and C) from peroxisomal fractions solubilized by 5% digitonin and analysed by mass specrometry we did not detect any major peroxisomal protein complexes, however the other peroxisomal proteins were detected. The Western Blot on 2D/SDS BN-PAGE gel (Fig. 4D) detected the presence of Pex14p but because the molecular weight of Pex14p is around 47 kDa the band which was observed, running at 20 kDa, probably contains a degradation product of Pex14.

Our analyses indicate that isolation of peroxin complexes from peroxisomes is not an easy task. It can be due to the well-known fact that peroxisomal membranes contain only low numbers of integral membrane components, in contrast to mitochondrial membranes, which are densily packed with large membrane proteins, with over 30 subunits for the yeast complex I. Hence it now appears crucial to purify such membranes to homogeneity, if possible, because otherwise they give a huge contamination. With classical methods like differential and sucrose centrifugation steps it is quite difficult to perform this, given the fact that

mitochondrial membrane proteins are possibly in the order of 50 times more abundant. Some novel cell and organelle separation methods will be discussed at the end of this discussion.

It is possible that our Pex protein complexes, followed by the marker Pex14p, were lost during sample preparation which includes 1) separation of peroxisomes by ultracentrifugation, 2) detergent solubilization, 3) removal of unsolubilized material by ultracentrifugation and 4) gel chromatography. Firstly, it is unlikely that whole peroxisomes are lost during ultracentrifugation, because the applied sedimention force is strong enough to spin them down. Moreover, the presence of Pex14p was detected by immunoblotting before subjecting it to BN-PAGE electrophoresis (data not shown). Secondly, the most important step during sample preparation for BN-PAGE is adding the detergent solubilization. However, we cannot compare the samples before and after detergent solubilization (digitonin or DDM), because there are intact mitochondria in the fractions and they would close the slots of the BN gel so that nothing could enter into the matrix of the gel. We also checked different detergents under variable conditions and none of them worked fine. One further check could be to test the presence of the Pex14p by SDS-PAGE and Western blotting. Thirdly, we cannot make a full comparison after adding the detergent, because proteins remaining in the very last pellet after centrifugation could not be resuspended at all. Again, these proteins, in the form of aggregates, can not be separated on a BN gel, like mitochondria.

We conclude that the problem of the absence of Pex proteins is due to sample preparation before BN-PAGE, but that this conclusion was not so evident from previous work. For example, the method which was used by Marco Lutz (2004; in Chapter 3 of his Ph.D thesis) and Agne et al. (2003) did not differ substantially from ours, because the same detergents (digitonin and DDM) were applied and also similar buffers to isolate the peroxisomal membranes. However, Lutz did not show any Coomassie-stained 2D BN/SDS gels. Pex proteins only were detected by immunostaining of 2D BN/SDS gels, which does not tell us much about purity. Nevertheless, he detected several mitochondrial protein bands and he also showed that solubilization did not result in loss in Pex14p. However, we still cannot explain why we could not detect any Pex protein complexes after solubilization. Even, if we would specifically loose peroxisomal membranes during sample preparation, this still would not explain why we see so many mitochondrial proteins.

In general, the peroxisomal isolation and membrane solubilization need to be improved. The yield of the peroxisomes is still very low and the minor contamination with mitochondria in the peroxisomal peak fractions, leads to an overrepresentation of mitochondrial proteins due to the very high protein content of mitochondrial membranes which are too difficult to remove during the isolation procedures. There are several ways to apply separation methods which are not based on differential centrifugation. Hansel et al. (1991) proposed an Immunomagnetic Cell Separation system to separate neutrophils from eosinophils. Superparamagnetic particles were coupled to a monoclonal antibody against CD16, a molecule present on neutrophils but not on eosinophils. A peripheral blood granulocyte preparation, containing neutrophils and eosinophils, was incubated with these anti-CD16 particles. In the magnetic field of a permanent magnet, magnetically labelled neutrophils were then retained on columns with a ferromagnetic matrix. By this negative selection procedure, eosinophils of 99.5% purity were obtained. This method has been widely applied in biochemistry. Rodriguez-Paris et al. (1993) 5. J.M. Rodriguez-Paris, K.V. Nolta and T.L. Steck. *J. Biol. Chem.* (1993), pp. 9110–9116. View Record in Scopus Cited By in Scopus have used magnetic chromatography to separate lysosomes that were loaded with iron dextran by endocytosis. Another novel method is free-flow electrophoresis (FFE) which is used together with differential centrifugation and density gradient purification methods. FFE was used to increase the purity of mitochondrial isolates from *Arabidopsis thaliana* by separating them from plastids and peroxisomes according to differences in the surface charge of each organelle, yielding mitochondria that have seven times less contamination (Eubel et al. 2007). At a charge difference of 800 V, mitochondria, peroxisomes, and other cellular material could be separated in FFE, without overlap (Eubel et al. 2008). We expect that FFE will also work for separating yeast peroxisomes and mitochondria, if the optimal charge difference is found experimentally.

In conclusion, with novel separation methods the isolation procedure of peroxisomes could be improved in the near future. Together with novel purification protocols this will open new territories in the study of the structure of large, intact peroxisomal membrane complexes.

Acknowledgements

We thank Wim Huibers for performing mass spectrometry experiments and Stephanie Sunderhaus for expert advise and help in performing BN-PAGE gels.

REFERENCES

Agne, B., Meindl, N.M., Niederhoff, K., Einwächter, H., Rehling, P., Sickmann, A., Meyer, H.E., Girzalsky, W. and Kunau, W.H. (2003) Pex8p: An Intraperoxisomal Organizer of the Peroxisomal Import Machinery. Molecular Cell, Vol. 11, 635–646.

Chang, C.C., Warren, D.S., Sacksteder, K.A. and Gould, S.J. (1999) PEX12 interacts with PEX5 and PEX10 and acts downstream of receptor docking in peroxisomal matrix protein import. J. Cell Biol. 147, 761–774.

Collins, C.S., Kalish, J.E., Morrell, J.C., McCaffery, J.M. and Gould, S.J. (2000) The peroxisome biogenesis factors Pex4p, Pex22p, Pex1p, and Pex6p act in the terminal steps of peroxisomal matrix protein import. Mol. Cell. Biol. 20, 7516–7526.

Dodt, G. and Gould, S.J. (1996) Multiple PEX genes are required for proper subcellular distribution and stability of Pex5p, the PTS1 receptor: evidence that PTS1 protein import is mediated by a cycling receptor. J. Cell Biol. 135, 1763–1774.

Douma, A.C, Veenhuis, M., Koning, W. de, Evers, M.E. and Harder, W. (1985) Dihydroxyacetone synthase is localized in the peroxisomal matrix of methanol grown Hansenula polymorpha. Arch. Microbiolog. 143, 237-243.

Dudkina, N.V., Sunderhaus, S., Braun, H.P. and Boekema, E.J (2006) Characterization of dimeric ATP synthase and cristae membrane ultrastructure from *Saccharomyces* and *Polytomella* mitochondria. FEBS Lett. 580, 3427-3432.

Erdmann, R., Veenhuis, M., Mertens, D. and Kunau, W.-H. (1989) Isolation of peroxisome-deficient mutants of *Saccharomyces cerevisiae*. Proc. Natl. Acad. Sci. USA 86, 5419–5423.

Erdmann, R., Wiebel, F.F., Flessau, A., Rytka, J., Beyer, A., Fröhlich, K.U. and Kunau, W.-H. (1991) PAS1, a yeast gene required for peroxisome biogenesis, encodes a member of a novel family of putative ATPases. Cell 64, 499–510.

Eubel, H., Lee, C.P., Kuo, J., Meyer, E.H., Taylor, N.L. and Millar, A.H. (2007) Free-flow electrophoresis for purification of plant mitochondria by surface charge. Plant J 52, 583–594.

Eubel, H., Meyer, E.H., Taylor, N.L., Bussell, J.D., O'Toole, N., Heazlewood, J.L., Castleden, I., Small, I.D., Smith, S.M. and Millar, A.H. (2008) Novel Proteins, Putative Membrane Transporters, and an Integrated Metabolic Network Are Revealed by Quantitative Proteomic Analysis of Arabidopsis Cell Culture Peroxisomes. Plant Physiol. 148, 1809–1829.

Gould, S.J. and Collins, C.S. (2002) Peroxisomal-protein import: is it really that complex? Nat. Rev. Mol. Cell Biol. *3*, 382–389.

Hansel, T.T., DeVries, I.J.M., Iff, T., Rihs, S., Wandzilak, M., Betz, S., Blaser, K. and Walker, C. (1991) An improved immunomagnetic procedure for the isolation of highly purified human blood eosinophils. J. Immunological Methods 145, 105-110.

Kunau, W.H. (1998) Peroxisome biogenesis: from yeast to man. Current Opinion in Microbiology 1, 232-237.

Lutz, M. (2004) Thesis: properties of fungal microbodies.

Marzioch, M., Erdmann, R., Veenhuis, M. and Kunau, W.H. (1994) PAS7 encodes a novel yeast member of the WD-40 protein family essential for import of 3-oxoacyl-CoA thiolase, a PTS2-containing protein, into peroxisomes. EMBO J. 13, 4908–4918.

Moscicka, K.B., Klompmaker, S.H., Wang, D., van der Klei, I.J. and Boekema, E.J. (2007) The *Hansenula polymorpha* peroxisomal targeting signal 1 receptor, Pex5p, functions as a tetramer. FEBS Lett. 581, 1758-1762.

Neuhoff, V., Stamm, R. and Eibl, H. (1985) Clear background and highly sensitive protein staining with coomassie blue dyes in polyacrylamide gels: a systematic analysis. Electrophoresis 6, 427-448.

Neuhoff, V., Stamm, R., Pardowitz, I., Arold, N., Erhardt, W. and Taube, D. (1990) Essential problems in quantification of proteins following colloidal staining with coomassie brilliant blue dyes in polycrylamide gels, and their solution. Electrophoresis 11, 101-117.

Okumoto, K., Abe, I. and Fujiki, Y. (2000) Molecular Anatomy of the Peroxin Pex12p. J. Biol. Chem. 275, 25700-25710.

Rodriguez-Paris, J.M., Nolta K.V. and Steck. T.L. (1993) Characterization of lysosomes isolated from Dictyostelium discoideum by magnetic fractionation. J. Biol. Chem. 268, 9110 –9116.

Sacksteder, K.A. and Gould, S.J. (2000) The genetics of peroxisome biogenesis. Annu. Rev. Genet. 34, 623–652.

Schägger, H. and von Jagow, G. (1987) Tricine-sodium dodecyl sulfate-polyacrylamide gel electrophoresis for the separation of proteins in the range from 1 to 100 kDa. Anal Biochem. 166, 368-379.

Schliebs, W., Saidowsky, J., Agianian, B., Dodt, G., Herberg, F.W. and Kunau, W.H. (1999) Recombinant Human Peroxisomal Targeting Signal Receptor PEX5. J. Biol Chem. 274, 5666–5673.

Subramani, S., Koller, A. and Snyder, W.B. (2000) Import of peroxisomal matrix and membrane proteins. Annu. Rev. Biochem. 69, 399–418.

Sulter, G.J., Harder, W. and Veenhuis, M. (1993) Structural and functional aspects of peroxisomal membranes in yeast. FEMS Microbiol. Rev. 11, 285-296

Van den Bosch, H., Schutgens, R.B.H., Wanders, F.L.I.A. and Tager, J.M. (1992) Biochemistry of peroxisomes. Annu. Rev. Biochem. 61, 157-197.

Van Dijken, J.P., Otto, R. and Harder, W. (1976) Growth of Hansenula polymorpha in methanol-limited chemostat. Physiological responses due to the involment of methanol oxidase as a key enzyme in methanol metabolism. Arch. Microbiol. 111, 137-144.

Van der Zand, A., Braakman, I., Geuze, H.J. and Tabak, H.F. (2006) The return of the peroxisome. J. Cell Sci. 119, 989–994.

Verduyn, C., van Dijken, J.P. and Scheffers, W.A. (1984) Colometric alcohol assays with alcohol oxydase. J. Microbiol. Methods 2, 15-25

Vizeacoumar, F.J., Torres-Guzman, J.C., Bouard, D., Aitchison, J.D. and Rachubinski, R.A. (2004) Pex30p, Pex31p and Pex32p form a family of peroxisomal integral membrane proteins regulating peroxisome size and number in *Saccharomyces cerevisiae*. Mol. Biol. Cell 15, 665–677.

Chapter 4

Structural characterization of CitS, GltS and GltT transporters by single particle electron microscopy.

Katarzyna B. Mościcka , Tomasz Krupnik , Juke S. Lolkema & Egbert J. Boekema

ABSTRACT

Three secondary transporter proteins: GltT of *Bacillus stearothermophilus,* CitS of *Klebsiella pneumoniae* and GltS of *Escherichia coli* were studied by single particle electron microscopy. The proteins were extracted from the membrane by detergent solubilization and purified to homogeneity by Ni^{2+}-affinity chromatography. Image processing showed a GltT particle with three-fold symmetry, which is in line with the trimer observed in the crystal structure of a homologous protein, Glt_{Ph} of *Pyrococcus horikoshi*. The CitS protein showed up in two main views as a kidney-shaped particle and a biscuit-shaped particle, both with a long axis of 160 Å and a short axis of 84 Å. The GltS protein was similarly shaped but somewhat smaller with dimensions of 150 Å x 84 Å. Comparison of the shapes and dimensions of the CitS and GltS particles with the GltT particle suggested that the former two were in the dimeric state.

A 10 kDa protein tag (Biotin Acceptor Domain, BAD) was fused to the N-terminus of the CitS protein or inserted in the central cytoplasmic loop, which connects the two putative domains of the protein. Both constructs were shown to be active citrate transporters and in the dimeric state after purification in detergent. Single particle analysis of the two proteins revealed differently shaped particles relative to the untagged protein. N-terminally tagged CitS revealed a more globular shape relative to the wild type. The aspect ratios were 1.77 and 1.9, respectively. In contrast, the inserted BAD domain resulted in an extended particle with an aspect ratio of 2.14. A model is presented for the relative orientation of monomers in the CitS dimer.

Submitted to Journal Mol. Biol.

INTRODUCTION

Secondary transporters use the free energy stored in ion and/or solute gradients to drive the transport of a solute across the cytoplasmic or internal membranes of biological cells. They are widely spread throughout all kingdoms of life; they are found in every biological cell and a specific transporter protein can probably be found for every low-molecular weight compound in nature. Their high abundance is reflected in the great diversity of sequences coding for secondary transporters. The transporter classification system (TC system) developed in the Saier laboratory is based on sequence homology and lists some 95 different gene (super)families coding for secondary transporters (subclass TC 2.A) (Pao et al. 1999). Many of these families are likely to be evolutionary related, and the high number of encoded protein families is likely to represent a much smaller number of structures and an even smaller number of translocation mechanisms. Hydropathy profile alignment has been proposed to group families of transport proteins or, more in general, membrane proteins with similar structures, into structural classes (Lolkema and Slotboom 1998). The hydropathy profiles would report a specific folding pattern of proteins in membranes and, therefore, capable of detecting distant evolutionary relationships between protein families.

This study involved three different secondary transporters that are found in two structural classes. GltT of *Bacillus stearothermophilus* is a member of the Dicarboxylate/Amino Acid Cation Symporter (DAACS) family. GltT translocates glutamate and aspartate (Slotboom and Lolkema 1999) coupled to H^+. The DAACS family includes transporters that are found in neurons and glial cells in the mammalian central nervous system that catalyze the reuptake of the excitatory neurotransmitter glutamate from the synaptic cleft (Fairman et al.1995; Kanai et al. 1992; Pines et al. 1992; and Storck et al. 1992). The DAACS family forms a structural class by itself, named Secondary Transporters [4] or (ST[4]). A member of the family (GlT_{Ph} of *Pyrococcus horikoshi)* has been crystallized and the three dimensional structure was solved at a resolution of 2.69 Å (Boudker and Gouaux 2007). The other two secondary transporters, CitS of *Klebsiella pneumoniae* and GltS of *Escherichia coli*, are both found in structural class ST[3]. CitS transports citrate in symport with two sodium ions and one proton. It belongs to the family of 2-hydroxycarboxylate transporters (2HCT) that contains transporters exclusively found in bacteria (Sobczak and

Lolkema 2003). GltS transports glutamate in symport with Na^+ ions. GltS belongs to the Glutamate Sodium Symporter (ESS) family. Members of the 2HCT and ESS families cannot be regarded to be homologous by sequence similarity, but are classified in one and the same class because they show highly similar hydropathy profiles. Insight into the structure of class ST[3] proteins comes mainly from studies of CitS of *Klebsiella pneumoniae* (van Geest and Lolkema 1999 and 2000; reviewed in Sobczak and Lolkema, 2005). The structural model of the transporters shows a core of two homologous domains consisting of five trans membrane segments (TMS) each that are connected by a large cytoplasmic loop region. Because of the odd number of helices, the two domains would have opposite orientations in the membrane ('inverted topology'). In between the 4^{th} and 5^{th} TMS in each domain, the connecting loop folds back in between the TMSs to form so-called 'pore loop' or 'reentrant loop' structures. It is believed that in the 3D structure, the pore-loops of the two domains are in close vicinity and form the translocation pore. The CitS protein has an additional TMS at the N-terminal end of the core structure, placing the N-terminus in the cytoplasm. Alignment of the hydropathy profiles of the ESS and 2HCT families suggested that this additional TMS is missing in the GltS protein. Experimental evidence has been reported that confirms a similar membrane topology and the presence of the pore-loop structure in the C-terminal domain of the CitS and GltS proteins (Dobrowolski et al. 2008; Dobrowolski et al. 2009).

Our understanding of the structure of these proteins is still limited. A proven method to study the structure of (membrane) proteins is single particle analysis of electron microscopy (EM) projections. Over the last 25 years it has improved to a well-established technique to obtain information at a medium resolution (10–20 Å), and to near-atomic resolution for some highly symmetric objects (Frank et al. 2002; Van Heel et al. 2000). Single particle averaging is simple and attractive if applied to negatively stained specimens with a mass between about 100 and 2000 kDa, since one can process many thousands of projections within a few days, which is necessary to obtain high quality 2D projection maps. The statistical analysis and classification procedures used in single particle analysis are often effective in the sorting of different projection views originating from different conformations or subunit compositions.

In this study, the quaternary structure of the transporters GltT, CitS and GltS is studied using single particle electron microscopy. Since the particles are expected to be at the lower size limit of what is feasible for the technique (the monomeric molecular masses of GltT, CitS and GltS are 46.6, 49.1 and 43.5 kDa, respectively) the GltT protein was included as a reference particle. Ample evidence has been presented that the GltT protein assembles into a trimeric structure (Lolkema and Slotboom 1998; Boudker and Gouaux 2004; Groeneveld and Slotboom 2007). We present EM data that indicate that the other two transporters from the ESS and 2HCT families, share a similar subunit structure. Because of the small dimensions of proteins with a mass around 100 kDa, the low signal-to-noise ratio of transmission EM images of biomacromolecules, and the unstructured detergent shell around membrane proteins, single particle EM analysis is not (yet) able to reveal much detail in such proteins. We were able to show differences in size of dimers of CitS and GltS (~ 100 kDa) and in size and shape of CitS transporters to which the Biotin Acceptor Domain (BAD) of the oxaloacetate decarboxylase of *Klebsiella pneumoniae* with a mass of 10 kDa was attached.

MATERIALS AND METHODS

Cell growth and membrane preparation

Escherichia coli strain DH5α was used as a host to express the transporter proteins and derivatives. Freshly transformed bacteria were used to inoculate an over-night growing pre-culture. 25 ml of pre-culture was added to 1 liter of Luria Broth (LB) medium at 37°C and containing 50 μg/ml amphycilin (Roche Diagnostic GmbH, Manninheim, Germany) under continuous shaking (200 rpm). At an OD_{660} of 0.6, 0.1% arabinose (Sigma-Aldrich GmbH, Steinheim, Germany) was added to induce expression of the transporters after which the culture was allowed to grow for an additional one hour. Subsequently cells were harvested by spinning at 8000 rpm in 4°C for 10 min, washed with 50 ml cold 50 mM KPi, pH 7, at 4 ^{o}C and resuspended in 5 ml of the same buffer containing 1 μg/mL DNAse.

The cell suspension was passed three times through a pressure-cell-distrupter at 13,5 MPa at 4°C. Following a low spin at 8000 rpm for 10 min at 4°C to remove debris and unbroken cells, the supernatant was centrifuged at 80000 rpm for 25 min at 4°C (high spin). The membrane fraction was resuspended and washed once with 50 mM Kpi, pH 7, buffer containing 1 M NaCl. The membranes were resuspended in 1 mL of 50 mM Kpi, pH 7, buffer and stored in liquid N_2 untill use.

Purification of transporter proteins

Transporter proteins were solubilized from the membranes by partial extraction. Membranes from a 1 L culture were incubated for 1 hour at 4°C under continuous shaking in 50 mM Kpi, pH 7, buffer containing 400 mM NaCl, 10% glycerol and 0.5 % DDM. Undissolved membrane material which contained the transporter proteins was recovered by spinning at 80000 rpm for 25 min at 4°C. The extraction procedure was repeated with the same buffer with 1% Triton X-100 instead of DDM. The transporter proteins were recovered in the supernatant after spinning, passed through a 0.2 µm filter and applied to a 1mL bed volume Ni-NTA column (HisTrap HP) in an AKTA HPLC system. Before, the column was conditioned for 5 min at 1 ml/min flow rate of the carrier buffer (50 mM Kpi, pH 8, 600 mM NaCl, 10% glycerol, 0.03% DDM, 20 mM imidazole). The loaded column was washed with 10 ml of 6% of the elution buffer (50 mM KPi pH 7, 600 mM NaCl, 10% glycerol, 0.03% DDM, 500 mM imidazole). The proteins were eluted in a linear gradient of 6% to 80% of the elution buffer. The OD_{280} of the eluate wash measured continuously, after which the eluate was collected in fractions of 0.5 mL.

Construction of plasmids

Plasmids pBADGltS (Dobrowolski et al, 2005), pBADCitS (Sobczak and Lolkema, 2003), and pGltThis were constructed before (Slotboom et al, 1996), as well as pSB260 (van Geest and Lolkema, 1996). Plasmid pCitS-BAD1 was obtained by ligation of the gene coding for the BAD domain flanked at both sides by NcoI restriction sites in pSB260 into pBADCitS digested with the same restriction enzyme using standard procedures. Plasmid pCitS-BAD260 was obtained by recloning the BAD containing CitS gene in pSB260 into pBADCitS.

Cross-linking with glutaraldehyde

For each experiment, a 50 mM glutaraldehyde (Singma-Aldrich GmbH, Steinheim, Germany) solution in water was freshly prepared. Protein samples were treated with 2 mM glutaraldehyde solution for 10 min at room temperature. The reaction was stopped by making the solution 100 mM in Tris-HCl pH 7 and incubating the sample for another 10 min at room temperature after which the samples were analyzed by SDS-PAGE.

Right-side-out (RSO) membrane preparation Cells cultures were grown, induced and harvested as described before. Cells of a 1 L culture were washed in 350 ml of 10 mM Tris-

HCl at 4°C and resuspended in 150 ml of 30 mM Tris-HCl, pH 8.0, 20 % sucrose at 37°C. After 10 min of incubation with 10 mM K-EDTA, pH 6, 100 µg/ml lysozyme was added and the cell suspension was incubated for an additional 15 min. Cells were collected by centrifugation, resuspended in 2 mL of 30 mM Tris-HCl pH 8.0, 20 % sucrose and, subsequently, diluted into 700 ml of KP_i , pH 7, at 37 ^{0}C. Following incubation for 15 min at the same temperature in the presence of 10 µg/ml DNAse and RNAse, 7 mL of a 1M $MgSO_4$ solution was added. After incubation for 15 min the membranes were collected by centrifugation for 60 min at 8000 rpm at 4 °C. The pellet was resuspended in 60 ml of 100 mM Kpi, pH 7, after which unbroken cells and debris was removed by spinning at 2500 rpm for 45 min at 4 °C (low spin). RSO membranes were collected from the supernatant by spinning at 20,000 rpm for 30 min at 4°C (high spin). RSO vesicles were resuspended in 50 mM KPi pH 7.0 and aliquoted in 150 µl portions that were stored at -80 °C. The concentration of the membrane protein in the RSO vesicles was assayed by the BioRad colorimetric protein assay.

Transport studies

RSO membrane vesicles were diluted to 1 mg/ml in 50 mM KPi pH 6 containing 100 mM NaCl. 100 µl aliquots were incubated for 2 min at 30°C with 10 mM K-ascorbate and 100 µM PMS under a flow of water-saturated air and continuous stirring with a magnetic bar. At t=0, 1 µl of 0.29 mM [1,5-^{14}C]-citrate (114 mCi/mmol, Amersham Pharmacia, Roosendaal, The Netherlands) was added to final concentration of 2.9 µM. Uptake was stopped at 5, 10, 20, 40, 60 seconds by addition of 2 mL ice-cold 0.1 M LiCl followed by immediate filtering over cellulose nitrate filter (0.45 µm pore size) and washing of the filter with an additional 2 mL of the LiCl solution. Filters were collected and their radioactivity was measured in a liquid scintillation counter.

SDS-PAGE

Protein samples were mixed with loading buffer (250 mM Tris-HCl pH 6.8, 10% SDS, 50% glycerol, 0.05% bromophenolblue) in a 1:4 ratio and loaded onto a polyacrylamide gel consisting of a stacking gel (4% polyacrylamide, 0.1% SDS, 0.375M Tris-HCl, pH 8.7) and separating gel (12% polyacrylamide, 0.1% SDS, 0.125M Tris-HCl, pH 6.8). The gel was run at a constant current of 25 mA for 45 min. The gel was stained in a buffer containing 25%

ETOH, 20% acetic acid, 0.25g/l Coomassie Brilliant blue R250, 0.25g/l $CuSO_4$ (Laemmli, 1970).

Electron Microscopy and Single-Particle Analysis

Negatively stained specimens of GltT, CitS and GltS were prepared with 2% uranyl acetate on glow-discharged carbon-coated copper grids. Electron microscopy was performed on a Philips CM12 electron microscope operated at 120 kV. Images were recorded with a Gatan 4K slow-scan CCD camera at 100,000 x magnification with a pixel size (after binning the images) of 3.00 Å at the specimen level, with "GRACE" software for semi-automated specimen selection and data acquisition. About 6,000 images were recorded and about 5,000 single particle projections from GltT, 80,000 projections from CitS, 30,000 from GltS and 28,000 single mutant N-terminus BAD CitS and CitS-BAD_{260} projections were selected, respectively. Single-particle analysis was performed with the Groningen Image Processing ("GRIP") software package on a PC cluster. Selected single-particle projections (96 x 96 pixel frame) were aligned by a multireference alignment and reference-free alignment procedures according to (Van Heel et al. 2000; Penczek et al. 1992). Next, particles were subjected to multivariate statistical analysis, followed by hierarchical ascendant classification (Van Heel et al. 2000). The resolution of the class averages was measured by Fourier Ring Correlation according to (Van Heel 1987). After several cycles of multireference alignments, statistical analysis and classification the best projections from each set were averaged.

RESULTS

Purification of GltS, CitS and GltT transporter proteins

Three secondary transporter proteins, GltT of *Bacillus stearothermophilus*, CitS of *Klebsiella pneumoniae* and GltS of *Escherichia coli* were expressed in *E. coli* DH5α harboring plasmids pBADGltT (Slotboom et al. 1999), pBADCitS (Sobczak and Lolkema 2003) and pBADGltS (Sobczak et al. 2007), respectively. The plasmids code for the transport proteins with N-terminal His_6-tags. The transporters were solubilized from the membrane by partial extraction using the detergents Triton X-100 and dodecylmaltoside as described in the Methods section. Solubilized proteins were loaded onto a Ni^{2+}-NTA affinity column and, after washing, bound proteins were eluted from the column by a linear imidazole gradient ranging from 50 – 400 mM (Figure 1). Protein in the eluent was detected by the extinction at 280 nm

and the fractions were assayed for the presence of the transporter proteins by SDS-PAGE. The CitS and GltS proteins eluted at more or less the same imidazole concentration of 120 mM, while the GltT protein clearly bound stronger to the resin, eluting at 200 mM imidazole. SDS-PAGE following pooling of the peak fractions and concentration by ultrafiltration showed that the procedure resulted in highly pure protein preparations (Figure 1B). The apparent molecular masses of GltS, CitS and GltT were 35, 40 and 36 kDa. The yield of the procedure, which largely reflects the different levels of expression in the *Escherichia coli* host strain were 0.083, 0.3 and 0.21 mg of protein per liter of cell culture for GltS, CitS and GltT, respectively.

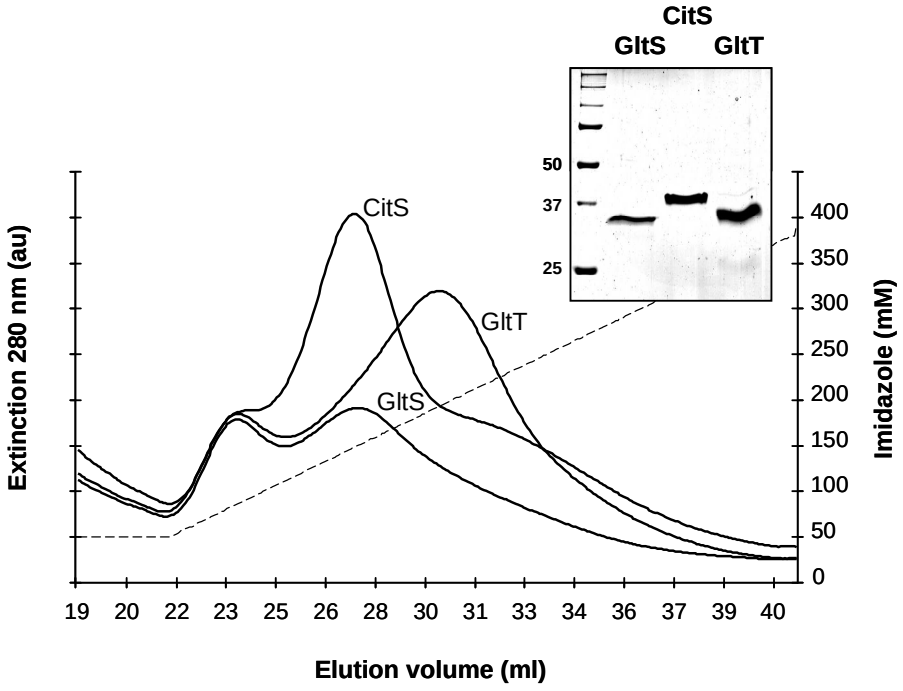

Figure 1. *Ni^{2+}-affinity chromatography purification of GltS, CitS and GltT proteins. Main plot. Elution profile of GltS, CitS and GltT. The dashed line indicates the imidazole gradient. Insert. SDS-PAGE of purified GltS (lane 1), CitS (lane 2) and GltT (lane 3). Fractions of 1 mL collected at 26-29 mL of elution volume for CitS and GltS and 30-33 mL for GltT were pooled and concentrated by ultrafiltration before analyzing by SDS-PAGE. Estimated molecular masses were 35, 40 and 36 kDa, respectively. Left lane: marker proteins: 50 (a), 37 (b) and 25 (c) kDa. The gel was stained with Coomassie Brilliant Blue.*

EM analysis of CitS, GltS and GltT.

Purified GltT, CitS and GltS transporter proteins were examined by electron microscopy (EM). Large numbers of monodisperse particles were present and a total number of about 130,000 projections of negatively stained GltT, CitS and GltS proteins was analyzed by single particle analysis. After several cycles of multi-reference alignment, multivariate statistical analysis and classification, final class sums from all analyzed particles (GltT, CitS and GltS) were obtained (Figure 2). The averaged EM projection maps of negatively stained GltT indicated high numbers of particles showing three-fold symmetry (Fig. 2A and B). The EM image of the GltT particle measures 118 Å in diameter and is likely to correspond to a top view projection of the GltT trimer (Yernool et al. 2004; Gendreau et al. 2004) which is in line with the known high resolution X-ray structure of the homologous transporter Glt_{Ph} resolved previously (Boudker et al. 2007) . Glt_{Ph} shows a similar three fold symmetry when viewed along an axis perpendicular to the membrane (Fig. 1B). The space filling model, based on the x-ray structure of Glt_{Ph} is a little bit smaller than the EM image of GltT because solubilized membrane proteins are surrounded by a detergent layer around the protein, which is not penetrated by the negative stain (Boekema et al. 1999). Particles with three-fold symmetry were almost the only type of projection that was observed. No side-views were found.

Analysis of 80,000 projections of the CitS protein indicated a high numbers of elongated particles (Fig. 2C and D). After several cycles of multireference alignments, statistical analysis and data classification, the best projections from each set were selected, combined and averaged. CitS appears to have two main types of projection views. One appears to be a biscuit-shape particle with a the long axis of 160 Å and a short axis of 84 Å (Fig. 2C). The second is a kidney-shape particle measuring 160 Å for the long axis and 81 Å for the short axis (Fig. 2D). CitS has been demonstrated to be a dimeric protein in detergent solution (Kastner et al, 2003; Pos et al, 1994; Veenhoff et al, 2001). Therefore, the biscuit-shaped particle is likely to reflect a top view because of its close-to 2-fold rotational symmetry, while the kidney-shaped projection is likely to represent a side view projection (mirror symmetry). The assignment will be discussed in more detail in the Discussion section.

A set of 30,000 EM projections of GltS were analyzed in a similar way as described above for GltT and CitS. The best projections from each set were averaged and the sums of the best classes are presented in Figure 2E and 2F. Similarly to CitS mainly two types of projection views of GltS were found (Figures 2E and 2F). The short axis of the projections were similar as observed for the CitS images (84 Å), while the long axis was significantly shorter (150 Å

vs. 160 Å). The difference in shape between the two main projections of the GltS particle is smaller than observed for CitS (compare Figures 2C,D and 2D,F). The image shown in Figure 2D is somewhat asymmetric along the long axis suggesting a tilted particle. A small constriction in the middle of the projections may be observed suggesting similarity to the kidney-shaped projection of CitS in Figure 2D.

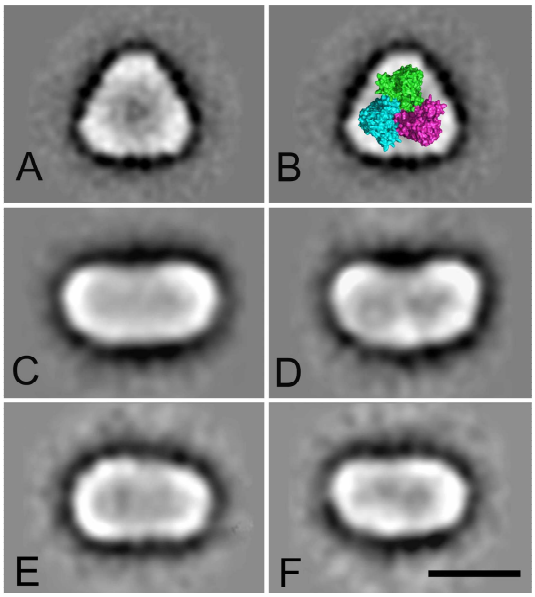

Figure 2. *Single particle analysis of top-view projections of GltS, CitS and GltT. Averaged top view projection of GltT with a sum of 5,000 particles from Bacillus stearothermophilus. (A) High-resolution $GltT_{Ph}$ X-ray model in a position similar to the EM projection of image B. The mass around the X-ray model could suggest the extra stain or detergent layer around the protein. (C,D) Averaged top view projections of CitS with a sum of 80,000 particles from Klebsiella pneumoniae. (E, F) Averaged top view projections of GltS particles with a sum of 28,000 particles from Escherichia coli. Space bar is 100 nm.*

Biotin Acceptor Domain (BAD) tagged CitS proteins.

The Biotin Acceptor Domain (BAD) domain of the oxaloacetate decarboxylase of *Klebsiella pneumoniae* is a ~10 kDa protein moiety. The gene coding for BAD was fused at the 5' end of the *citS* gene yielding plasmid pCitS-BAD1 and inserted in the *citS* gene at the position corresponding to amino acid residue 260 of the CitS protein yielding plasmid pCitS-BAD260. The plasmids code for one hybrid protein consisting of the CitS with BAD fused at the N-terminus and the other with BAD inserted in the central cytoplasmic loop in between the two putative domains of CitS. Both constructs contain a His_6-tag at the N-terminus.

Membrane vesicles with a right-side-out (RSO) orientation were prepared from *E. coli* DH5α cells expressing wild-type CitS and the two hybrid proteins and were assayed for citrate uptake activity. Membrane vesicles prepared from the host strain are completely devoid of citrate uptake activity because of the lack of expression of citrate transporters during aerobic growth of *E. coli* (not shown; Lolkema et al. 1994). The initial rate of uptake of citrate driven by a proton motive force imposed by the artificial electron donor system K-ascorbate/phenazine methosulfate (PMS) was roughly 40 % less for the RSO membranes containing the two hybrid proteins than for those containing wild-type CitS (Figure 3A). The level of expression was determined by purifying the proteins from the membranes by Ni^{2+}-NTA affinity chromatography using a batch-wise protocol. SDS-PAGE analysis of the partially purified proteins revealed that the two hybrid protein have apparent molecular masses of 50 kDa (Figure 3B, lanes 3 and 4) which is about 10 kDa more than the untagged CitS protein as expected (lane 2). A degradation product of CitS with an apparent molecular mass of 26 kDa was observed which is most likely the result of proteolytic activity during the lengthy procedure at elevated temperature of preparing RSO membranes. The intensity of the bands of the two hybrid proteins are more or less the same, but both were clearly less intense than observed for wild-type CitS (lane 2). The lower expression level of the two hybrid proteins largely explains the difference in citrate uptake activity of the different RSO membrane preparations in Figure 3A. Introduction of BAD at the N-terminus and at position 260 of the CitS protein does not seem to significantly affect the transport activity of the CitS moieties. The result is in line with the positive phenotype of *E. coli* cells expressing the hybrid proteins on Simmons agar indicator plates (van Geest and Lolkema 1999).

The CitS protein can be shown to be present as a dimer in the detergent solubilized state by cross-linking with glutaraldehyde. Treatment of CitS with 2 mM glutaraldehyde for 10 min shifts the protein band on SDS-PAGE up to a protein with an apparent molecular mass of 100 kDa (Figure 4). Pretreatment of the sample with SDS prevents the up shift demonstrating that cross-linking in the native state is not the result of collisions between monomeric particles. The two hybrid proteins were purified to homogeneity as described above. Similarly as observed for the CitS protein, treatment of the hybrid proteins with glutaraldehyde resulted in an upshift of the proteins on SDS-PAGE that was not observed with the denatured proteins (Figure 4). It follows that introduction of BAD at the N-terminus and at position 260 of the CitS protein does not interfere with the dimeric state of the CitS moieties. Treatment of the protein with glutaraldehyde results in more diffuse protein bands

which is most likely the result of heterogeneity caused by random labelling of the protein and intramolecular cross-linking.

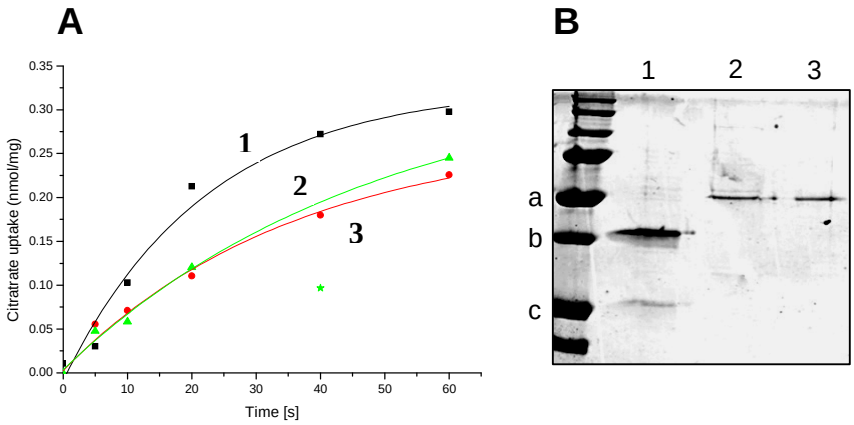

***Figure 3**. Transport activity of BAD-tagged CitS transporters in RSO membranes. (**A**) Uptake of ^{14}C-citrate by RSO membranes containing wt-CitS line 1), N-terminal BAD- tagged CitS (CitS-BAD1, line 2) and CitS with BAD inserted at position 260 (CitS-BAD260, line 3). Membrane protein concentrations were 1 mg/ml. Citrate uptake was expressed in nmol per mg of membrane protein in the sample. (**B**) SDS PAGE of partial purified CitS moieties from the RSO membrane vesicles. Lane 1, wt-CitS, lane 2, CitS-BAD1, lane 3, CitS-BAD 260, left lane, marker proteins: 50 kDa (a), 37kDa (b), 25kDa(c).*

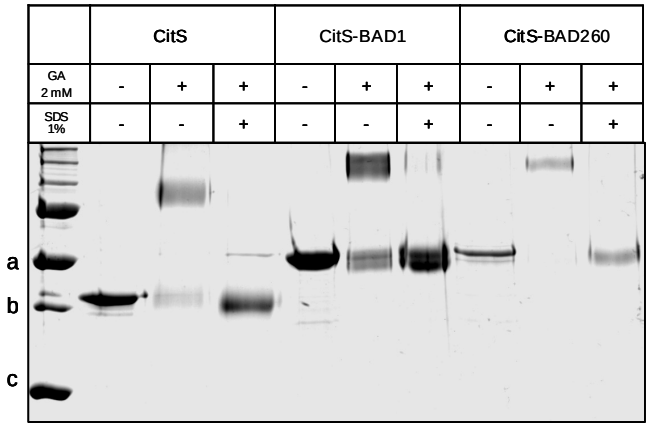

***Figure 4**. Cross-linking of wt-CitS, CitS-BAD1 and CitS-BAD260 by glutaraldehyde. The CitS moieties were treated or not with 2 mM glutaraldehyde in the absence and presence of 1 % SDS as indicated. Left lane, marker proteins, 50 kDa (a), 37 kDa (b), 25 kDa (c). Proteins were stained with Coomassie Brilliant Blue.*

Electron Microscopy of BAD tagged CitS

The effect of the addition of the BAD domains on the sizes and shapes of the CitS protein was studied by EM. Analysis by multireference alignment, multivariate statistical analysis and classification of 14,000 projections indicated that both CitS-BAD1 and CitS-BAD260 yielded a single type of projection map, shown in Figures 5C and 5D, respectively. The general quality of the projection maps of the BAD tagged CitS proteins was lower than observed with wild-type CitS, resulting in a more blurred appearance. The poor quality of the images of both CitS with the BAD domain fused to the N-terminus and CitS with BAD inserted in cytoplasmic loop complicated the alignment and classification procedure which caused lower resolution. When compared to wild type CitS (Figure 5A and B) with a resolution of about 15 Å, the BAD tagged particles have a resolution of at best 20 Å.

In spite of the lower resolution, the sums obtained after reference alignment indicated changes in the overall shape of the BAD tagged CitS proteins. CitS with the BAD domain fused to the N-terminus resulted in a more globular shape of the particle (Fig. 5C). In contrast, CitS with BAD inserted in the cytoplasmic loop inbetween the two putative domains resulted in more extended particles (Fig. 5D). The dimensions of the different particles were summarized in Table 1. The BAD domain adds approximately 25% protein mass to the CitS particle. The increase of the surface of the EM projections was a bit higher with a factor of 1.3 and 1.37 for CitS-BAD1 and CitS-BAD260, respectively. This most likely due to the lower resolution of the latter. The aspect ratios of the particles were increasing in the order CitS-BAD1, CitS, CitS-BAD260.

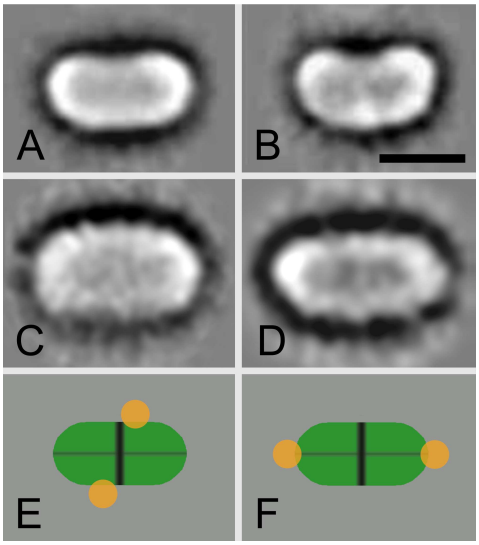

Figure 5. *A gallery of 2D projection maps from single particle EM of averaged BAD tagged CitS transporter proteins (A,B) top view of dimeric CitS. (C) Averaged projection of CitS with BAD inserted in the cytoplasmic loop of CitS (C) and with BAD fused to the N-terminus of CitS. (E,F) Schemes for BAD- tagged CitS proteins explaining the images in panels C and D. BAD domains (yellow), CitS (green) The thick solid line indicates the subunit interface, the thin line the putative interface between the N- and C-terminal domains of CitS. Space bar for all frames equals 100 nm.*

	long axis	**short axis**	**aspect ratio**	**surface in nm^2**	**Predicted surface in nm^2**
CitS	160	84	1.91	116 nm^2	-
CitS-BAD1	177	100	1.77	150 nm^2	140
CitS-BAD260	180	84	2.14	160 nm^2	140
GltS	150	84	1.78	84 nm^2	-

Table 1*. Dimensions and aspect ratios of wt and BAD tagged CitS proteins. The predicted surface area was calculated assuming an increase in surface that is proportional to the increase in protein mass. Surface area of the wild-type is much smaller while the area of mutants is comparably similar. The dimension aspect ratios are consistently increasing in the order: CitS-BAD1 ,CitS and CitS-BAD260.*

DISCUSSION

The investigation of the secondary transporters GltT, CitS and GltS by electron microscopy and single particle averaging gives several new insights into the architecture of these relatively small proteins. The glutamate transporter GltT found in *Bacillus stearothermophilus* and *Bacillus caldotenax* (Tolner et al. 1992) is a protein with a molecular mass of about 42 kDa. In the detergent solubilized state, the protein was shown to be a homotrimer by chemical cross-linking (Yernool et al. 2003) which is in line with the trimer observed in the high resolution structure of the homologous transporter Glt_{Ph} of the archaeon *Pyrococcus horikoshi* (Yernool et al. 2004). The dominant projection image obtained after single particle averaging of purified GltT in detergent was a triangular particle with a clear three-fold rotational symmetry at about 14 Å resolution (Figure 2A). This strongly suggests that the image represents a view along an axis perpendicular to the membrane (top view). One of the reasons might be that the grids were glow discharged before preparing electron microscopy specimens. This enhances the absorption of particles with their hydrophilic parts, which results in predomination of top-view projections. A top view of a space filling model of the Glt_{Ph} trimeric structure (Figure 2B) superimposed on the image is a bit smaller which is due to the fact that solubilized membrane proteins are surrounded by a detergent layer, which is not penetrated by the negatively charged stain (Boekema et al. 1999). The EM analysis of GltT presented here, demonstrates that the shape of proteins as small as ~120kDa can be successfully determined by electron microscopy.

The citrate transporter CitS of *Klebsiella* pneumoniae is a protein of 46 kDa. No high resolution structure of the protein is available, but several lines of evidence indicate that CitS is a dimeric protein in detergent solution (Pos, Krupnik, see Sobczak and Lolkema 2003). EM analysis of purified CitS revealed two dominant classes of 2 D projection maps. Both projections showed elongated particles with a long axis about twice the length of the short axis (roughly 160 x 80 Å). One of the projections had a biscuit-shape, the other a kidney-shape (Figures 2C and D, respectively). The two classes represent two views of the protein rotated around the long axis. Secondary transporter proteins are largely embedded in the phospolipid bilayer without too much of their mass protruding into the inside or outside water phase. Considering that the thickness of the membrane layer is around 40-50 Å, the long axis

of both projections has to be in the plane of the membrane. Then, in the two projections, the short axis is either also in the plane of the membrane (view from within the membrane, side view) or perpendicular to the membrane (view on the membrane, top view). Since the orientation of an integral membrane protein in the membrane is fixed (positive-inside rule; von Heyne et al. 1991), a (homo)dimeric structure of a membrane protein forces certain symmetries upon the projections. In side view projection, one half should be the mirror image of the other half, which, in support for a dimeric structure of CitS, is observed for both projections. However, the top view should have two-fold rotational symmetry which is only compatible with the biscuit-shaped and not with the kidney-shaped image. It follows that the kidney-shaped image represents the side view of the CitS dimer. CitS would be a particle with an indentation at one side of the membrane at the interface of the subunits. The two EM images of the GltS protein reveal the same overall shape as observed for CitS but are somewhat smaller which is in line with their smaller molecular mass (Figure 2E,F and Table 1). The size of the particles suggests that GltS is a dimer as well. The shape is resembling the top view image of CitS while the corresponding side view was not observed. It is concluded that the dimeric structure of those two proteins is preserved despite their far evolutionary distance.

The structural model for the monomeric subunits of CitS and GltS consists of two homologous domains with the substrate and co-ion translocation sites at the interface of the two domains (Sobczak and Lolkema, 2005). In a simple three-dimensional model, the loop that connects the two domains would be at the 'closed' side of the monomer (the 'back') and the N- and C-terminal ends of the protein at the 'open' opposite side (the 'head'). We have attempted to determine the relative orientation of the monomers in the CitS dimer by tagging the central loop and the N-terminus with an additional protein mass and, subsequently, locating the additional mass in the EM images. The biotin acceptor domain (BAD) of the oxaloacetate decarboxylase of *Klebsiella pneumoniae* that was used as tag is a 10 kDa protein which amounts to ~20% of the transporter protein mass. Both CitS-BAD1 (N-terminus) and CitS-BAD260 (central loop) had retained the Na^+-citrate transport activity and dimeric structure. The increase in surface of the EM images of the two tagged CitS proteins was indeed observed, but slightly more than expected (Table 1). This is probably related to the lower resolution obtained for the images of the tagged proteins which may be caused by a relatively high degree of flexibility between tag and transporter protein. The lower resolution,

estimated at 20 Å, may also have blurred the difference between top views and side views resulting in only one type of projection maps (Fig. 5C and D). Nevertheless, tagging the CitS protein at these two different sites results in a remarkable difference in shape of the particles. Relative to wild-type CitS, CitS with the BAD domain fused at the N-terminus appeared to have more globular shape with an aspect ratio of 1.77 *vs.* 1.91 for the untagged protein (Table 1). In contrast, CitS with BAD inserted in the cytoplasmic loop resulted in more extended particles with an aspect ratio of 2.14. The position of the additional cmass in both images suggest that the cytoplasmic loop between the two domains is placed at the end of the long axis and not involved in formation of the subunit interface, while the N-terminus is located at the interface in the dimer (Fig. 5E). It is concluded that the CitS dimer is 'head-to-head'.

REFERENCES

Boekema, E.J., van Roon, H., van Breemen, J.F.L and Dekker, J.P. (1999) Supramolecular organization of photosystem II and its light-harvesting antenna in partially solubilized photosystem II membranes. Eur. J. Biochem. 266, 444-452.

Boudker, O., Ryan, R.M., Yernool, D., Shimamoto, K., Gouaux, E. (2007) Coupling substrate and ion binding to extracellular gate of a sodium-dependent aspartate transporter. Nature 445, 387-393.

Dobrowolski, A., Sobczak-Elbourne, I. and Lolkema, J.S. (2007) Membrane Topology Prediction by Hydropathy Profile Alignment: Membrane Topology of the Na+-Glutamate Transporter GltS. Biochemistry 46, 2326-2332.

Fairman, W.A., Vandenberg, R.J., Arriza, J.L., Kavanaugh, M.P. and Amara, S.G. (1995) An excitatory amino-acid transporter with properties of a ligand-gated chloride channel. Nature 375, 599–603.

Frank, J. (2002) Single-particle imaging of macromolecules by cryoelectron microscopy. Annu. Rev. Biophys. Biomol. Struct. 31, 309–319.

Gaillard, I., Slotboom, D.J., Knol, J., Lolkema, J.S. and Konings, W.N. (1996) Purification and Reconstitution of the Glutamate Carrier GltT of the Thermophilic Bacterium *Bacillus stearothermophilus*. Biochemistry 35, 6150 -6156.

Gendreau, S., Voswinkel, S., Torres-Salazar, D., Lang, N., Heidtmann, H., Detro-Dassen, S., Schmalzing, G., Hidalgo, P., Fahlke, C. (2004) A trimeric quaternary structure is conserved in bacterial and human glutamate transporters. J. Biol. Chem. 279, 39505-12.

Groeneveld, M., Slotboom, D.J. (2007) Rigidity of the subunit interfaces of the trimeric glutamate transporter GltT during translocation. J Mol Biol. 372, 565-70.

Heyne, R.I., De Vrij, W., Crielaard, W. and Konings, W.N. (1991) Sodium ion-dependent amino acid transport in membrane vesicles of *Bacillus stearothermophilus*. J. Bacteriol. 173, 791-800.

Kanai, Y. and Hediger, M.A. (1992) Primary structure and functional characterization of a high-affinity glutamate transporter. Nature 360, 467–471.

Kästner, C.N., Prummer, M., Sick, B., Renn, A., Wild, U.P., Dimroth, P. 2003. The citrate carrier CitS probed by single-molecule fluorescence spectroscopy. Biophys. J. 84:1651-59.

Konings, W.N., Kaback, H.R. and Lolkema, J.S. (1996) Transport processes in eukaryotic and prokaryotic organisms. Elsevier Science B.V., Amsterdam, The Netherlands.

Lolkema, J.S., Enequist, H., van der Rest, M.E. (1994) Transport of citrate catalyzed by the sodium-dependent citrate carrier of *Klebsiella pneumoniae* is obligatorily coupled to the transport of two sodium ions. Eur J Biochem. 220, *469-75*.

Lolkema, J.S. and Slotboom, D.J. (1998) Estimation of structural similarity of membrane proteins by hydropathy profile alignment. Mol. Membr. Biol. 15, 33–42.

Lolkema, J.S. and Slotboom, D.J. (1998) Hydropathy profile alignment. A tool to search for structural homologues of membrane proteins. FEMS Microbiol. Rev. 22, 305–322.

Lolkema, J.S., Dobrowolski, A. and Slotboom, D.J. (2008) Evolution of Antiparallel Two-domain Membrane Proteins: Tracing Multiple Gene Duplication Events in the DUF606 Family. J. Mol. Biol. 378, 596–606.

Pao, S.S., Paulsen, I.T. and Saier Jr., M.H. (1999) Major facilitator superfamily. J. Mol. Microbiol. Biotechnol. 1: 257-279.

Penczek, P., Radermacher, M. and Frank, J. (1992) Three dimensional reconstruction of single particles embedded in ice. Ultramicr. 40, 33-53.

Pines, G., Danbolt, N.C., Bjoras, M., Zhang, Y., Bendahan, A., Eide, L., Koepsell, H., Storm-Mathisen, J., Seeberg, E. and Kanner, B. I. (1992) Cloning and expression of a rat brain L-glutamate transporter. Nature 360, 464–467.

Pos, K.M., Bott, M., and P. Dimroth. 1994. Purification of two active fusion proteins of the Na(+)-dependent citrate carrier of Klebsiella pneumoniae. FEBS Lett. 347:37-41.

Saier, Jr., M.H. (2000) A functional-phylogenetic classification system for transmembrane solute transporters. Microbiol. Mol. Biol. Rev. 64, 354-411.

Slotboom, D.J., Koning, W.N. and Lolkema, J.S. (1999) Structural features of the glutamate transporter family. Microbiol. and Molecular Rev. 63, 293–307.

Slotboom, D.J, Sobczak, I., Konings, W.N., Lolkema, J.S. (1999) A conserved serine-rich stretch in the glutamate transporter family forms a substrate-sensitive reentrant loop. Proc Natl Acad Sci U S A. 96, 14282-7.

Sobczak, I. and Lolkema, J.S. (2003) Accessibility of Cysteine Residues in a Cytoplasmic Loop of CitS of *Klebsiella pneumoniae* is Controlled by the Catalytic State of the Transporter. Biochemistry 42, 9789-9796.

Storck, T., Schulte, S., Hofmann, K. and Stoffel, W. (1992) Structure, expression, and functional analysis of a Na(1)-dependent glutamate/aspartate transporter from rat brain. Proc. Natl. Acad. Sci. USA 89, 10955–10959.

Tolner, B., Poolman, B. and Konings, W.N.(1992) Characterization and functional expression in Escherichia coli of the sodium/proton/glutamate symport proteins of Bacillus stearothermophilus and Bacillus caldotenax. Mol. Microbiol. 6 , 2845-2856

Van Geest, M. and Lolkema, J.S. (1996) Membrane topology of the Na^+ ion dependent citrate carrier of *Klebsiella pneumoniae.* J. Biol. Chem. 271, 25582 - 25589.

Van Geest, M. and Lolkema, J.S. (1999) Transmembrane Segment (TMS) VIII of the Na^+/Citrate Transporter CitS Requires Downstream TMS IX for Insertion in the *Escherichia coli* Membrane. J. Biol. Chem. 274, 29705 - 29711.

Van Geest, M. and Lolkema, J.S. (2000) Membrane topology of the Na^+/citrate transporter CitS of *Klebsiella pneumoniae* by insertion mutagenesis. Biochimica et Biophysica Acta 1466, 328-338.

Van Heel, M. (1987) Similarity measures between images. Ultramicr. 21, 95-100.

Van Heel, M., Gowen, B., Matadeen, R., Orlova, E.V., Finn, R., Pape, T., Cohen, D., Stark, H., Schmidt, R., Schatz, M., Patwardhan, A. (2000) Single-particle electron cryo-microscopy: towards atomic resolution. Q. Rev. Biophys. 33, 307-369.

Veenhoff, L.M., Heuberger, E.H.M.L., Duurkens, H.H., Poolman, B. 2001. Oligomeric state of membrane transport proteins analyzed with blue native electrophoresis and analytical ultracentrifugation. J. Mol. Biol. 317:591-600.

Stark, H., Schmidt, R., Schatz, M. and Patwardhan, A. (2000) Single-particle electron cryo-microscopy: towards atomic resolution. Quat. Rev. Biophys. 33, 307–369.

Yernool, D., Boudker, O., Folta-Stogniew, E. and Gouaux, E. (2003) Trimeric subunit stoichiometry of the glutamate transporters from Bacillus caldotenax and Bacillus stearothermophilus. Biochemistry 42, 12981-12988.

Yernool, D., Boudker, O., Jin, Y., Gouaux, E. (2004) Structure of a glutamate transporter homologue from Pyrococcus horikoshii. Nature 431, 811-818.

Chapter 5

Structural characterization of outer membrane components of the Type IV pili system in pathogenic *Neisseria* by single particle electron microscopy

Katarzyna B. Mościcka*, Samta Jain*, Martine Bos, Wilko Keegstra, Egbert J. Boekema, and Chris van der Does

* contributed equally.

ABSTRACT

The structure of the PilQ secretins from *Neisseria gonorrhoeae* and *Neisseria meningitidis*, embedded in isolated outer membranes, was investigated by transmission electron microscopy. Two-dimensional projection maps of the PilQ oligomers were obtained by single particle averaging. Remarkably, by analyzing oligomers within the native membrane, additional domains could be revealed which were not observed in studies using purified proteins. PilQ complexes of *N. gonorrhoeae* showed a double ring structure with a clear 14-fold symmetry of the outer ring, and a 14-15-fold symmetry in the inner ring. From the 14 protein densities of the outer ring 7 external spikes are protruding. PilQ complexes of *N. meningitidis* also consisted of two rings, but also complexes partly or completely lacking the outer ring were observed. The outer ring of the *N. meningitidis* PilQ had a 19-fold symmetry. In the *N. meningitidis* structures, no external spikes, were observed. The inner ring structures observed for both *N. gonorrhoeae* and *N. meningitidis* were of similar size as the structures previously observed from the isolated PilP/PilQ complexes, demonstrating that the second ring and the external spikes do not contain domains of the PilQ or PilP proteins. To investigate the composition of the outer ring and the spikes, the structure of PilQ complexes

within membranes of several *N. gonorrhoeae* knock-out mutants was investigated. A knock-out of PilP, a lipoprotein shown to interact with PilQ did not show spikes, indicating that this protein might be directly or indirectly involved in the spike composition. Remarkably the PilP knock-out also showed a change in the symmetry of the outer ring from 14 to 19 fold. A PilF mutant also did not show spikes, but maintained the 14-fold symmetry of the outer membrane. PilF is an ATPase located in the inner membrane, involved in pilus assembly, suggesting that localization of the spike-protein depends on functional assembly of the pilus. The PilC2 and PilW mutants yielded similar structures as observed for the wild-type, indicating that they are not involved in these structures.Single particle analysis also showed that the structure composed of two rings and spikes has a high rotational flexibility, especially the connection of the two rings is flexible. This suggests that the second ring and spikes my have a role in stabilizing the anchoring of the PilP/PilQ complexes with the membranes.

INTRODUCTION

Neisseria species are gram-negative bacteria, whose pathogenic members are associated with significant morbidity and mortality for their exclusively human hosts. *Neisseria meningitidis*, which normally inhabits the human nasopharynx, and *Neisseria gonorrhoeae*, which normally colonizes mucosal surfaces, are responsible for bacterial meningitis and septicemia, and the sexually transmitted disease gonorrhea, respectively (Tønjum and Koomey 1997). During the infection process, a remarkable variety of adhesins is involved in the modulation of the interaction with the host cell. Among these adhesins are type IV pili which mediate binding of the bacteria to host cells. Type IV pili are long fibrous structures emanating from the bacterial surface involved in a variety of processes. Type IV pili not only mediate cellular attachment to tissue receptors (Jönsson et al. 1994), but are also involved in several other processes, including bacterial auto-agglutination (Frøholm et al. 1973; Swanson et al. 1971), twitching motility (Henrichsen et al. 1972), biofilm formation and natural competence for DNA uptake (Frøholm et al. 1973; Mathis and Scocca 1984).

Type IV pili are long (>1–5 µm), thin (60–70 Å), mechanically strong polymeric fibers which can be extented and retracted. The pilus consists of 500–2000 subunits of the major pilin protein, PilE (Parge et al, 1995) and is assembled by a complex machinery consisting of up to 30 proteins (Wolfgang et al. 2000, Morand et al, 2004, Carbonnelle et al. 2005; Tønjum

and Koomey 1997). This machinery shows similarity to the apparatus for secretion of proteins of the general (type II) secretory pathway (Nunn, 1999; Peabody et al. 2003; Pugsley 1993). The first step of assembly of the pilus is the insertion of PilE into the cytoplasmic membrane. In the cytoplasmic membrane the hydrophobic leader peptide is removed and the freed N-terminal amino acid is methylated by the pre-pilin peptidase PilD (Strom et al. 1993). It was proposed that the PilE subunits are assembled and extruded from the inner membrane by the PilF ATPase (a homologue of GspE, and a member of the AAA chaperone/mechanico-enzyme family) with the aid of a polytopic inner membrane protein PilG. Remarkably a similar ATPase as PilF, PilT is involved in the dissasembly of the PilE subunits at the cytoplasmic membrane, resulting in retraction of the pilus. Several other neisserial proteins, called pseudopilins or minor pilins, which show homology in their N-terminal hydrophobic leader peptide with the PilE signal peptide, are processed by PilD and can also be intergrated into the growing pilus. The pilus passes the outer membrane through PilQ (Drake and Koomey 1995; Tønjum et al. 1995). PilQ is an antigenically conserved, abundant outer membrane protein, and a member of the GspD secretin superfamily of integral outer membrane proteins involved in different processes like type II and type III secretion (Pugsley 1993).

Examination of the purified secretins of members of this superfamily, such as XcpQ and PilQ from *Pseudomonas aeruginosa* (Bitter et al. 1998), PulD from *Klebsiella oxytoca* (Hardie et al. 1996), the pIV protein, through which filamentous phages are secreted (Daefler et al. 1997; Linderoth et al. 1996) and PilQ of *N. meningitidis* (Collins et al. 2001, Collins et al. 2003) by transmission electron microscopy (TEM) indicated that these proteins form a multimeric ring-like structure. A 3D structure of the PilQ complex was determined by using single particle averaging methods applied to transmission electron microscopy (EM) images of the purified multimer visualized by cryo-negative EM staining. This structure showed a large central cavity, which was closed at the poles by ‘plug’ and ‘cap’ features, and four ‘arm’ features at the sides with an apparent cavity around 60 Å in diameter). A higher resolution 3D structure of a secretin was obtained for PulD of *K. oxytoca*. This complex consists of a dodecameric structure composed of two rings that sandwich a closed disc. The two rings form chambers on either side of a central plug that is part of the middle disc.

Members of the secretin superfamily often strongly interact with small lipoproteins, also known as pilotins, or pilot proteins. These lipoproteins are involved in oligomerization, stabilization, and/or outer membrane localization of the secretin. For example, the *K. oxytoca*

PulD requires PulS for proper outer membrane association; in its absence, PulD remains associated to the inner membrane. MxiM of *Shigella flexneri* and YscW of *Yersinia enterocolitica* are required for outer membrane localization of the Type III secretion secretins MxiD and YscC respectively (Burghout et al. 2004; Schuch and Maurelli 2001). The interaction between MxiM and MxiD has been studied using NMR spectroscopy (Okon et al. 2008). It has been demonstrated that PilP and PilW interact with the Neisserial PilQ. PilP was shown to co-purify with PilQ and to localize to the cap region of the PilQ complex. Although PilQ does not need PilP for its stabilization or membrane localization *pilP* mutants showed a loss of piliation and natural competence and greatly reduced amounts of PilQ in the outer membrane. In a *pilW* mutant, the total amount or outer membrane localization of PilQ was not changed, but the stability of the PilQ multimer was strongly affected. Another protein that has been proposed to interact with PilQ is PilC. Within the pathogenic *Neisseria* species, two copies of PilC (PilC1 and PilC2) are found. In *N. gonorrhoeae,* both copies can be exchanged and function as pilus tip adhesins, while in *N. meningitidis*, only PilC1 promotes adhesion. The PilC proteins are associated with the outer membrane but can also be recovered from purified pili, were they seem to be located at the top of the pilus (Rahman et al.1997).

Although the observations made by different authors have been useful in establishing that secretins adopt ring-like structures with 12-14 fold symmetry, there are still many questions remaining. Structural information about the interaction of the secretins with other components is lacking. Since all structural information about the secretins obtained to date has been obtained from purified proteins, and multi-subunit membrane complexes can loose subunits during the purification procedure (Folea et al. 2008), we set out to study the structure of the PilQ secretin within the membrane using Transmission Electron Microscopy and single particle averaging. Using isolated outer membranes we were able to determine the 2-dimensional structure of the PilQ oligomers of *N. gonorrhoeae* and *N. meningitidis.* Remarkably, using this approach, additional domains could be observed which were not observed in studies using purified proteins. PilQ complexes of *N. gonorrhoeae* showed a double ring structure with a 14-fold symmetry of the outer ring, and external spikes on the outer ring with a 7-fold symmetry. PilQ complexes of *N. meningitidis* also consisted of complexes consisting of two rings, but also structures lacking or having a partial outer ring were observed. The outer ring of the *N. menigitidis* PilQ had a 19-fold symmetry. In the *N. meningitidis* structures, no external spikes were observed. The inner ring structures observed for both *N. gonorrhoeae* and *N. meningitidis* were of similar size and shape as the structures

previously observed from the isolated PilP/PilQ complexes demonstrating that the second ring and the external spikes consist of proteins most likely do not consist of PilQ or PilP proteins.

To obtain further information on the PilQ complex, we studied the structure of the complex in membrane derived from *pilP*, *pilW*, *pilF* and *pilC2* knock outs. While no differences were observed in the *pilW* and *pilC2* knock-outs, remarkable difference were observed for the *pilF* and *pilP* knock-outs. The *pilF* knock-out lost the outer spikes, while the *pilP* not only lost the outer spikes, but also changed the symmetry of the outer ring from 14 to 19. Implications for the assembly and structure of the observed PilQ mega-complex are discussed.

MATERIALS AND METHODS

Strains, plasmids, primers and media

Neisseria gonorrhoeae strain MS11, *Neisseria meningitidis* strains HB1 and M986 and further strains created in this study are described in Table 1. *N. gonorrhoeae* strains were grown at 37 ºC in 5% CO_2 on GCB (Difco) plates containing Kellog's supplement (Kellog et al. 1963) or GCB liquid medium (GCBL) containing 0.042% $NaHCO_3$ and Kellog's supplements. *N. meningitidis* was also grown at 37 ºC in 5% CO_2 on GC-agar plates or in tryptic soy broth (TSB). When necessary, erythromycin was used at 5 μg/ml.

Construction of knock-out strains

Knock-outs in PilC, PilW and PilF were made using the insertion-duplication mutagenesis method (Hamilton et al. 2005). Using this method, the gene is disrupted and expression of genes downstream of the disrupted gene is driven from the erythromycin promotor. PCR products encoding 541 bp (primers PilC-for and PilC-rev), 452 bp (primers PilW-for and PilW-rev) and 524 bp (primers PilF-for and PilF-rev) fragments of PilC, PilW and PilF were generated by performing a PCR on isolated chromosomal DNA of *N. gonorrhoeae* strain MS11 (for a list of used primers, see Table 2). PilC and PilW PCR fragments were digested with *Bam*HI and *Knp*I and ligated into the *Bam*HI/*Kpn*I sites of pIND3 (Hamilton et al. 2001) resulting in plasmids pSJ030 and pSJ032 respectively. The PilF PCR fragment was digested with *Xho*I *and Kpn*I and ligated into *Xho*I */Kpn*I site of pIND3 resulting in plasmid pEP057. Plasmids pSJ030 and pSJ032 were transformed to MS11 and plasmid pEP057 was transformed to EP019 (derivative of MS11A strain) and colonies were selected on GCB plates containing erytromycin. Correct clones were identified by performing a PCR on isolated

chromosomal DNA of these colonies resulting in strains SJ030-MS, SJ032-MS and EP060 respectively (Table 1B). To create marker-less non-polar knock-outs of PilP and PilQ, PCR fragments of the flanking regions of the respective genes were annealed using the splicing by overlapping extension PCR (SOE-PCR) (Horton et al. 1990) method. To create the PCR products for PilP and PilQ, the primer combinations of PilP-for1/PilP-rev1 and PilP-for2/PilP-rev2 and PilQ-for1/PilQ-rev1 and PIlQ-for2/PilQ-rev2) were used. The obtained PCR products were diluted and amplified with the external primers which also contained the gonoccocal DNA uptake sequence (DUS). The PCR product was transformed to strain MS11 and the mutant colonies were checked using colony PCR. Correct clones were identified by performing a PCR on isolated chromosomal DNA of several colonies resulting in strains SJ031-MS and SJ001-MS (Table 1B). To further confirm the correct deletion of the gene, the deletion site and the flanking regions were determined by sequencing.

Membrane Preparation

To isolate membranes of *N. gonorrhoeae*, the strain was plated on GCB plates with the appropriate antibiotic, and (when possible) piliated cells were scraped from the plate and transferred to 3 ml GCBL medium. Cells were grown to an OD660 of 0.6 and consecutively diluted into increasing volumes until a final volume of 1 liter with an OD660 of 1.0 was obtained. Cells were centrifuged at 8000 rpm and resuspended in 50 mM Tris-HCl pH 7.5. Cells were broken by three passes through a French press at 15psi. Cell debris was removed by centrifugation at 6000 rpm for 10 min. The membranes were spun down at 40,000 rpm for 1 hr, resuspended in 1 ml of 50 mM Tris-HCl pH7.5 and overlaid on a 4 step (1, 1.8, 0.8 and 0.8 ml) sucrose gradient of 54, 51, 45 and 36 (w/v) sucrose) and centrifuged at 80,000 rpm for 30 mins. The lower two fractions were collected, diluted in 50 mM Tris-HCl pH 7.5 and membranes were collected by centrifugation at 40,000 rpm for 1 hr and resuspended in 1 ml 50 mM Tris-HCl pH 7.5. To isolate membranes of *N. meningitidis*, the strain was inoculated from an overnight GC-agar plate in 40 ml tryptic soy broth (TSB) at an OD550 of 0.1 and grown for 7 hours to OD_{550} of 4. Cells were collected by centrifugation, resuspended in 50 mM Tris/HCl, 5 mM EDTA pH8 and frozen at -80°C. After thawing, aliquots were plated to verify killing of the bacteria. The suspensions were sonicated for 4 minutes (Branson 450, setting 6, output 40%) and spun at 10.000 rpm (12.000xg) in an SS34 rotor in a Sorvall RC 5B centrifuge. The resulting supernatant was spun for 8 minutes at 40000 rpm (100.000xg) in a Ti-70 rotor in a Beckmann LE-80K ultracentrifuge. Cell envelope pellets were dissolved in 2 mM Tris/HCl pH 7.6 and overlaid on a 4 step (1, 1.8, 0.8 and 0.8 ml) sucrose gradient of 54,

51, 45 and 36 (w/v) sucrose) and centrifuged at 80,000 rpm for 30 mins. The lower two fractions were collected, diluted in 50 mM Tris-HCl pH 7.5 and membranes were collected by centrifugation at 40,000 rpm for 1 hr. The final membrane preparation was resuspended in 50mM Tris-HCl, pH 7.5, for EM analysis.

Electron Microscopy and single particle analysis

For image processing, whole membranes from *Neisseria gonorrhoeae* and *Neisseria meningitidis* were negatively stained with 2% uranyl acetate on glow-discharged carbon-coated copper grids. Electron microscopy was performed on a Philips CM120 equipped with a LaB_6 tip operating at 120 kV. The "GRACE" system for semi-automated specimen selection and data acquisition (Oostergetel et al. 1998) was used to record 2048 x 2048 pixel images at 60000x calibrated magnification with a Gatan 4000 SP 4K slow-scan CCD camera. About 8000 images were recorded, and about 20000 single particle projections of the PilQ complex from *Neisseria gonorrhoea*, 8000 projections of the PilQ complex from *Neisseria meningitidis*, 7000 projections of the PilC knock-out, 6000 of PilW knock-out and around 5000 of the PilP knock-out projections from *N. gonorrhoea* were selected, respectively. Single particle analysis was performed using the Groningen Image Processing ("GRIP") software packages on a PC cluster. Single particles of PilQ were repeatedly aligned and classified and finally the best 100% of the data set was taken for the final sums.

Table 1: strains used in the study

Strains	Description	Reference
HB1	*Neisseria meningitidis* strain	Bos et al, 2005
M986	*Neisseria meningitidis* strain	Tsai et al, 1980
MS11	*Neisseria gonorrhoeae* strain	Swanson et al, 1971
SJ001-MS	MS11 strain with PilQ truncation	This work
SJ030-MS	MS11 strain transformed with pSJ030; non polar insertion in PilC, ErmC	This work
SJ031-MS	MS11 strain transformed with PCR product to introduce truncation in PilP	This work
SJ032-MS	MS11 strain transformed with pSJ032; non polar insertion in PilW, ErmC	This work
EP060	EP019 strain transformed with pEP057; non polar Insertion in PilF, ErmC	This work

Table 2: Primers used in this study.

PilC-for	5’-TGGCGGTACCCTCGCTGCCCAAATTGAAAG-3’
PilC-rev	5’-GCGCGGATCCGTAAATACGCTATTATCATGGACG-3’
PilW-for	5’-GCGCGGTACCTTGTCCGCGATGCAAGAATG-3’
PilW-rev	5’-GCGCGGATCCCGACCGCATAGGCATTGACCAC-3’
PilF-for	5’-ATGCTCGAGACGGCGCGACACCCATATTC-3’
PilF-rev	5’-TACGGTACCCGGCAAGCCTGTCGATTTCC-3’
PilP-for1	5’-GGTTTCCCTAACGTAAGTTATTTTTGCTCGGCATTTTGTG-3’
PilP-rev1	5’-ATGCCGTCTGACTTCACCTGCTCAACCTTCC-3’
PilP-for2	5’-TTCAGACGGCATGCCGCCAATTCGATAATGCC-3’
PilP-rev2	5’-ACTTACGTTAGGGAAACCATGAATACCAAACTGACAAAAATC-3’
PilQ-for1	5’-GCTGACTATGACGTCCAGACATCAAAGTTTCCTCCCTGCC-3’
PilQ-rev1	5’-TTCAGACGGCATGCCGCCAATTCGATAATGCC-3’
PIlQ-for2	5’-ATGCCGTCTGAAACCTTTCCAAGCACCTACCC-3’
PilQ-rev2	5’-GACGTCATAGTCAGCATGGAGTAATCCTCTTCTTAAT-3’

RESULTS

Transmission electron microscopy on isolated membranes of Neisseria gonorrhoeae

To study the structure of the PilQ secretin of *N. gonorrhoeae* in its native environment, total membranes were isolated and separated on a sucrose gradient. Fractions containing the highest amount of PilQ (from 45 to 51 % (w/v) sucrose) were collected and concentrated. This fraction contained both inner and outer membranes as determined by antibodies against SecY and DsbA (as inner membrane markers) and Omp85 and Imp (as outer membrane markers) (data not shown). These mixed membranes were analyzed with transmission electron microscopy. Indeed both inner membranes which appear as vesicles and outer membranes which appear as flattened sheets could be identified (data not shown). The membranes form rather intact closed vesicles, because upon air-dried negative staining, the

membranes collapse and became superimposed. This can be seen at the edges where a white rim marks the curvature (Fig. 1A). The outer membranes contained prominent stain-filled indentations (Fig. 1A) which were absent in the inner membranes, with an average density of 350 indentations per μm^2. Since these stain-filled indentations could be formed by the PilQ secretin, a *pilQ* knock-out strain was constructed. The absence of PilQ within membranes isolated from this strain was confirmed by Western blotting using an anti-PilQ antibody (data not shown), and isolated membranes of this strain were checked by electron microscopy (Fig. 1B). The stain filled indentations were absent in the membranes of the *pilQ* knock-out demonstrating that the stain filled indentations are indeed related to PilQ.

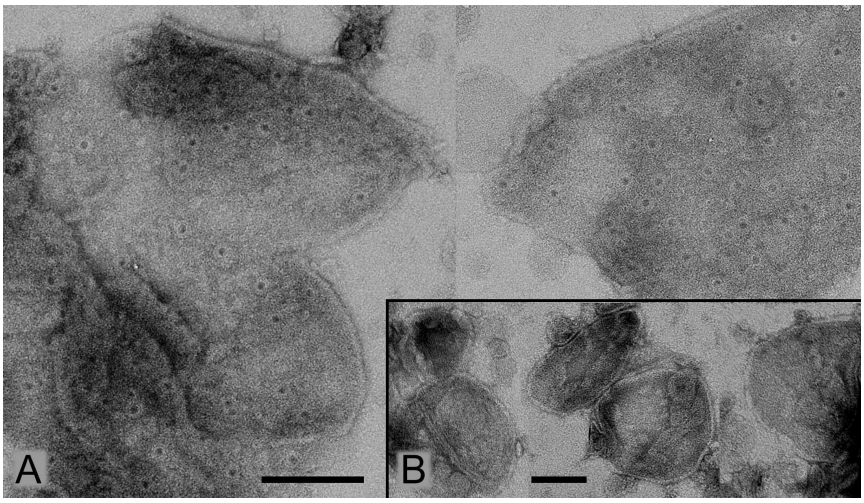

Figure 1. *Overview of negatively stained Neisseria gonorrhoeae membranes.* ***(A)*** *Membranes isolated from strain MS11.* ***(B)*** *Membranes isolated from a pilQ knock-out strain. Space bar for frames in A and B is 1000 Å.*

Projection structure of N.gonorrhoeae PilQ

To further analyze the PilQ structure, a large data set of about 20,000 single projections of the stain-filled indentations was obtained from EM images and this data set was analyzed by single particle analysis. After several cycles of multi-reference alignment, multivariate statistical analysis and classification, final class sums from all analyzed particles were obtained (Fig. 2A). The 2D map shows a circular particle composed of a double ring with extending spike-like densities. The inner ring has a diameter of 150 Å and has a large central cavity, whereas the second ring has a diameter of 210 Å. The spikes further extend the

diameter to 310 Å. The second ring clearly has a 14-fold symmetry, while the spike-like densities show a 7-fold symmetry. After applying 7-fold symmetry, the features of both the second ring and the spikes improve (Fig. 2B). If this figure is used for further improvement as a reference in a next alignment procedure, it appears that the spike features become stronger, but at the cost of the resolution of the outer ring, which now becomes less well defined (Fig. 2C). This suggests that the structure has some flexibility between the second ring and the spikes. The symmetry of the inner ring could not be resolved from either the class averages without symmetry applied or from the class averages with 7-fold symmetry applied. In an attempt to determine the symmetry of the inner ring, the second ring was masked out during analysis. After repeated alignment and classification the final projection map showed two striking features. First, densities in the inner ring come into focus (Fig. 2D). At least 11 densities are well separated, with a average center-to-center distance of about 25 Å (red bars, Fig. 2E). However, in two areas the features are not well resolved (blurred red bars), despite the fact that we increased the number of analyzed projections from 20,000 to 36,000. This indicates that at the current resolution of this map, which is in the range of the 25 Å of the center-to-center distance of the inner ring densities, we can not prove the symmetry. It appears most likely to be 14 or 15. By imposing 14-fold symmetry, as performed in Fig. 2F, the features become stronger enhanced than with any other imposed symmetry between 12 and 16. A second striking result from this analysis is the total disappearance of the features of the second ring. This shows that also the association of the inner and outer ring is remarkably flexible, much more flexible than between the second ring and the outer spikes.

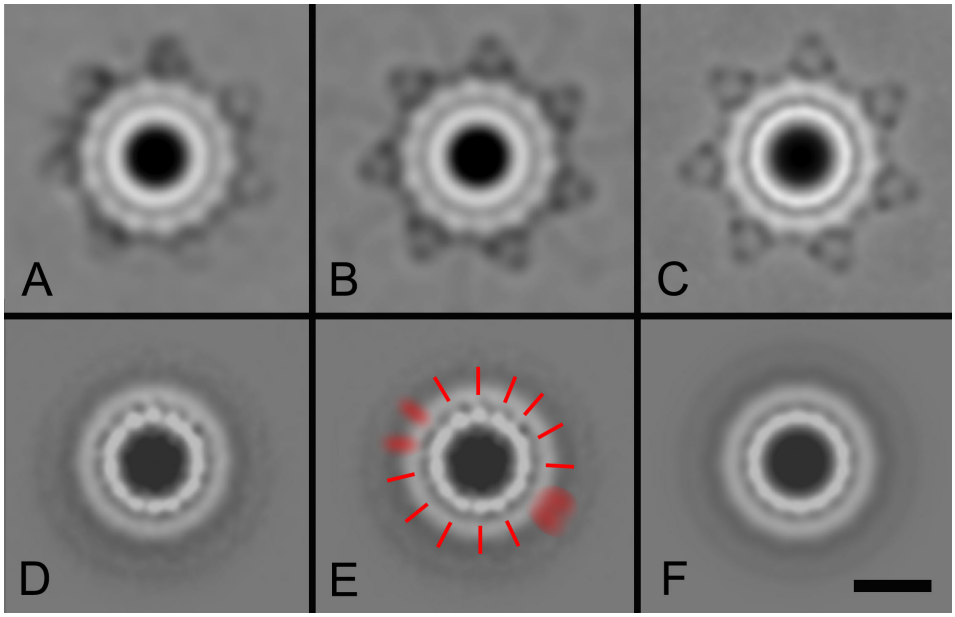

Figure 2*. Class averages of single particle electron microscopy images of the PilQ complex from N. gonorrhoeae.* ***(A)*** *wild-type projection map* ***(B)*** *with 7-fold symmetry imposed on the outer spikes* ***(C)*** *with 7-fold symmetry imposed using the class average of (C) as template* ***(D)*** *class average of the inner ring, after masking out the second ring and spikes* ***(E)*** *inner ring 2D map with positions of densities indicated* ***(F)*** *inner ring 2D map with imposed 14-fold symmetry. The projection map of the PiliQ complex in frame A has a resolution of 20 Å. The scale bar is 100 Å.*

Transmission electron microscopy on isolated membranes of Neisseria meningitidis

The PilQ and PilP proteins from *N. gonorrhoeae* and *N. meningitidis* are highly homologous (89 % identity and 91 % similarity for PilQ and 98 % identity and 98 % similarity for PilP). The structure of the purified PilQ/PilP complex was previously analyzed by transmission electron microscopy (Collins et al. 2001, Collins et al. 2003, Collins et al. 2004). To enable us to compare the previously published structure of the solubilized *N.meningitidis* PilQ/PilP complex to the structures of *N. gonorrhoeae* and *N. meningitidis* PilP/PilQ in the membrane, membranes of *N. meningitidis* were isolated and analyzed by transmission electron microscopy. The membranes of *N. meningitidis* also showed the presence of pores, but in much smaller numbers compared to *N. gonorrhoeae*. Moreover, the pores were less homogeneously distributed in the membrane, and some of them are found in

small clusters (Fig 3A). Single particle analysis showed a structure composed of only one ring (Fig. 3B) or with an additional second ring in about 20% of the data set (Fig. 3C). Some particles (10 %) showed an incomplete second ring (Fig. 3D). The inner and outer rings have the same diameter as observed in the *N. gonorrhoeae* structure (Fig. 3E). Remarkably, there is no indication for spikes attached to the second ring. The motif in the second ring, is also substantially smaller than in *N. gonorrhoeae*, indicating that it is possibly composed of a larger number of copies of a smaller protein. Symmetry analysis was performed to evaluate the number of copies. It appears that imposing 2-, 3-, or 7- fold does not enhance the features (not shown). Since the motif is smaller than in *N. gonorrhoeae*, symmetries above 14 were evaluated (Fig. 3F-J). This approach strongly points to a 19-fold symmetry in the second ring. Based on the high similarities of the PilP and PilQ proteins of N.meningitis and N.gonorrhoeae, the observed differences were unexpected. To ensure that the lack of spikes is a general feature of *N. meningitidis*, and not caused by the strain used, two different *N. meningitidis* strains, M986 and HB-1, which are different clonal lineages were used. Both strains gave very similar results. To further exclude that the *N. menigitidis* strains used in our study contained any mutations affecting *pilP* or *pilQ*, the entire PilP/PilQ operon and flanking regions were sequenced, but no differences were observed with the published sequence of strain (Bentley et al. 2007).

Previously, a purified *N. meningitidis* PilQ complex was studied by electron microscopy. The PilQ complex appeared as single rings with a diameter of approximately 15.5 to 16.5 nm and 6.0- to 6.5-nm-diameter cavities in the central region (Collins et al. 2001). These rings are comparible to the inner ring of both the *N. menigitidis* and *N. gonorrhoeae* structures. Data reported for oligomeric rings of PilQ and XcpQ of *Pseudomonas aeruginosa* show rings of 198 Å and 183 Å (Bitter et al 1998), but it is not clear if these structures are actually composed of two rings, since no image processing was performed.

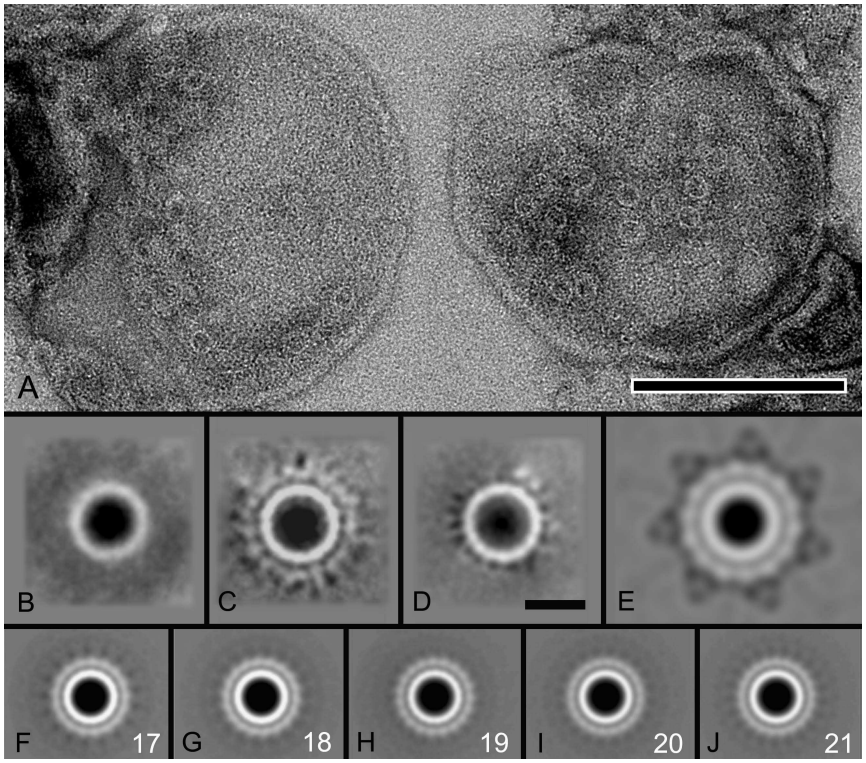

Figure 3*. Electron microscopical analysis of the PilQ complexes in isolated membranes. (A) Neisseria meningitidis membranes negatively stained with 2% uranyl acetate (B-D) Average of 8,000 projections of the PilQ complexes from N. meningitidis showing classes with single, double and incomplete rings, respectively. (E) Average of 10,000 projections of PilQ complex from N. gonorrhoeae showing inner and the outer ring having 14- fold symmetry. (F-J) To investigate the number of copies of the outer ring, 17- to 21-fold rotational symmetry (white numbering) was imposed on the classes after completion of the analysis. Strongest rotational symmetry within the second ring is in frame H. Scale bar in equals 1000 in (A) and 100 Å in (B-J) .*

Structure and assembly of the PilQ complex of N. gonorrhoeae

Our analysis of the structure of the PilQ complex in isolated outer membranes unequivocally shows extra subunits not observed in purified PilQ/PilP complexes. To try to identify the different subunits, we set-out to knock-out possible candidates for the extra observed densities. PilC is a protein normally present in two copies, involved in adhesion to

epithelial cells, and is located in the outer membrane and at the tip of the pilus. Since the MS11 strain used for our study, contains a non functional copy of *pilC1* (Rudel et. al. 1995), we first generated a pilC2 knock-out. PilC2 is a protein with a molecular weight of 110 kDa. Single particle analysis was performed as on WT membrane pore complexes, and 6,000 projections were analyzed. The *pilC* knock-out yielded projection maps showing a similar structure as observed for WT with the presence of double rings plus 7 spikes (Fig. 4C). Again the features become more visible after imposing symmetry (Fig. 4D). This demonstrates that PilC2 is not a subunit of the observed PilQ complex. In a next step, a knock-out of pilW, a lipoprotein with a molecular mass of 28 kDa of the mature protein which was shown to be involved in stabilization of the PilQ oligomer was generated. As observed for the *pilC* knock-out no differences from WT were observed when 6,000 projections were analyzed. The membranes also contained a similar density of particles. This demonstrates that stable PilQ complexes can indeed still be formed within the membrane in the absence of PilW, and that PilW is not a subunit of the PilQ complex we observed.

PilP is an 18 kDa lipoprotein shown to co-purify stoichiometrically with PilQ. Both in *N. meningitidis* and *N. gonorrhoeae* PilP and PilQ are located within one operon and are co-transcribed (Balasingham et al. 2007). *PilP* mutants show a loss of piliation and natural competence and strongly reduced amounts of PilQ in the outer membrane (Drake et al. 1997). A previous study in which a comparison was made of the 3D reconstructions of *N. meningitidis* PilQ complexes derived from WT strains and of a strain lacking the PilP protein showed that PilP localized to the cap region of the PilQ complex (Balasingham et al. 2007). Comparison of these results with our structures suggests that the PilP protein is a component of the outer ring or involved in its assembly. To study the localization of PilP in PilQ complexes within the membrane, a *pilP* knock-out was created in *N. gonorrhoeae*, As expected, the density of PilQ complexes observed in the membranes derived from the *pilP* knock-out was reduced to only ~30 % compared to the WT membranes, showing that our *pilP* mutant either affects the expression or the stability of the *pilQ* mutant. More remarkable differences were observed when the class averages of 6.000 particles without (Fig. 4G) and with applied symmetry (Fig. 4H) were compared to the class averages obtained from WT membranes. The *pilP* knock-out has not only lost the extending spike-like densities, but also the symmetry of the outer ring has changed from 14 to 19. Based on a possible localization of PilP between the inner and outer rings of the PilQ complex (see above), it could be proposed that deletion of PilP affects the interface between the inner and outer ring, resulting in a re-

assembly of the second ring. The reassembled second ring does not appear to be able to bind the spike-like extensions. Even more surprisingly, the structure of the PilQ complex in membranes derived of the *N. gonorrhoeae pilP* knock-out shows a remarkable similarity to the structure of the PilQ complex isolated from WT *N.meningitidis* membranes. Why the absence of PilP in the structure of the *N. gonorrhoeae* PilQ complex results in a structural change to a complex resembling the PilQ complex in *N. meningitidis* remains an open question (See discussion).

It has previously been shown that incubation of purified PilQ complexes with isolated pili can induce structural changes in PilQ (Collins et al. 2005). It was proposed that these structural changes could be explained by an outward movement of the arms and dissociation of the cap feature of the PilQ oligomer on binding to the pilus. To compare the structures of PilQ complexes that have interacted with the pilus and PilQ complexes that have not interacted with the pilus, membranes derived from a *pilF* knock-out were studied. PilF is an ATPase, localized in the inner membrane and essential for the assembly and extrusion of pilin sub-units. Remarkably, when the class averages of 6.000 particles obtained from membranes of the *pilF* knock-out without (Fig. 4I) and with applied symmetry (Fig. 4J) were compared to the class averages obtained from WT membranes, it appeared that the PilQ structure has lost the extending spike-like densities. This suggest that either the PilQ complex changes its conformation upon interaction with the pilus resulting in assembly of the extending spike-like structures, or that the spike-like structures are either formed by the pilus protein PilE or by a protein transported across the outer membrane along with the extension of the pilus.

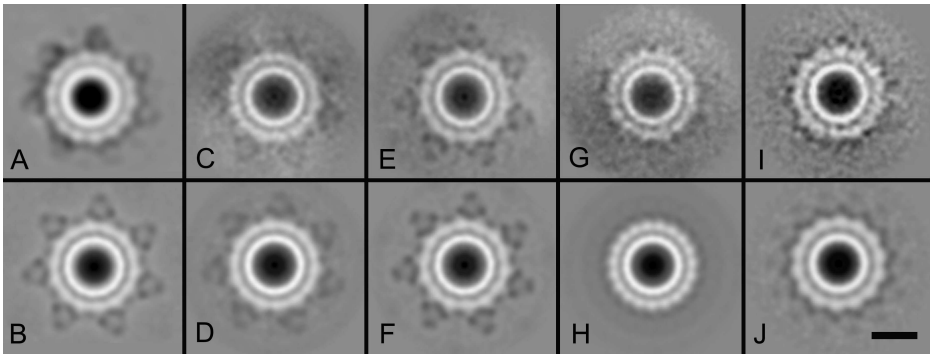

Figure 4. *Single particle analysis of particles derived of isolated membranes of different N. gonorrhoeae knock-out strains. Projection maps derived from membranes isolated from (A) N.gonorrhoeae strain MS11, (B) with 7-fold symmetry imposed, (C) the PilC mutant, (D) the PilC mutant with 7-fold symmetry imposed, (E) the PilW mutant, (F) the PilW mutant with 7-fold symmetry imposed, (G) the PilP mutant, (H) the PilP mutant with 19-fold symmetry imposed (I)the pilF mutant, and (J) the PilF mutant with 14-fold symmetry imposed on I. Scale bar equals 100 Å.*

DISCUSSION

In this study we set out to study the structure of the PilQ secretin within the outer membrane using transmission electron microscopy and single particle averaging. Our approach revealed features of a large structure not seen before. Compared to the previously published structures derived from purified PilP/PilQ complexes of *N. meningidis*, the complexes observed in *N. meningitidis* membranes contained an extra proteinous ring with a 19 fold symmetry. In our analysis we also observed structures lacking or having a partial outer ring, indicating that the extra domains are not tightly attached and can possibly also be dissociated during the membrane isolation procedure. Apparently this extra ring structure is also lost during the previously described purfication of the PilQ/PilP complexes (Balasingham et al. 2007). Remarkably, the complexes observed in membranes isolated from *N. gonorrhoeae* (which expresses highly similar PilQ and PilP proteins) appear much more stable, and showed a double ring structure with a 14-fold symmetry of the outer ring, from which seven external spikes are protruding. These data demonstrate that the study of these multi-componet membrane inserted complexes within their native lipid environment by electron microscopy can identify extra components and/or structures which are lost after purification.

Compared to the previously published structures derived from purified PilP/PilQ complexes of *N.meningitidis* shows that the inner ring in our structures most likely consists of PilQ and PilP. The symmetry of the inner ring of *N. meningitidis* has previously been determined to be 12, while the symmetries of the *K. oxocyta* PulD and the pIV protein of filamentous phages were respectively 12 and 14. We were unfortunately not able to conclusively determine the symmetry of the inner ring of *N. gonorrhoeae*, but our analysis indicates that the symmetry of the inner ring of *N. gonorrhoeae* is most likely 14, and thus could differ from the inner ring of *N. meningitidis*.

Another remarkable feature of the studied secretin complexes is the high flexibility between the different rings and the spikes. In particular, the fact that the number of protein copies in the second ring changes from 14 to 19 in a mutant lacking the spikes, is uncommon but intriguing. There is one other system of flexible interacting membrane proteins, that we like to discuss here in some detail, which has some similar structural aspects. Monomeric photosystem I (PSI) is a membrane protein complex of 330 kDa, which is mainly present as trimers in cyanobacteria. Under stress conditions it forms supercomplexes with a 37 kDa integral membrane protein named IsiA (see for details http://www.uniprot.org/uniprot/Q55274). These complexes have been extensively studied by electron microscopy (Yeremenko et al. 2004, Kouřil et al. 2005) and it was shown that IsiA can form complete and incomplete single and double rings around monomeric or trimeric PSI. The number of IsiA copies was variable; in the case of monomers the inner IsiA ring was composed of 12, 13 or 14 copies and these numbers matched with 19, 20 or 21 copies in the outer ring. One conclusion was that within these PSI-IsiA supercomplexes the double rings of IsiA are flexibly attached. For complexes with 14 / 21 IsiA copies, analysis showed that the rotational flexibility between both rings was about 2-3°, on the average. In this work on the secretin complex of the type IV pilus, we noticed a same type of rotational flexibility between the first and second ring and and a smaller fliexibility between the second ring and the spikes.

A second finding on the PSI-IsiA supercomplexes could also be relevant for the type IV secretion complex. On trimers with two IsiA rings, the inner ring is composed of 18 copies and the outer ring is formed by 25. However, the positions of IsiA in *incomplete* second rings with 12-19 copies were slightly different. If extrapolated to complete rings they appeared to consist of only 24 copies. These data illustrate how IsiA is flexibly attached to PSI

(Kouřil et al. 2005 and unpublished data). In a similar way, it could be possible that the protein(s) making the second ring around the secretin of the type IV pilus are flexible in their self-association. In one spike-less *N. gonorrhoeae* mutant and in *N. meningitidis* the ring contains 19 copies, but the association of spikes, each binding two second ring proteins, triggers ring formation with only 14 copies. There is, however, no evidence that the second rings of 14 and 19 copies in Neisseria contain the same protein(s).

Within this study we also tried to identify the proteins located within the second ring and in the spike-like extensions, and showed that neither PilC2 or PilW are components of the outer ring or the spike-like extensions. Remarkably, our study showed that the PilQ structure in the *pilP* knock-out has not only lost the extending spike-like densities, but also the symmetry of the outer ring has changed from 14 to 19. A previous study showed, however, that PilP localized to the cap region of the PilQ complex (Balasingham et al. 2007), which would place the PilP protein on the interface between the inner and outer ring, making it unlikely that PilP forms either the second ring or the spike-like extension. Finally, it became apparent that in the PilF knock-out the PilQ structure has lost the extending spike-like densities. Since PilF is an ATPase located in the inner membrane, it is unlikely that this protein is part of the spike-like extensions. Thus inactivation of the assembly and extrusion of the pilus results in loss of the spike-like extensions. This suggests that either the PilQ complex changes its conformation upon interaction with the pilus resulting in assembly of the extending spike-like structures, or that the spike-like structure are either formed by the pilus protein PilE or a protein transported across the outer membrane along with the extension of the pilus. We have therefore still not identified the proteins in the outer ring and spike-like extensions.

REFERENCES

Balasingham, S.V., Collins, R.F., Assalkhou, R., Homberset, H., Frye, S.A., Derrick, J.P. and Tønjum, T. (2007) Interactions between the Lipoprotein PilP and the Secretin PilQ in *Neisseria meningitidis.* J. Bacteriol. 189, 5716–5727.

Bentley, S.D., Vernikos, G.S., Snyder, L.A., Churcher, C., Arrowsmith, C., Chillingworth, T., Cronin, A., Davis P.H., Holroyd, N.E., Jagels, K., Maddison, M., Moule, S., Rabbinowitsch,

E., Sharp, S., Unwin, L., Whitehead, S., Quail, M.A., Achtman, M., Barrell, B., Saunders, N.J. and Parkhill, J. (2007) Meningococcal genetic variation mechanisms viewed through comparative analysis of serogroup C strain FAM18. PloS Genet. 16, 3, e23.

Bitter, W., Koster, M. Latijnhouwers, M., de Cock, H. and Tommassen, J. (1998) Formation of oligomeric rings by XcpQ and PilQ, which are involved in protein transport across the outer membrane of *Pseudomonas aeruginosa*. Mol. Microbiol. 27, 209–219.

Bos, M.P., Robert, V. and Tommassen, J. (2007) Functioning of outer membrane protein assembly factor Omp85 requires a single POTRA domain. EMBO Rep. 8, 1149-1154.

Burghout, P., Beckers, F., de Wit, E., van Boxtel, R., Cornelis, G.R., Tommassen, J. and Koster, M. (2004) Role of the pilot protein YscW in the biogenesis of the YscC secretin in Yersinia Enterocolitica. J. Bacteriol. 186, 5366-5375.

Carbonnelle, E., Helaine, S., Prouvensier, L., Nassif, X. and Pelicic, V. (2005) Type IV pilus biogenesis in *Neisseria meningitidis*: PilW is involved in a step occuring after pilus assembly, essential for fiber stability and function. Mol. Microbiol. 55, 54–64.

Collins, R.F., Davidsen, L., Derrick, J.P., Ford, R.C. and Tønjum, T. (2001) Analysis of the PilQ secretin from *Neisseria meningitidis* by transmission electron microscopy reveals a dodecameric quaternary structure. J. Bacteriol. 183, 3825–3832.

Collins, R.F., Ford, R.C., Kitmitto, A., Olsen, R.O., Tønjum, T. and Derrick, J.P. (2003) Three-dimensional structure of the *Neisseria meningitidis* secretin PilQ determined from negative-stain transmission electron microscopy. J. Bacteriol. 185, 2611–2617.

Collins, R.F., Frye, S.A., Kitmitto, A., Ford, R.C., Tonjum, T. and Derrick, J.P. (2004) Structure of the *Neisseria meningitidis* outer membrane PilQ secretin complex at 12 Å resolution. J Biol Chem 279, 39750–39756.

Collins, R.F., Frye, S.A., Balashingham, S., Kitmitto, A., Ford, R.C., Tønjum, T. and Derrick, J.P. (2005) Interaction with Type IV pili induces structural changes in the bacterial outer membrane secretin PilQ. J. Biol. Chem. 280, 18923-18930.

Daefler, S., Russel, M. and Model, P. (1997) Module swaps between related translocator proteins pIV(f1), pIV(IKe) and PulD: identification of a specificity domain. J. Mol. Biol. 266, 978-992.

Drake, S.L. and Koomey, M. (1995) The product of the pilQ gene is essential for the biogenesis of type IV pili in *Neisseria gonorrhoeae*. Mol. Microbiol. 18, 975–986.

Drake, S.L., Sandstedt, S.A. and Koomey, M. (1997) PilP, a pilus biogenesis lipoprotein in *Neisseria gonorrhoeae*, affects expression of PilQ as a high-molecularmass multimer. Mol. Microbiol. 23, 657–668.

Folea, I.M., Zhang, P., Nowaczyk, M.M., Ogawa, T., Aro, E.M. and Boekema, E.J. (2008) Single particle analysis of thylakoid proteins from *Thermosynechococcus elongatus* and Synechocystis 6803:Localization of the CupA subunit of NDH-1. FEBS Lett. 582, 249-254.

Frøholm, L.O., Jyssum, K. and Bøvre, K. (1973) Electron microscopical and cultural features of *Neisseria meningitidis* competence variants. Acta Pathol Microbiol Scand [B] 81, 525–537.

Hamilton, H.L., Schwartz, K.J and Dillard, J.P. (2001) Insertion-duplication mutagenesis of Neisseria: Use in characterization of DNA transfer genes in the gonococcal genetic island. J. Bacteriology 183, 4718-4726.

Hamilton, H.L., Dominguez, N.M., Schwartz, K.J, Hackett, K.T. and Dillard, J.P. (2005) *Neisseria gonorrhoeae* secretes chromosomal DNA via a novel type IV secretion system. Mol. Microbiol. 55, 1704-1721.

Hardie, K.R., Seydel, A., Guilvout, I. and Pugsley, A.P. (1996) The secretin-specific, chaperone-like protein of the general secretory pathway: separation of proteolytic protection and piloting functions. Mol Microbiol. 22, 967-976.

Henrichsen, J., Froholm, L.O. and Bovre, K. (1972) Studies on bacterial surface translocation. 2. Correlation of twitching motility and fimbriation in colony variants of *Moraxella nonliquefaciens, M. bovis*, and *M. kingii*. Acta Pathol Microbiol Scand [B] 80, 445–452.

Horton, R.M., Cai, Z.L., Ho, S.N. and Pease, L.R. (1990). Gene splicing by overlap extension: tailor-made genes using the polymerase chain reaction. Biotechniques 8, 528–535.

Jönsson, A.B., Ilver, D., Falk, P., Pepose, J. and Normark, S. (1994) Sequence changes in the pilus subunit lead to tropism variation of *Neisseria gonorrhoeae* to human tissue. Mol Microbiol 13, 403–416.

Kellogg, D.S. Jr., Peacock, W.L. Jr., Deacon, W.E., Brown, L. and Pirkle, C.I. (1963) *Neisseria Gonorrhoeae* I.Virulence Genetically Linked to Clonal Variation. J Bacteriol. 5, 1274–1279.

Kouřil R, Arteni AA, Lax J, Yeremenko N, D'Haene S, Rögner M, Matthijs HCP, Dekker JP, Boekema EJ (2005) Structure and functional role of supercomplexes of IsiA and Photosystem I in cyanobacterial photosynthesis. FEBS Lett 579, 3253-3257.

Linderoth, N.A., Model, P. and Russel, M. (1996) Essential role of a sodium dodecyl sulfate-resistant protein IV multimer in assembly-export of filamentous phage. J Bacteriol. 178, 1962-1970.

Mathis, L.S. and Scocca, J.J. (1984) On the role of pili in transformation of *Neisseria gonorrhoeae*. J Gen Microbiol 130, 3165–3173.

Morand, P.C., Bille, E., Morelle, S., Eugène, E., Beretti, J., Wolfgang, M., Meyer, T.F., Koomey, M. and Nassif, X. (2004) Type IV pilus retraction in pathogenic *Neisseria* is regulated by the PilC proteins. EMBO J. 23, 2009–2017.

Nunn, D. (1999) Bacterial type II protein export and pilus biogenesis: more than just homologies? Trends Cell Biol. 9, 402–408.

Okon, M., Moraes, T.F., Lario, P.I., Creagh, A.L., Haynes, C.A., Strynadka, N.C. and McIntosh, L.P. (2008) Structural characterization of the type-III pilot-secretin complex from *Shigella flexneri*. Structure 16, 1544-1554.

Oostergetel, G.T., Keegstra, W. and Brisson, A. (1998) Automation of specimen selection and data acquisition for protein electron crystallography. Ultramicroscopy 74, 47-59.

Parge, H.E., Forest, K.T., Hickey, M.J., Christensen, D.A., Getzoff, E.D. and Tainer, J.A. (1995) Structure of the fiber-forming protein Pilin at 2.6-Angstrom resolution. Nature 378, 32-38.

Peabody, C.R., Chung, Y.J., Yen, M.R., Vidal-Ingigliardi, D., Pugsley, A.P. and Saier, M.H., Jr. (2003) Type II protein secretion and its relationship to bacterial type IV pili and archaeal flagella. Microbiology 149, 3051–3072.

Pugsley, A.P. (1993) The complete general secretory pathway in Gram-negative bacteria. Microbiol. Rev. 57, 50–108.

Rahman, M., Källström, H., Normark, S. and Jonsson, A.B. (1997) PilC of pathogenic *Neisseria* is associated with the bacterial cell surface. Mol. Microbiol. 25, 11-25.

Rudel, T., Boxberger, H.J. and Meyer, T.F. (1995) Pilus biogenesis and epithelial-cell adherence of *Neisseria-gonorrhoeae* PilC double knock-out mutants Mol. Microbiol. 17, 1057-1071.

Schuch, R. and Maurelli, A. (2001) MxiM and MxiJ, Base Elements of the Mxi-Spa Type III Secretion System of *Shigella*, Interact with and Stabilize the MxiD Secretin in the Cell Envelope. J. Bacteriol. 183, 6991-6998.

Strom, M.S., Nunn, D.N. and Lory. S. (1993) A single bifunctional enzyme, PilD, catalyzes cleavage and N-methylation of proteins belonging to the type IV pilin family. Proc. Natl. Acad. Sci U.S.A. 90, 2404-2408.

Swanson, J., Kraus, S.J. and Gotschlich, E.C. (1971) Studies on gonococcus infection. I. Pili and zones of adhesion: their relation to gonococcal growth patterns. J. Exp. Med. 134, 886–906.

Tønjum, T., Freitag, N.E., Namork, E. and Koomey, M. (1995) Identification and characterization of pilG, a highly conserved pilus assembly gene in pathogenic *Neisseria*. Mol. Microbiol. 16, 451–464.

Tønjum, T. and Koomey, M. (1997) The pilus colonization factor of pathogenic neisserial species: organelle biogenesis and structure/function relationships – a review. Gene 192, 155–163.

Tsai, C.M. and Frash, C.E. (1980) Chemical analysis of major Outer-Membrane Proteins of *Neisseria-Meningitidis* – Comparison of serotypes-2 and serotypes-11. J. Bacteriol. 141, 169-176.

Wolfgang, M., van Putten, J.P.M., Hayes, S.F., Dorward, D. and Koomey, M. (2000) Components and dynamics of fiber formation define a ubiquitous biogenesis pathway for bacterial pili. EMBO J. 19, 6408-6418**.**

Yeremenko N, Kouřil R, Ihalainen JA, D'Haene S, van Oosterwijk N, Andrizhiyevskaya EG, Keegstra W, Dekker HL, Hagemann M, Boekema EJ, Matthijs HCP, Dekker JP (2004) Supramolecular organization and dual function of the IsiA Chlorophyll-Binding protein in cyanobacteria. Biochemistry 43, 10308-10313.

Summary

Biological membranes are vital components of all living systems, forming the boundaries of cells and their organelles. They consist of a lipid bilayer and embedded proteins, which are nanomachines that fulfill key functions such as energy conversion, solute transport, secretion, and signal transduction. Some membrane proteins form domains, which can vary and adapt to the functional state of the cell. Intact membrane complexes or solubilized membrane-bound complexes can be studied by electron microscopy (EM) and single particle analysis. This technique allows obtaining structural information in a rather easy way up to 10-20 Å resolution without using crystals, which are obligatory in X-ray diffraction studies. The technique has gained in popularity at the cost of the crystallographic approach, which uses two-dimensional (2-D) crystals. Such 2-D crystals of purified membrane proteins, reconstituted in the presence of lipids, provide a close to native environment and allow the structure and function of membrane proteins to be assessed. It was demonstrated in the nineties that electron crystallography can solve high-resolution structures of membrane proteins and very recently single particle averaging established itself also as a high resolution technique. A cryo-EM reconstruction of viral protein 6 (VP6) of a rotavirus was similar in clarity to a 3.8-Å resolution map obtained from x-ray crystallography. At this resolution, most of the amino acid side chains produced recognizable density. For non-symmetric objects such as membrane proteins this resolution is not achievable, but single particle averaging at lower resolution is still attractive if applied to negatively stained specimens with a mass between about 200 kDa and 2000 kDa. A major reason is that thousands of projections can be processed very fast, yielding 2D projection maps of at least 20 Å resolution. The statistical analysis and classification procedures used in single particle analysis have been developed for sorting different projection views originating from different conformations or subunit compositions.

In this thesis we present here some examples which show that single particle electron microscopy can be wider applied than just performing a structure determination of a highly purified large protein complex. Obtaining two-dimensional projection maps is a fast process but assignment of these maps can be a tedious process. The method is very suitable for determination of transient complexes or complexes that are inherently heterogeneous or

simply small. The method works on the level of a specialized membrane, as we show here for the membrane complex of two pathogenic *Neisseria* species.

Chapter 1 gives a general introduction about the protein structure, with an emphasis on membrane proteins. It also includes general information about the examined organisms, some important cellular processes and protein complexes, relevant to the topics studied in this thesis. Theoretical aspects of electron microscopy (EM), specimen preparation and image analysis are also presented. This chapter further contains a compilation of the recent progress in the field of electron microscopy, with an emphasis on structural biology.

Chapter 2 presents a study on some membrane-associated peroxins (Pex proteins). These particular Pex proteins are involved in protein import over the membrane in peroxisomes. Studies were performed with a model organism, the yeast *Hansenula polymorpha*. Single particle electron microscopy was used to analyze the structure of purified Pex5p and its possible association with Pex20p. The results showed that Pex5p can physically interact with Pex20p. We observed that a multimeric Pex20p complex can bind to the periphery of the Pex5p tetramer. Moreover, in this Pex5p-Pex20p complex, the conformation of tetrameric Pex5p was changed from a closed conformation with a diameter of 115 Å into an open conformation of 134 Å. EM data also showed that the Pex5p-Pex20p complex was capable to bind native, folded catalase, a peroxisomal PTS1 protein. This suggests that the Pex5p-Pex20p complex may be functional as receptor complex.

After completing the practical work of Chapter 2, we realized that peroxisomal membrane protein complexes are good candidates for further EM investigation since virtually no direct structural information of these complexes is available. In **chapter 3** a pilot study of the major peroxisomal membrane complexes in the yeast species *Saccharomyces cerevisiae* and *Hansenula polymorpha* is presented. We monitored the presence and purification of large, hypothetical pex complexes by western blotting with specific antibodies against Pex14p. The results showed that upon 1D and 2D/SDS Blue Native gel electrophoresis from peroxisomal fractions only a few protein bands could be attributed to peroxisomes. Moreover, no large Pex protein complexes were found, which we also proved by mass spectrometry. It was realized that this could be related to the relatively low protein content of the peroxisomal membranes compared to mitochondrial membranes. By using differential and sucrose density centrifugation to obtain a rather pure peroxisomal fraction, we faced the problem that

mitochondria were a major contaminant in the best purified peak fractions. We conclude that further purification of the initial membranes is crucial, which requires more advanced techniques and better separation protocols to separate peroxisomes from mitochondria.

Chapter 4 of this thesis presents three secondary transporter proteins: GltT of *Bacillus stearothermophilus,* CitS of *Klebsiella pneumoniae* and GltS of *Escherichia coli,* which were studied by single particle electron microscopy. Image processing showed that a GltT particle map with three-fold symmetry is in line with the trimer observed in the crystal structure of a homologous protein, Glt_{Ph} of *Pyrococcus horikoshi*. The other secondary transporter: CitS showed two main views as a kidney-shaped particle and a biscuit-shaped particle, both with a long axis of 160 Å and a short axis of 84 Å. The last examined secondary transporter: GltS was similarly shaped but smaller with dimensions of 150 Å x 84 Å. By comparing the shapes and dimensions of the CitS and GltS particles with the GltT particle, we suggest that the former two were in the dimeric state. In addition, a 10 kDa protein tag (Biotin Acceptor Domain, BAD) was fused to the N-terminus of the CitS protein or inserted in the central cytoplasmic loop which connects the two putative domains of the protein. Results from single particle EM analysis of the two proteins revealed differently shaped particles relative to the untagged protein. N-terminally tagged CitS revealed a more globular shape relative to the wild type. The aspect ratios were 1.77 and 1.9, respectively. We observed, that the inserted BAD domain resulted in an extended particle with an aspect ratio of 2.14. A model is presented for the relative orientation of monomers in the CitS dimer.

In **chapter 5** we studied the structure of the PilQ secretins from *Neisseria gonorrhoeae* and *Neisseria meningitidis.* The complex embedded in isolated outer membranes, was investigated by electron microscopy and single particle image analysis. Results showed that analyzed oligomers within the native membrane, revealed additional domains, which were not observed in studies using purified proteins. The structure of PilQ complexes of *N. gonorrhoeae* showed a double ring structure with a clear 14-fold symmetry of the outer ring, and a 14-15-fold symmetry in the inner ring. In addition, from the 14 protein densities of the outer ring 7 external spikes are protruding. Moreover, PilQ complexes of *N. meningitidis* also consisted of two rings, together with complexes partly or completely lacking the outer ring. Our results showed, that the outer ring of the *N. menigitidis* PilQ had a 19-fold symmetry and no external spikes were observed. The inner ring structures for both *N. gonorrhoeae* and *N. meningitidis* were of similar size as the structures previously observed from the isolated PilP/PilQ

complexes, demonstrating that the second ring and the external spikes do not contain domains of the PilQ or PilP proteins.

Further investigation of the composition of the outer ring and the spikes of the PilQ complexes from several *N. gonorrhoeae* knock-out mutants showed some changes in the composition of the outer rings. A knock-out of PilP did not show presence of the spikes, which means that this protein might be directly or indirectly involved in the spike composition. Moreover, the PilP knock-out also showed a change in the symmetry of the outer ring from 14 to 19 fold. A PilF mutant also did not show spikes either, however, maintained the 14-fold symmetry of the outer membrane. We concluded, that PilC2 and PilW mutants yielded similar structures as observed for the wild-type, indicating that they are not involved in these structures. These results and our observations could indicate that our structure composed of two rings and spikes is a high rotational flexibility, especially the connection of the two rings is flexible. Therefore, we concluded that the second ring and spikes my have a role in stabilizing the anchoring of the PilP/PilQ complexes with the membranes.

Nederlandse Samenvatting

Biologische membranen zijn onmisbare componenten van alle levende organismen en ze vormen de begrenzing van cellen en hun organellen. Ze bestaan uit een dubbele lipidelaag, waarin membraaneiwitten zijn ingebed. Deze hebben heel diverse functies, sommige zijn betrokken bij de energiehuishouding, andere dragen signalen over of zijn betrokken bij transport. Intacte membraancomplexen of gezuiverde eiwitten kunnen worden bestudeerd met behulp van elektronenmicroscopie (EM) en losse-deeltjes beeldverwerking. Een resolutie van 10-20 Å is vrij eenvoudig haalbaar met deze methode in het geval van membraaneiwitten. Er zijn ook een heleboel systemen te bedenken die met veel meer resolutie zijn te analyseren, zoals viruseiwitten. Hier is heel recent hoge-resolutie bereikt, die het mogelijk maakte om op aminozuur niveau een eiwit in kaart te brengen. Het gaat hierbij veelal om objecten met hele hoge symmetrie, die wordt benut om met een relatief kleine aantal deeltjes veel detail zichtbaar te maken.

Losse-deeltjes beeldverwerking is heel geschikt voor grote flexibele membraaneiwitten, en het proefschrift geeft hiervan diverse voorbeelden. We hoeven hierbij niet alleen te denken aan gezuiverde complexen, want bijvoorbeeld het laatste hoofdstuk van dit proefschrift gaat over een membraaneiwit dat als complex in de natieve membraan is geanalyseerd. Dit werk is verricht aan twee pathogene *Neisseria* soorten.

Hoofdstuk 1 geeft een algemene introductie over eiwitstructuur en over de achtergrond van de in dit proefschrift bestudeerde eiwitten. We geven ook details over elektronenmicroscopie, beeldverwerking en over de nieuwste ontwikkelingen in dit veld.

Hoofdstuk 2 presenteert een studie over peroxins, afgekort Pex eiwitten. Dat zijn eiwitten die te maken hebben met de eiwitimport in een organel, genaamd peroxisoom. Het modelorganisme *Hansenula polymorpha* werd gebruikt om gezuiverde Pex eiwitten te besturen met EM en beeldverwerking. Het blijkt dat het Pex5p eiwit een tetrameer eiwit is; de tetrameren kunnen een complex aangaan met een multimeer van het Pex20p eiwit. We hebben niet kunnen bepalen hoeveel kopieën van Pex20p in dit multimeer aanwezig zijn, maar wel hebben we laten zien dat het Pex5p-Pex20p complex in staat is van conformatie te veranderen, waarbij de tetrameren van een gesloten conformatie met een diameter van 115 Å

over gaan naar een open conformatie met een diameter van 134 Å. Ook zijn ze in staat om katalase, een peroxisomaal PTS1 eiwit, te binden. Vandaar dat we veronderstellen dat het Pex5p-Pex20p complex als een functioneel receptorcomplex werkt.

Het werk in Hoofdstuk 2 heeft ons gestimuleerd om te kijken naar andere PEX complexen, aangezien hier vrijwel niets over bekend is, althans over directe structuurinformatie. **Hoofdstuk 3** beschrijft een pilot study over peroxisomale membraancomplexen in twee gisten. We hebben diverse technieken gebruikt, zoals BN-PAGE om de opzuivering van veronderstelde grote eiwitcomplexen te volgen. Kort samengevat zijn we niet in staat geweest om dergelijke complexen aan te tonen. Dit kan onder andere liggen aan het feit dat het erg lastig is om goed gezuiverde peroxisomen te krijgen met de klassieke methode van differentiele en dichtheids centrifugatie. In de membranen zitten namelijk relatief buitengewoon weinig PEX eiwitten. Mitochondriën hebben daarentegen membranen die helemaal vol zitten met grote eiwitcomplexen.

Hoofdstuk 4 van dit proefschrift gaat over drie secondaire transporteiwitten, genaamd GltT uit *Bacillus stearothermophilus*, CitS uit *Klebsiella pneumoniae* en GltS uit *Escherichia coli.* Alledrie zijn bestudeerd met EM en beeldverwerking. De projectiemap van GltT laat zien dat dit deeltje drie-tallige symmetrie heeft, in overeenkomst met een hoge-resolutie map bepaald aan de hand van kristallen van een homoloog eiwit, Glt_{Ph} uit *Pyrococcus horikoshi*. We hebben deze deeltjes geanalyseerd om te zien of de beeldverwerking betrouwbaar is, aangezien deze transporteiwitten bijzonder klein zijn, aan de ondergrens van wat met losse-deeltjes beeldverwerking kan worden geanalyseerd. De andere twee transporters blijken beide een dimeer te zijn. Om nog wat meer over de positie van onderdelen van het eiwit te weten te kunnen komen is een Biotine Acceptor Domain (BAD) met een massa van 10000 dalton gefuseerd met de N-terminus van het CitS eiwit of gefuseerd met het centrale deel van het eiwit. De fusie-eiwitten hebben duidelijk een andere vorm en hierdoor hebben we een globaal model voor de positie van de monomeren in het dimeer kunnen maken.

In **hoofdstuk 5** hebben we de structuur van het PilQ secretine complex van de bacteriën *Neisseria gonorrhoeae* en *Neisseria meningitidis* bestudeerd. Dit complex hebben we bekeken in geïsoleerde buitenmembranen, zonder het verder te zuiveren, door middel van elektronenmicroscopie en beeldverwerking. Het PilQ secretine complex is een oligomeer in de membraan, maar heeft extra domeinen die niet meer aan het gezuiverde complex vast

zitten. Het PilQ complex uit *N. gonorrhoeae* bestaat uit een dubbele ringstructuur die een duidelijke 14-tallige symmetrie in de buitenste ring heeft. De symmetrie van de binnenring is niet helemaal duidelijk, maar vermoedelijk 14-15-tallig. Aan de buitenste ring steken 7 kopieën van een onbekend eiwit ver naar buiten. Het PilQ secretine complex van *N. meningitidis* bestaat ook uit twee ringen, maar 7 eiwituitsteeksels ontbreken volledig. Bovendien heeft de buitenste ring geen 14- maar 19-tallige symmetrie. Verder is deze ring in een vrij groot deel van de complexen geheel of gedeeltelijk afwezig. We hebben de samenstelling van de complexen onderzocht door te kijken naar mutanten die bepaalde eiwitten niet maken.

Een mutant die het PilP eiwit niet maakt, heeft geen eiwituitsteeksels meer. Twee andere mutanten, waar de PilC2 en PilW eiwitten ontbreken hebben echter hetzelfde PilQ secretine complex, waaruit we kunnen concluderen dat deze eiwitten niet bij de stuctuur betrokken zijn. Als laatste bleek uit de beeldverwerking dat de structuur bijzonder flexibel is; de binnen- en buitenring kunnen ten opzichte van elkaar iets verdraaid.

Acknowledgments

The time has come finally for me. You noticed that less and less people before you are left to promote, and suddenly one day you realize it is your turn. For me the journey is almost at an end it would not have been possible without the help of many people. Many of them have been a part of my whole PhD life, others shared just short moments of that time; none of them should be forgotten. I am indebted to prof. Dr. Egbert J. Boekema, my supervisor and promoter. He invited me to Groningen to do my PhD research and work with electron microscope, which was a new challenge for me, as a person who did not have any experience in this field. He always motivated me and found time to comfort me. For all this help, I want to thank You very much. It was a great pleasure to have You as my promoter and it was very nice to work in your group.

I would like to mention some persons who made my time in Groningen more joyful: Iwona Sobczak-Elbourne and Asia Majchrzykiewicz (our dinner evenings and talks till late hours). I also want to thank all my colleagues from Electron Microscopy Group especially Mihaela Folea (for our talks, dinners and shopping events) and Wilma Bergsma-Schutter (who was a great companion in our room and she always cheered me up), Mirjam (my new nice companion in our room), Roman and Jelle (for their great sense of humor), Natasha, Sami, Musa, Ana, Gert Oostergetel (for helping and teaching me how to work with microscopes), Wilko Keegstra (for teaching me the fundaments of image processing), Mark Stuart (for sharing his knowledge of membrane purifications and cryo demonstration), Jan Zagers (for immediate response when I had a problem with microscope), Roberta (for the nice complements), Emilie, Francesca, Milena and Bartek. I would like to thank you Hilda (you are a great person!!) for all the help with forms, rules, laws and all related paperwork, which are often not understandable for foreigners. Life is easier with people like you around. Thank you all it was nice to be a part of the group!

I would like to mention all the people from the X-ray group with some of you I had always nice conversations. Many thanks to Wim Huibers (for your help with Mass Spectrometry), Karin (for your patiance for EM results) and Gosia (for nice conversations during the breaks which you took when you search for the pili in EM).

I also want to thank Prof. dr. Ida van der Klei and the members from Molecular Cell Biology Group for help and support. Special thanks to Sandra, Eda, Shirisha who introduced me to protein research during my PhD.

Many thanks to Dr. Juke Lolkema and Tomek Krupnik from Molecular Microbiology Group and also to Dr. Chris van der Does and Samta Jain (you always provided me with very good membrane samples and I could always count on you). Finally I wish to acknowledge Prof. dr. Hans-Peter Braun and his group members (especially Steffi) for all the help during my time in Hannover. It was a pleasure working with such a nice group, even when the results were not always successful. Thank you all!

I would like to say few words to my parents. I am very happy that I came to the Netherlands and decided to study here and do my PhD. I want to thank especially my father for that, he advised to do that. Thank you for it! I know that both of you always believed in me and gave me all the help and love you could. Thank for the all support!

Finally, I want to dedicate the last lines to my dearest person to me. My boyfriend Gerjo, we met here in the Netherlands (in Wageningen). During the time of my MSc-study and PhD, you were always here to give me all support during good and stressful days. Dank je wel!

Kasia M.

Podziękowania

Przyszla i na mnie pora. Początkowo zauważasz, ze coraz mniej osób zostało przed tobą, które się wkrótce obronią, aż któregoś dnia zdajesz sobie sprawę, że to już twoja kolej. Dla mnie ta podróż dobiegła prawie końca, ale nie byłaby możliwa bez wielu osób. Wiele z nich była częścią mojego życia, inni dzielili krótkie momenty w tym czasie; nikt z nich nie będzie zapomniany. Za moje osiągnięcia jestem najbardziej wdzięczna Prof. dr. Egbertowi J. Boekemie, mojemu opiekunowi i promotorowi. On zaprosił mnie do Groningen aby podjąć studia doktoranckie nad praca z mikroskopem elektronowym, co było nowym doświadczeniem dla mnie jako osoby która ukończyła studia na wydziale ogrodniczym. On zawsze mnie motywowal i zawsze znalazł dla mnie czas na słowa otuchy podczas problemów z doświadczeniami. Za wszystko i za całą pomoc chcę mu bardzo podziękować, to był wielki zaszczyt, że byłeś moim promotorem i było mi bardzo miło pracować w Twojej grupie.

Chciałabym też wspomnieć parę osób, które dużo dla mnie znaczą: głównie Iwona Sobczak-Elbourne i Asia Majrzykiewicz (z naszych wspólnych obiadów i dlugich rozmow do pozna w nocy). Chcę też podziękować wszystkim moim kolegom z grupy mikroskopów elektronowych szczególnie Mihaeli Folei (za nasze wspólne rozmowy, zakupy) i Wilmie Bergsmie-Shutter (która była wspaniałym towarzyszem w naszym pokoju i zawsze podtrzymywała mnie na duchu), Mijam (mojej nowej milej towarzysce, która dzielila ze mna pokoj), Romanowi i Jelle (za szczególne poczucie humoru), Nataszy, Samiemu, Musie, Anie, Gertowi Oostergetel (za pomoc i nauczanie mnie do pracy z mikroskopami), Wilkowi Keegstra (za nauczenie mnie podstaw oprocesowywania zdjęc), Markowi Stuartowi (za dzielenie się swoją wiedzą na temat płukania membran), Janowi Zagers (za nastychmiastową reakcje gdy mialam problem z mikroskopem), Robercie (Ty zawsze powiedziałaś mi mily komplement), Emilie, Francesce, Milenie a takze Bartkowi. Chciałabym także podziękować Tobie Hildo za całą pomoc z dokumentami, zasadami, prawami i całą papierkową robotę, które są szczególnie trudne dla obcokrajowców. Życie jest o wiele łatwiejsze z ludźmi takimi jak Ty dookoła nas. Dziękuje wszystkim, było mi miło być częścią tej grupy! Chce tez wspomniec ludzi z grupy krystalografow, z niektórymi z Was bardzo milo mi się rozmawialo. Na pewno tego nie zapomne. Chciałabym także wspomniec Wima Huibersa (dziekuje za

pomoc przy Mass Spectrometry), Karin (za cierpliwość przy czekaniu na wyniki) a także Gosi (za mile rozmowy w czasie przerw na szukanie fantastycznej pili).

Chciałabym także podziękować prof. dr. Idzie van der Klei i członkom jej grupy Molekularnej Biologii Komórki za okazaną mi pomoc i wsparcie. Specjalne podziękowania Sandrze, Edzie i Shirishii, które wprowadziły mnie w badania nad białkami w czasie bycia doktorantką.

Wiele podziękowań dla dr. Juke S. Lolkemy i Tomka Krupnika z grupy Molekularnej Mikrobiologii a także dla dr. Chrisa van der Doesa i Samty Jaim (zawsze dostawałam od was dobre próbki i zawsze mogłam na was liczyc).

Na końcu chciałabym zaakcentować moją wdzięczność prof. dr. Hansowi-Peterowi Braun i członkom jego grupy (szczególnie Steffi) za całą pomoc jaka od nich otrzymałam w czasie mojego pobytu w Hanowerze. To było dla mnie przyjemnością pracować z taką grupą, nawet jeśli nie miałam pozytywnych rezultatów. Dziękuję wam za wszystko!

Parę słów dedykuje moim rodzicom. Jestem bardzo szczęśliwa, że przyjechałam do Holandii i zdecydowałam studiować tutaj i zrobić mój doktorat. Chciałabym szczególnie podziękować mojemu tacie za to, on doradził mi ten pomysł. Dziękuje Ci za to! Wiem, że Wy zawsze we mnie wierzyliście i zapewnialiście mi dużo pomocy i wiele miłości. Dziękuję Wam za wszystko!

Na końcu, parę zdań do mojego najbliższej mi osoby. Gerjo, spotkaliśmy się tutaj (w Wageningen). W czasie moich studiów i mojego doktoratu zawsze byłeś przy mnie w ciągu dobrych i złych dni. Dziękuję!

Kasia M.